LBL-6819

ATMOSPHERIC AEROSOL RESEARCH

ANNUAL REPORT 1976-77

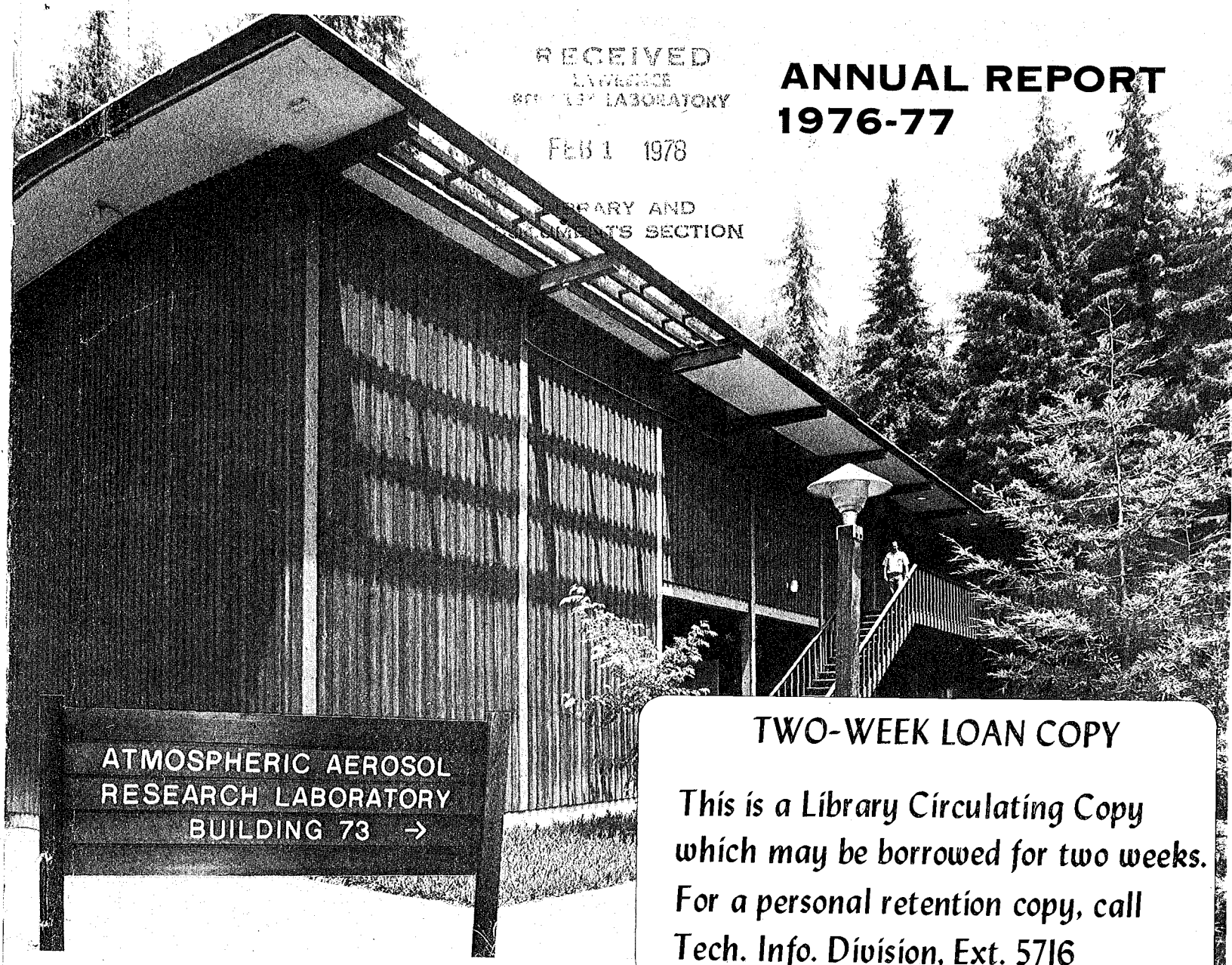

ENERGY & ENVIRONMENT DIVISION
LAWRENCE BERKELEY LABORATORY

UNIVERSITY OF CALIFORNIA, BERKELEY

PREPARED FOR THE DEPARTMENT OF ENERGY
UNDER CONTRACT W-7405-ENG-48

LBL-6819

UC-11
TID-4500-R66

LAWRENCE BERKELEY LABORATORY
ENERGY AND ENVIRONMENT DIVISION
ATMOSPHERIC AEROSOL RESEARCH

ANNUAL REPORT
1976-1977

PARTICIPANTS: T. Novakov, Principal Investigator
S.-G. Chang, Co-principal Investigator
C. D. Hollowell, Co-principal Investigator
H. Rosen, Co-principal Investigator
W. H. Benner
H. A. Brendel
R. Brodzinsky
M. Clemenson
R. L. Dod
R. D. Giauque
L. Gundel
A. D. A. Hansen
S. S. Markowitz
G. F. Mason
P. J. Pagni
R. C. Schmidt
G. W. Traynor
R. Toossi
L. Wroth

Editor: H. Rosen

TABLE OF CONTENTS

ACKNOWLEDGMENTS

The research described in this report is supported by the National Science Foundation—Research Applied to National Needs and the U.S. Department of Energy. We would like to express our appreciation and thanks to Dr. Richard A. Carrigan and Dr. Frank P. Hudson, program managers of the respective agencies.

We gratefully acknowledge and thank the following:

The Bay Area Air Pollution Control District and the South Coast Air Quality Management District for their cooperation with our program.

Presentation High School, Berkeley, for providing a site for our Mobile Atmospheric Research Laboratory.

Dr. Andrew M. Sessler, Director of Lawrence Berkeley Laboratory, and Dr. Robert J. Budnitz, Head of LBL's Energy & Environment Division, for their continued strong support of our program.

Dr. Billy W. Loo of LBL for advice on aerosol sampling and for elemental analyses of particulate samples using the X-ray fluorescence technique.

Prof. Mark Shapiro, California State University, Fullerton, for help in making arrangements for sampling in the Los Angeles Air Basin.

Mr. E. R. Mayo, Highway Superintendent, California State Department of Transportation, Caldecott Tunnel, and his staff for helping us in every way possible to conduct the experiments in the Caldecott Tunnel.

Dr. Chester Spicer, Batelle, Columbus Laboratories, Columbus, Ohio, for performing analyses of particulate samples.

We would also like to acknowledge fruitful discussions with Dr. Richard A. Carrigan, Prof. Glen Gordon, Prof. Jarvis Moyers, Prof. Robert J. Charlson, Prof. Milton Kerker, Prof. Leo Brewer, and Prof. Harold Johnston.

INTRODUCTION

Introduction

T. Novakov

During the early days of environmental awareness, primary particulate emissions were easily visible; and smoke or soot was the first air pollutant to be recognized and controlled. In fact, the word "smog" was coined from the words "smoke" and "fog". In more recent times, improvements in combustion technology and the use of better-grade fuels have led to the virtual elimination of visible smoke emissions. The emphasis of air pollution control slowly shifted away from primary particulate emissions toward controlling gaseous emissions. This trend culminated in southern California with the concept of Los Angeles-type photochemical smog, which is believed to contain neither smoke nor fog. According to a widely held view, the haze over the Los Angeles Air Basin on polluted days is due almost entirely to the photochemical conversion of certain invisible gases to light-scattering particles. In recent years there has also been a trend to consider aerosol pollution elsewhere in the United States and in the world as an essentially photochemical phenomenon. Control strategies based on the above view naturally stress the control of gaseous emissions, especially those responsible for the formation of ozone. Ozone, the principal product of photochemical processes, is considered essential in the formation of photochemical haze. Thus the control of pollution aerosol particles remains linked largely with present control strategy for oxidant and precursor gases.

Over the past 4 to 5 years, the principal research objective of LBL's Atmospheric Aerosol Research has been to assess the contribution of primary particulates to the ambient particulate burden and to evaluate the role of

these primary particles in the formation of secondary aerosol species. We chose this research objective because there is considerable evidence that primary carbonaceous or soot particles are still very important contributors to atmospheric pollution. The difference between our concept of soot and visible smoke is largely confined to the size of the particles. Smoke consists of large particles that are responsible for the opacity of plumes. Soot is any carbonaceous particulate material emitted from sources, even if these do not produce visible plumes or smoke. In most cases soot particles are very small when emitted, having diameters of the order of 100 Å, and are therefore invisible to the naked eye. Soot can also be described as a chemically complex carbonaceous material which consists of a "graphitic" component and an organic component. There are significant differences in the overall properties of the two components. For example, the graphitic component is nonvolatile, insoluble in organic solvents, and is a strongly light-absorbing material. In contrast, the organic component of soot is volatile, soluble in solvents, and does not appreciably absorb light. We have previously stated that we find that as much as 80% of the ambient particulate carbon, collected in different parts of California, is in the form of soot.[1,2]

The second view, which we have advocated over the years, is that soot particles are not only a major constituent of ambient particles but also are a catalytically and surface chemically active material largely responsible for the formation of sulfates resulting from fossil fuel combustion.[1] For example, we have expressed the view that the catalytic formation of sulfate on soot particles is expected to occur in the open atmosphere and especially in or near combustion sources, where both SO_2 and soot concentrations are highest.[1] We have also stated that the soot-catalyzed SO_2 oxidation plays a major role in atmospheres characterized by high concentrations of particulate carbon.

This annual report describes the results obtained during 1976-1977. The individual papers contained in the report attempt to provide answers to the following questions:

1. What fraction of the ambient particulate carbon is of primary origin?

2. What is the role of primary particulate carbon in the atmospheric oxidation of sulfur dioxide to sulfate?

3. What is the role of primary particulate carbon in the formation of suspended nitrogenous species?

Section I deals with the chemical and physical characterization of ambient and source particulates. The research reported in this section should provide at least a partial answer to the question of what fraction of the ambient particulate carbon is of primary origin. Two novel approaches have been used for this purpose: the first involves application of the optical absorption technique; the second uses laser Raman spectroscopy. The results show that the absorbing species in ambient and source particulate samples are "graphitic" soot and that a major fraction of the carbonaceous component of ambient aerosol particles in the San Francisco Bay Area and in the Los Angeles Air Basin are of primary origin. In this section further developments in the determination of low-Z elements in atmospheric particulates by nuclear reactions are also described.

Section II reviews our recent work on the role of primary particulate carbon in atmospheric reactions. We have extended our work on the role of soot particles as catalysts for SO_2 oxidation by studying the effect of liquid water on the soot-catalyzed reaction. The effects of liquid water are important because in plumes liquid water may condense on the soot particles. Furthermore, soot particles may encounter liquid water in their passage through fogs and clouds. This "wet" mechanism is much more efficient for SO_2 oxidation than the corresponding "dry" mechanism that we have suggested previously.[1]

For the dry mechanism we present a mathematical model applicable to plumes. This model will be extended to the "wet" mechanism. Surface reactions of NO_x and NH_3 with particulate carbon have continued to be an important part of our research. Results obtained by means of Fourier transform infrared spectroscopy on laboratory-synthesized samples have confirmed the existence of certain reduced nitrogen species that we have uncovered before by X-ray photoelectron spectroscopy.

Section III describes some of our field results. The principal aim of our field program is the study of winter air pollution in the Bay Area. These winter episodes are characterized by low oxidant concentrations but high particulate concentrations. The particulates are produced either by sources or by atmospheric reactions, but presumably not by ozone-related reactions. These results demonstrate that even in the virtual absence of ozone, there is still a severe air pollution problem whose abatement will require measures different from those designed for oxidant control.

References

1. T. Novakov, S.-G. Chang, and A. B. Harker, "Sulfates as pollution particulates: Catalytic formation on carbon (soot) particles," Science 186, 259 (1974).
2. S.-G. Chang and T. Novakov, "Formation of pollution particulate nitrogen compounds by NO-soot and NH_3-soot gas-particle surface reactions," Atmos. Environ. 9, 495 (1975).

SECTION I

CHARACTERIZATION OF AMBIENT AND SOURCE PARTICULATE SAMPLES

Characterization of the Carbonaceous Component of Ambient and Source Particulate Samples by an Optical Absorption Technique

H. Rosen, A. D. A. Hansen, R. L. Dod, and T. Novakov

One major uncertainty in the air pollution field is the extent to which the carbonaceous aerosol particle burden is due to secondary reactions or is of primary origin. Such a determination is clearly necessary for designing an effective control strategy; but due to the complex nature of the samples, it has been a difficult analytical problem to develop methods for discriminating between these two sources of carbon. One distinct feature of primary emissions, however, is that they appear to have a large "graphitic" soot component. This component offers an attractive tracer for primary emissions since it has some rather unique physical properties. These include a rather high oxidation threshold and a large and uniform absorptivity throughout the visible spectral region, which we suggest leads to the blackish or grayish appearance of ambient and source particulate samples. It should be emphasized that "graphitic" soot represents only one component of the primary carbonaceous aerosol particles, which in general also contain a large nonabsorbing and volatile organic fraction.

Here we report on measurements of the absorbing properties of ambient samples collected in Berkeley, California, in the winter and in Anaheim, California, in the summer. These results are compared with measurements made on various source particulate samples. A strong correlation between the carbon content and the absorptivity of the collected particulates is observed. This correlation, in combination with measurements of the wavelength dependence and temperature dependence of the absorptivity, suggests that the absorbing species is "graphitic" soot. A striking similarity is observed in the dependence of

the absorptivity on the carbon content for the Berkeley and Anaheim particulate samples (Fig. 1a). This is true is spite of the fact that several of the Anaheim samples were taken under high oxidant conditions, which are expected to promote secondary production of aerosol particles. Also, the absorptivity per unit mass of carbon for these ambient samples is found to be quite similar to that of various mobile source exhaust samples (Fig. 1b). These results seem to indicate that a large fraction of the carbonaceous aerosol particles in the summer and winter episodes investigated is primary in origin. Further studies are under way to test the generality of these results under a wide range of atmospheric conditions and for a variety of combustion sources.

Particulate samples were collected simultaneously on 1.2-μm Millipore filters and on quartz fiber filters that had been prefired to remove all combustible carbon. The total carbon on the quartz fiber filters was determined by combustion in an oxygen atmosphere, followed by separation and measurement of the evolved CO_2 with a gas chromatograph/thermal conductivity detector system.[1] After correction for differing flow rates, these values were then used to calculate the total carbon loadings on the corresponding Millipore filters. Optical attenuation measurements were made on the loaded Millipore filters by an apparatus incorporating a 1-mW He-Ne laser as a light source (λ = .6328 μm) and a photomultiplier as a detector. Essentially all of the light transmitted through the filter was collected and focused onto the photomultiplier by an f/1 lens. The average transmission through blank filters was assigned a value of 100%. This technique for measuring absorptivity is based on a principle similar to that of the opal glass technique developed by Lin et al.[2] The attenuation measured in the above fashion should be primarily due to absorption rather than scattering because most of the radiation scattered from ambient aerosol particles is in the forward direction and therefore should

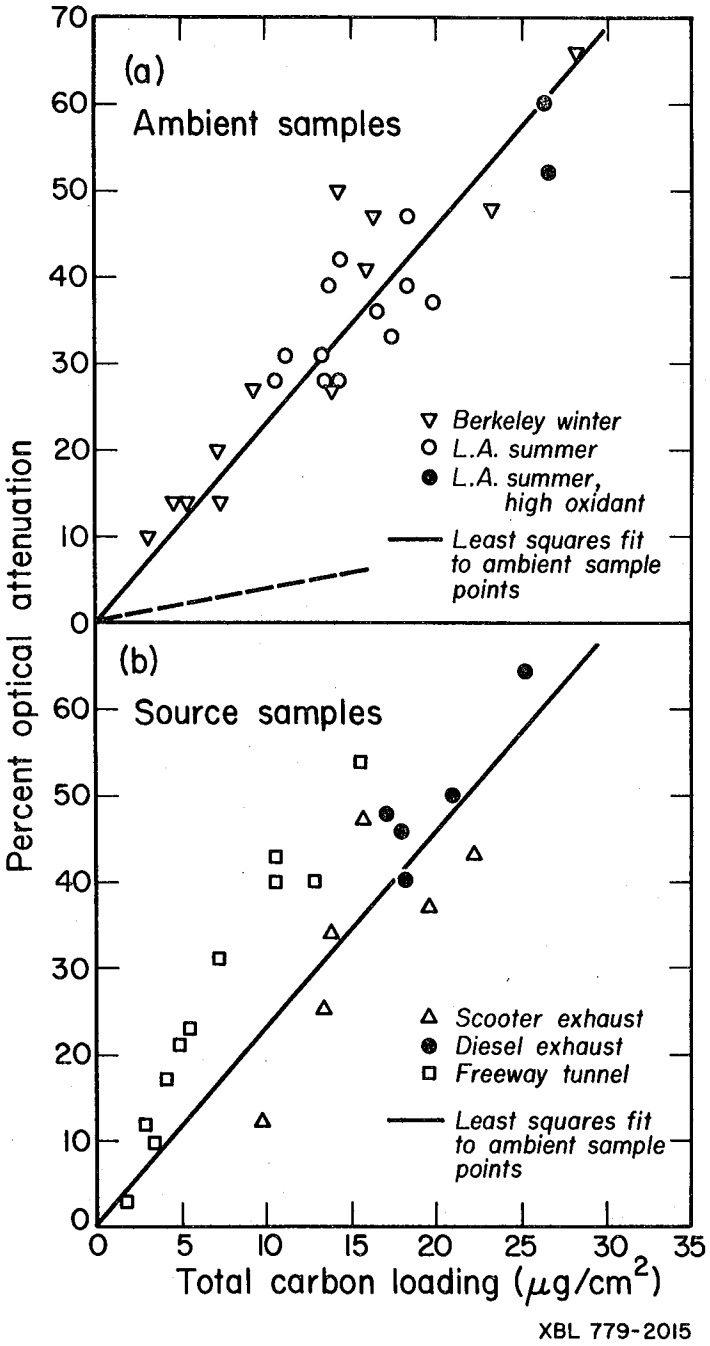

Figure 1. a) Optical attenuation vs. total carbon loading for ambient samples collected in Berkeley, California, in the winter and in Anaheim, California, in the summer. The peak ozone levels for the daily summer samples ranged from 30 ppb to 270 ppb. The points designated by a solid circle have ozone levels ≥ 250 ppb. The dashed line corresponds to the theoretical prediction from a mass balance calculation using Pb as a tracer and assuming the dominant sources of primary particulate carbon are automobiles.

b) Optical attenuation vs. total carbon loading for various mobile source samples.

not contribute to the attenuation since it is collected by the small-f-number lens.

The particulate samples used in these experiments were (1) ambient samples collected in the winter in Berkeley, California (sampling times, from 15 min-4 hr; flow rate, ≈ 70 liters/min); (2) ambient samples collected in the summer in Anaheim, California (sampling time, 24 hr; flow rate, ≈ 7 liters/min); (3) tunnel samples collected in a storage room between two bores of the Caldecott Tunnel, on a major San Francisco Bay Area commuter route with a traffic flow of approximately 10^5 vehicles/day; (4) garage samples collected from the rear of an underground parking garage, in which the automobile traffic flow was approximately 35 vehicles/hr with an average stay of 1-2 hr; (5) diesel exhaust samples from a small air-cooled engine; (6) motor scooter exhaust samples from a two-stroke engine operating at a slow idle; and (7) soot samples generated by a very rich acetylene flame.

We have measured the attenuation and total carbon content of a number of ambient and mobile-source exhaust samples. These results are shown in Figures 1a and 1b. In all cases there is a strong correlation between the carbon content and the attenuation. Since sulfur and nitrogen species in the form of common salts such as ammonium sulfate and ammonium nitrate are nonabsorbing in the visible region, and since there are no significant amounts of transition metals like Fe in these samples, we suggest that the absorption is due to the carbonaceous component of the aerosol particles.

It should be emphasized that the coverage of these samples is very light (≈ 1 monolayer of particles or less); and yet the absorptivity is quite high, implying that the refractive index of the absorbing species has a large imaginary part. The material most likely to be responsible for this absorption is "graphitic" soot, which has the requisite high imaginary index of refraction

(n_I = .46)[3] and has been shown to be a major species in both ambient and source samples[4] (see Section I, p. 18).

In order to gain a better understanding of the nature of these highly absorbing species, we have measured the wavelength and temperature dependence of the absorptivity for ambient, tunnel, and laboratory-generated soot samples (Figs. 2 and 3). The absorptivity shows a $1/\lambda$ wavelength dependence to within 20% over the visible spectral region (4500 Å - 7000 Å), as expected for a wavelength independent imaginary index of refraction and evidenced by the gray or black color of these samples. This result is consistent with the hypothesis that the absorption is due primarily to "graphitic" soot since it has been shown that the imaginary index of refraction of both acetylene and propane soot is essentially constant throughout the visible region.[3] In fact it is difficult to find many organic species which meet this criterion: of the 13,000 organics listed in the 54th edition of the CRC Handbook, only 5 are gray or black in appearance.

The temperature dependence of the absorptivity was determined by measuring the absorptivity of particulates collected on quartz fiber filters before and after heat treatment at various temperatures. The heat treatment procedure consisted in heating the sample at the prescribed temperature for 30 minutes in air. The results of these measurements are plotted in Figure 3, which shows clearly that in all cases the absorbing species are stable in air until approximately 400°C, and then undergo what is presumably a rapid oxidation process to essentially disappear by 500°C. Note that this threshold is similar to that of polycrystalline graphite.[5] The stability of the absorbing species at elevated temperatures again suggests that they are graphitic in structure, as most other organic species expected to be present in ambient and tunnel samples should oxidize or vaporize at significantly lower temperatures.

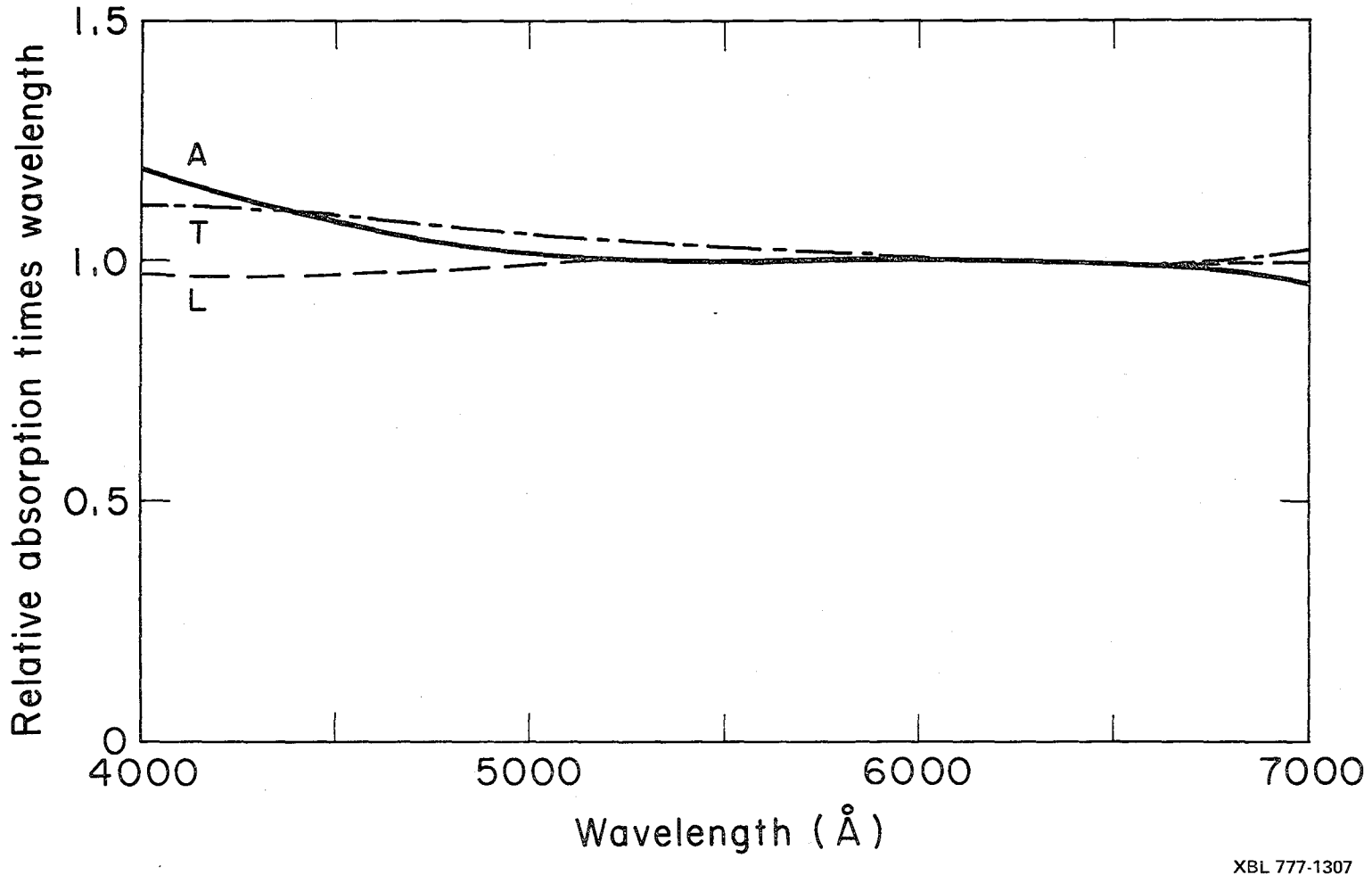

Figure 2. Plot of the product of absorptivity and wavelength versus wavelength for A — ambient samples, T — tunnel samples, and L — laboratory-generated soot samples. Such a plot would be flat for a wavelength-independent imaginary index of refraction.

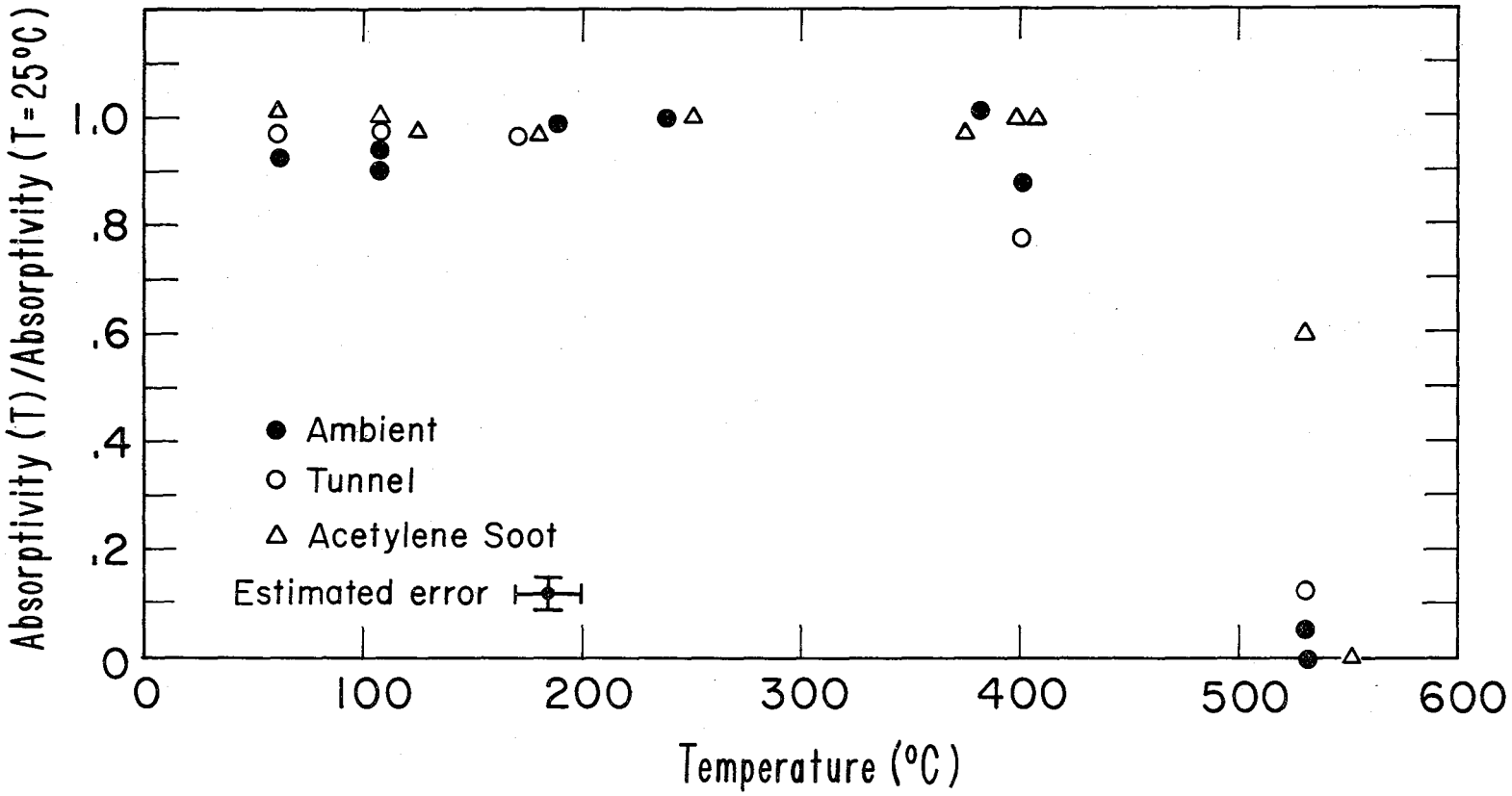

XBL 777-1308

Figure 3. Plot of the ratio of the absorptivity of various samples after heat treatment at temperature T to the absorptivity at T = 25°C as a function of heat treatment temperature. The heat treatment procedure consisted in heating the sample in air for 1/2 hour at the prescribed temperature.

The characterization of the carbonaceous component of ambient aerosol particles in terms of primary and secondary species is crucial to the determination of any effective control strategy. In this respect the results shown in Figures 1a and 1b could have important implications. The similarity between the absorbing properties of the winter and summer ambient samples and the mobile source samples is quite striking and can be interpreted to indicate that a large fraction of ambient particulate carbon is primary in origin. It would seem quite fortuitous for secondary atmospheric processes to generate carbonaceous species which just happen to have similar absorbing properties to mobile source samples. It is also evident from the strong correlation between the absorptivity and carbon content that "graphitic" soot seems to constitute an approximately constant fraction of the total carbon content of the ambient samples even for oxidant levels exceeding 250 ppb (see Fig. 1a). This is expected from primary emissions, but not from secondary processes which would be expected to show more variability depending on atmospheric conditions (relative humidity, gas concentrations, oxidant level, etc.).

It has been suggested that most of the carbonaceous species in the Los Angeles Air Basin in the summer are of secondary origin, based on the concept of mass balance using Pb as a tracer.[6,7] Most of the primary carbon is assumed to originate from mobile sources, while the contribution of other sources relative to the automobile is estimated from an emission inventory. The contribution of mobile sources is determined by assuming that such emissions are characterized by a C/Pb ratio of ~ 1.7.[7] In the ambient samples, C/Pb ratios of the order of 10 are found, and the deviation from the automotive C/Pb ratio, after taking into account a small contribution from other sources, is attributed to the secondary production of organic carbon. Both the summer and winter episodes that we have investigated show a similar discrepancy (C/Pb in the ambient

samples, ≃ 10, and C/Pb in the tunnel samples, ≃ 1). If we were to use the same analysis as above and further assume that black species ("graphitic" soot) are not produced in secondary processes, an approximate prediction of the absorptivity versus carbon content for our ambient samples would be given by dividing the slope of least squares fit of the tunnel points by 10. This line is shown in Figure 1a and clearly does not agree with the ambient measurements. This disagreement may be due to the fact that sources other than automobiles (e.g., diesels, home heating, aircraft, industry) make a major contribution to the carbon balance. It is also possible that there are some difficulties in using Pb as a tracer for mobile source emissions. For example, differences in the transport properties of lead and carbon could affect the C/Pb ratio. Also, we have found that the C/Pb ratio may depend markedly on driving conditions. Tunnel samples typically had a C/Pb ratio of ≃ 1 while parking garage samples taken under "start-stop" conditions had a C/Pb ratio of ≃ 8. This is quite reasonable since under these conditions we would expect the combustion process to be more incomplete and therefore produce more carbonaceous emissions.

References

1. A similar system is described by P.K. Mueller, R.W. Mosley, and L.B. Pierce, "Carbonate and non-carbonate carbon in atmospheric particulates," in Proceedings of the 2d International Clean Air Congress, New York, Acedemic, 1971.

2. C.-I. Lin, M. Baker, and R.J. Charlson, "Absorption coefficient of atmopsheric aerosol: A method for measurement," Applied Optics 12, 1356 (1973).

References (contd.)

3. W.H. Dalzell and A.F. Sarofim, "Optical constants of soot and their application to heat-flux calculations," J. Heat Transfer 91, 101 (1969).

4. H. Rosen and T. Novakov, "Raman scattering and the characterization of atmospheric aerosol particles," Nature 266, 708 (1977); H. Rosen and T. Novakov, "Identification of primary particulate carbon and sulfate species by Raman spectroscopy," Report LBL-5912, Lawrence Berkeley Laboratory, University of California, Berkeley, CA 94720; accepted by Atmospheric Environment.

5. See, for example, Union Poco Comparison Chart, Publication PGI-S-2021, Poco Graphite, Inc., 1601 South State Street, Decatur, TX 76234.

6. S.K. Friedlander, "Chemical element balances and identification of air pollution sources," Environ. Sci. and Technol. 7, 235 (1973).

7. G.M. Hidy, et al. Characterization of Aerosols in California (ACHEX): Final Report, Science Center, Rockwell International, Report SC524.25FR, 1974.

Application of Raman Scattering to the Characterization of Pollution Particulates

H. Rosen, A. D. A. Hansen, and T. Novakov

A. Identification of primary particulate carbon and sulfate species by Raman spectroscopy

In order to better assess the origin and the environmental effects of airborne particles, it is important to explore new techniques for their chemical characterization. During the past year, we have successfully obtained Raman spectra of both ambient and source-enriched particulate samples. As far as we know, this is the first application of this method to the characterization of pollution particulate samples.[1,2] Although the Raman scattering technique is in its early stages of development, it seems to hold considerable promise as a nondestructive, sensitive, and highly selective method for the characterization of pollution particulates.

The Raman spectra between 900 and 1950 cm^{-1} of ambient, automobile exhaust, and diesel exhaust particulates are compared with the spectra of activated carbon and polycrystalline graphite in Figure 4. The close correspondence of the spectra strongly suggests the presence of physical structures similar to activated carbon in both source-enriched and ambient samples. These graphitic species are presumably of primary origin, and throughout the text we shall use the term "graphitic" soot to describe them.

Typically about 10% of the weight in the small particle size fraction ($\leq$ 2.4 μ) of the ambient samples studied is sulfur. Therefore if the Raman cross section for sulfur species is comparable to that of "graphitic" soot, we would expect to observe such species. In Figure 5 we show the Raman spectrum of a heavily loaded ($\simeq$ 400 $\mu g/cm^2$) sample collected in St. Louis, Missouri,

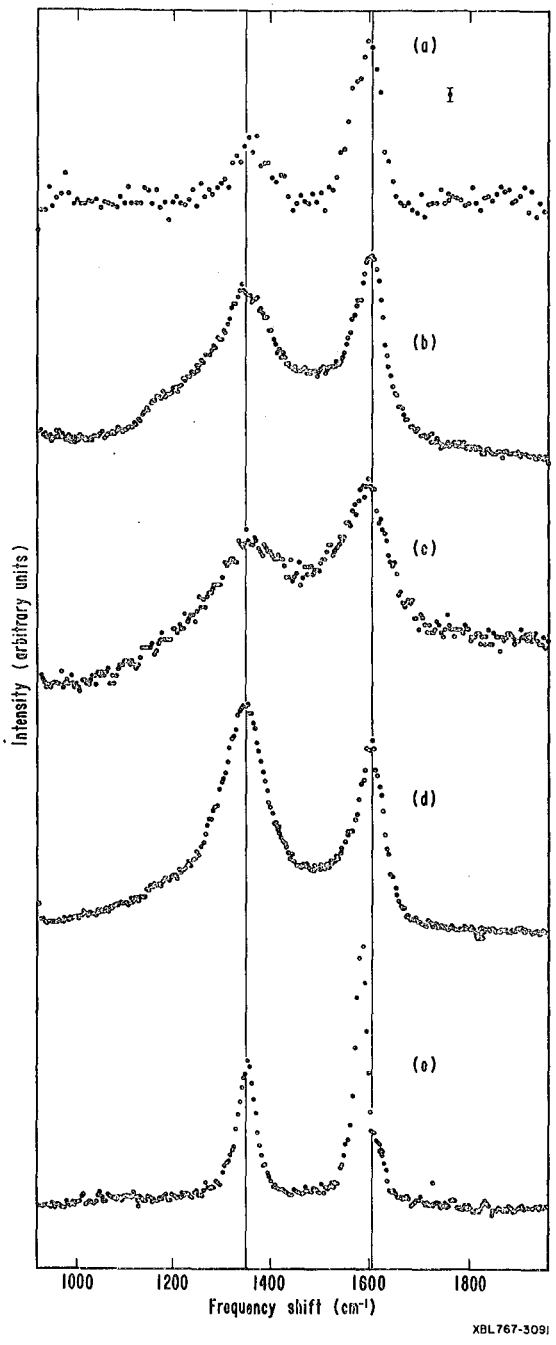

Figure 4. Raman spectra between 920 and 1950 cm^{-1} of: a) Ambient samples collected in 1975 as part of EPA's RAPS program. The sample was collected on a dichotomous sampler and was in the small size range fraction. b) Automobile exhaust collected from a number of cold starts of a poorly tuned automobile using lead-free gas and having no catalytic converter. c) Diesel exhaust. d) Activated carbon. e) Polycrystalline graphite.

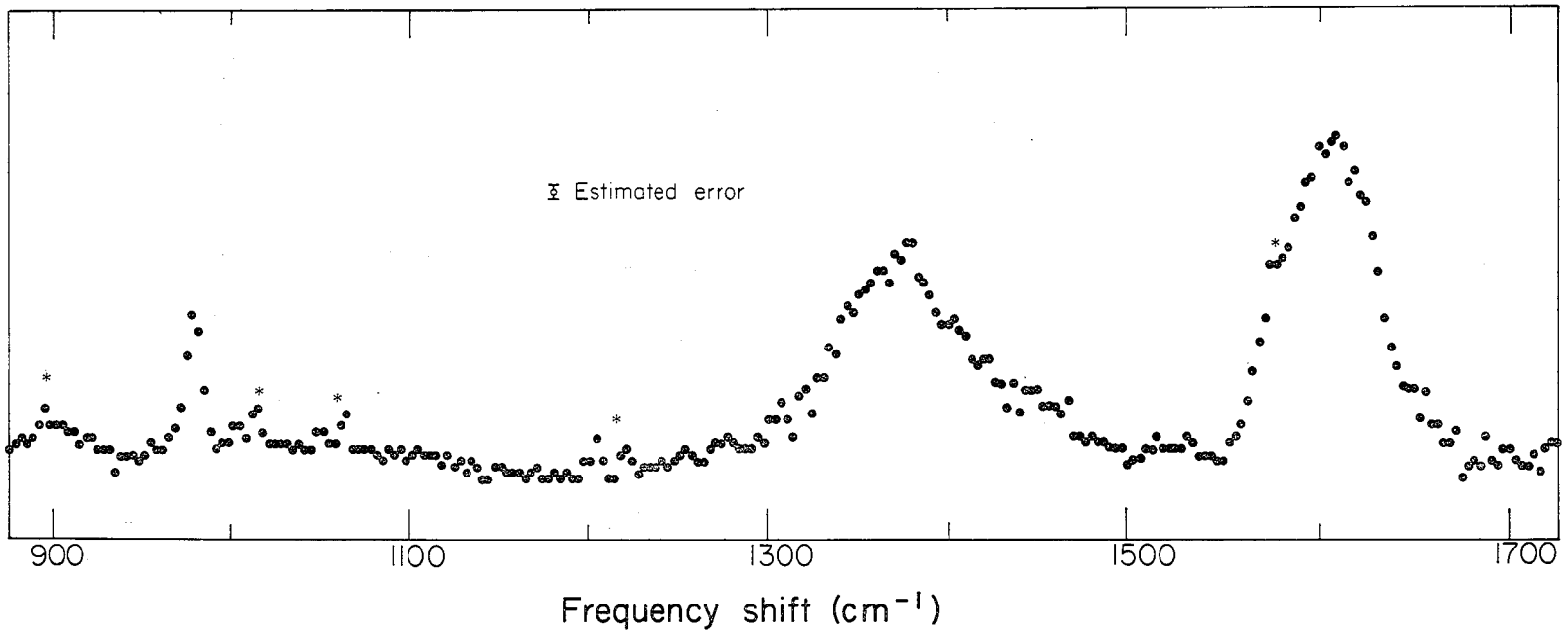

Figure 5. Raman spectrum of an ambient sample collected in 1975 as part of EPA's RAPS program in St. Louis, Missouri. The sample was collected on a dichotomous sampler (Ref. 5) and was in the small size range fraction. The spectrum was obtained with a slit width of 3 Å ($\sim$ 10 cm^{-1}) and integration time of 2 min/ch. The lines denoted by an asterisk correspond to grating ghosts.

in the spectral region between 900 and 1700 cm^{-1} after subtraction of the fluorescent background. The elemental composition of this sample as determined by X-ray fluorescence[3] is shown in Table I. The spectrum was obtained with a

Table I. Elemental composition of the ambient sample whose Raman spectrum is shown in Figure 5.[a]

Element	Nanogram/cm^2	Element	Nanogram/cm^2
Al	729	Ni	27
Ar	96	P	250
As	2	Pb	4,091
Br	389	Rb	6
Ca	650	S	45,781
Cl	95	Sc	565
Cr	13	Se	22
Cu	135	Si	1,593
Fe	1,034	Sr	2
Ga	0	Ti	112
Hg	13	V	38
K	1,084	Zn	505
Mn	82		

[a]Data obtained using the X-ray fluorescence analyzer developed by Jaklevic et al. (Ref. 3).

scan speed of 0.5 Å/min, an integration time of 2 min/ch, and a slit width of 3 Å (10 cm^{-1}). The spectral lines characteristic of "graphitic" soot are again evident. However, a sharp line is also observed near 976 cm^{-1}, which we assign to sulfate species. The lines denoted by an asterisk are due to grating ghosts. This spectrum clearly has better signal to noise than that of the ambient spectra shown in Figure 4. The improvement is due to the longer integration times used in this scan and the smaller slit widths, which tend to enhance the sharper features of the spectrum relative to the broad fluorescence background. The position of the sharp line was compared with that of the ν_1 vibration of

$(NH_4)_2SO_4$, which was used as a standard. The peak position was coincident to within ± 2 cm^{-1}, which is the estimated experimental error. This suggests that the line is indeed due to $(NH_4)_2SO_4$. It is clear from Figure 6, which shows the Raman spectra of sulfuric acid, ammonium bisulfate, and ammonium sulfate, that the Raman technique is highly selective and can certainly distinguish between these species. For sulfate salts like $CaSO_4$ and $PbSO_4$, the spectral changes are smaller; but the sharpness of the spectra allows one to detect small shifts and therefore discriminate among the various compounds.[4]

B. Raman study of the relationship between optical absorptivity and "graphitic" soot content

The absorptivity of urban aerosol particles is quite high as evidenced by the grayish or blackish appearance of even lightly loaded particulate samples. The results on pp. 12-14 of this report suggest that this absorptivity is due to the "graphitic" soot content of the aerosol particles. Since "graphitic" soot seems to offer a very attractive tracer for primary emissions, we would like to obtain more direct evidence that this is indeed the case. Our approach was to measure the Raman spectrum and absorptivity of the same sample and then to compare the integrated intensity of the "graphitic" Raman mode near 1600 cm^{-1} with the optical absorptivity. These measurements were done on acetylene soot samples, highway tunnel samples, and ambient samples collected in Berkeley. The results are shown in Figure 7. Within experimental error these data show that there is a direct correspondence between the optical absorptivity and the Raman intensity for all samples studied.

If we take the Raman intensity as a measure of the "graphitic" soot content of the aerosol particles, then these results clearly show that the optical absorptivity is also a quantitative measure of this species. The most obvious explanation for this correlation in these widely different samples is that the

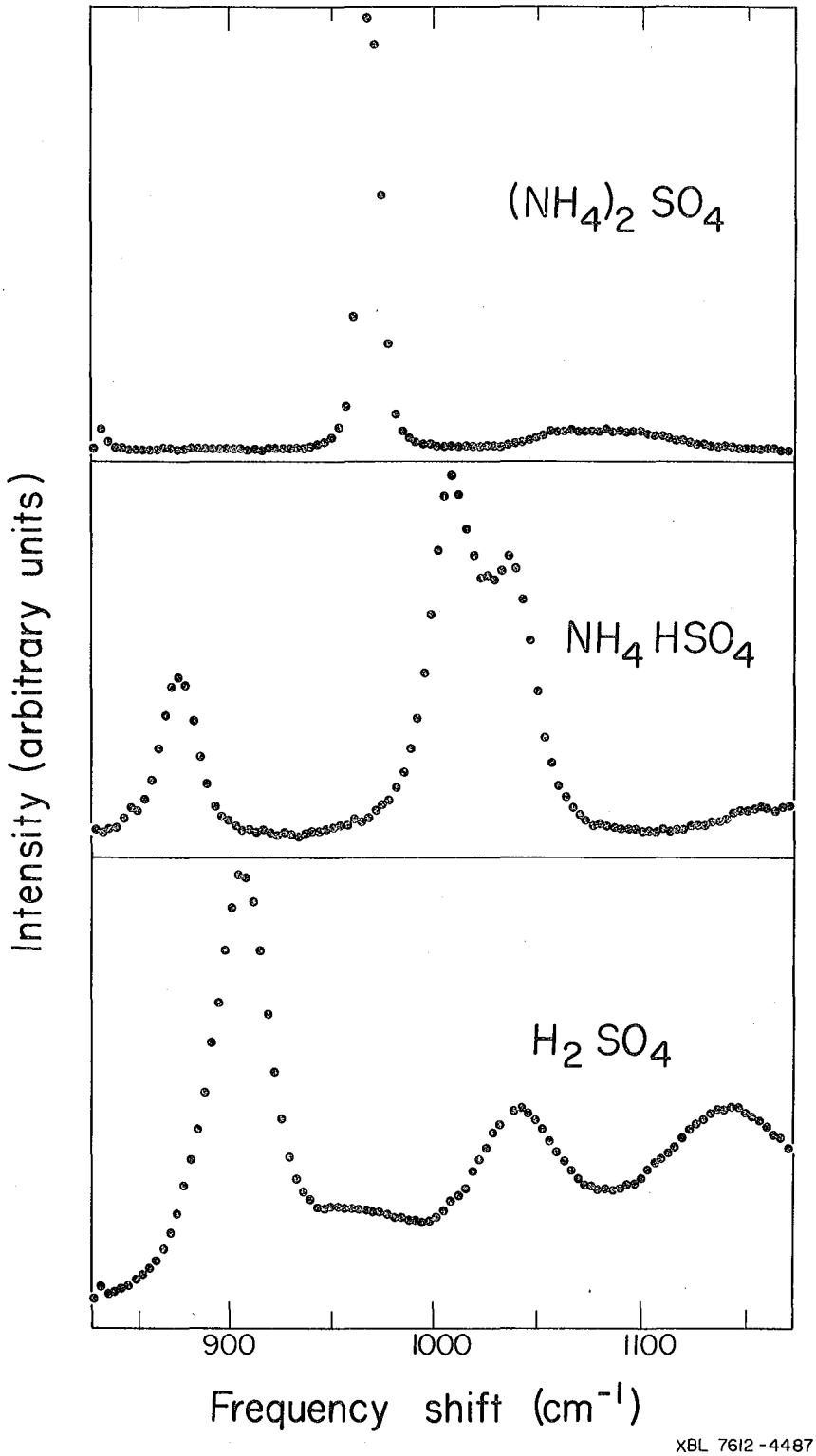

Figure 6. Raman spectra of $(NH_4)_2SO_4$, NH_4HSO_4, and H_2SO_4 in the spectral region between 850 and 1150 cm^{-1}. These spectra were obtained with a slit width of 3 Å ($\sim$ 10 cm^{-1}).

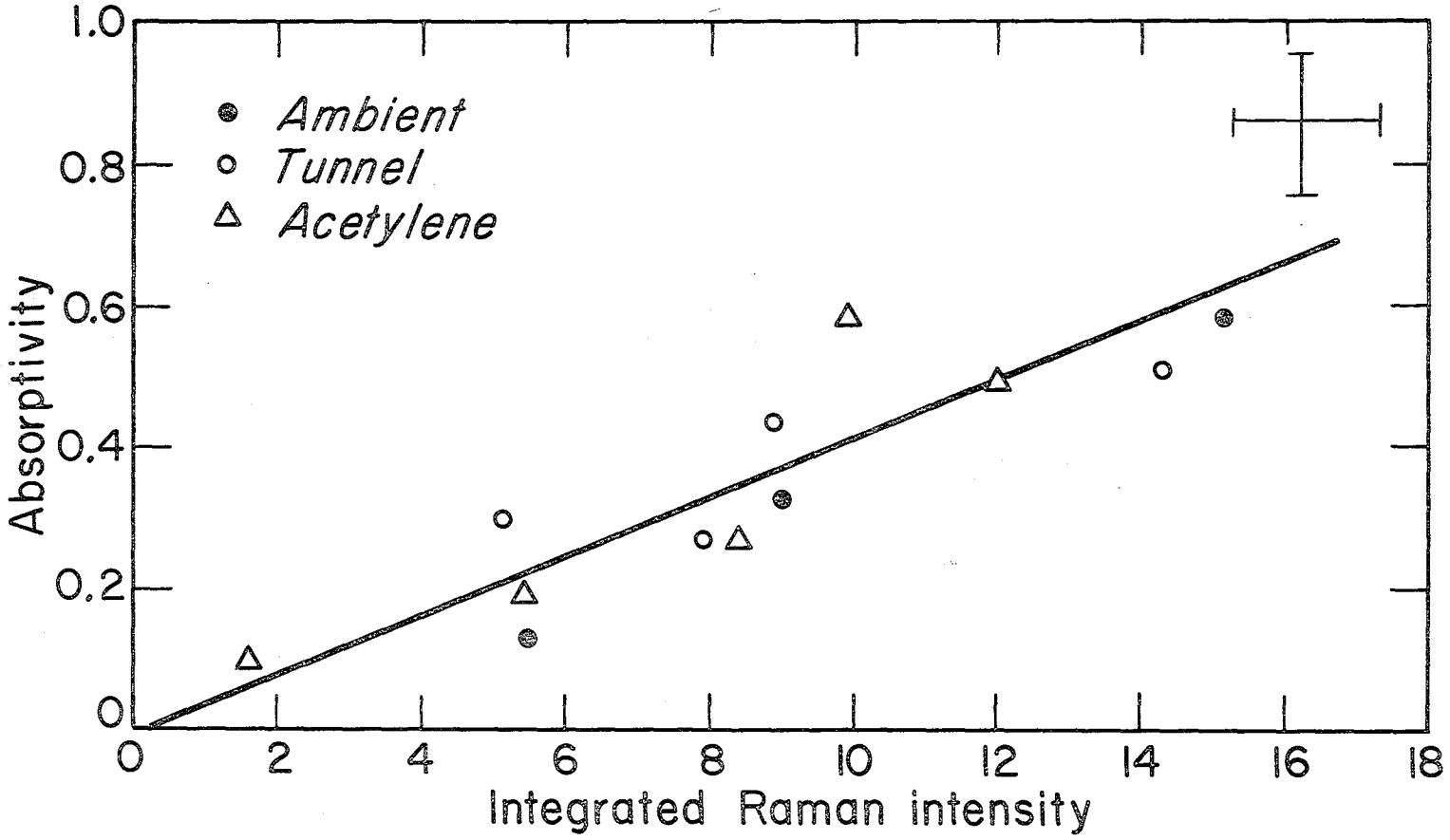

Figure 7. Plot of integrated Raman intensity of the 1600 cm^{-1} mode vs. optical absorptivity at 6328 Å for acetylene soot, tunnel, and ambient samples.

the absorptivity is due to the "graphitic" soot component of the aerosol particles. In the future other source and ambient samples will be studied to see if the correspondence is generally valid.

C. Study of the activation of graphite using Raman spectroscopy

Activated carbon is a well-known surface chemical and catalytically active material, which in many respects is similar to "graphitic" soot. It can be viewed as being made up of small crystallites of the order of 25 Å in size, which have layered graphitic structure. The chemical activity of the material is thought to be due to functional groups containing oxygen and hydrogen that are attached to the surface of these crystallites. However, the nature and the formation mechanism of these species are not well understood.

There have been several investigations of these species using the infrared technique, but these have had only limited success because of the difficulty in taking spectra on the highly absorbing carbon substrate. Our initial attempts in using the Raman scattering technique, which in many ways is complementary to the infrared technique, have been encouraging.

Our approach is to use polycrystalline graphite as a model substrate and to study its Raman spectrum as a function of activation temperature. The activation procedure involves exposure of the sample to O_2 + H_2O for a period of 1/2 hr at various temperatures. Our results in Figure 8 clearly show changes in the Raman spectrum as the activation temperature is varied. As the oxidation threshold for polycrystalline graphite is approached, the Raman mode near 1320 cm^{-1} begins to decrease in intensity, and a new sharp mode near 1620 cm^{-1} appears. This behavior continues up to about 675°C. As the temperature is raised beyond this point to 900°C, the 1350 cm^{-1} mode grows in intensity and the 1620 cm^{-1} mode disappears. If we can assume that there are no large changes in the graphite substrate at these temperatures, then these spectral changes

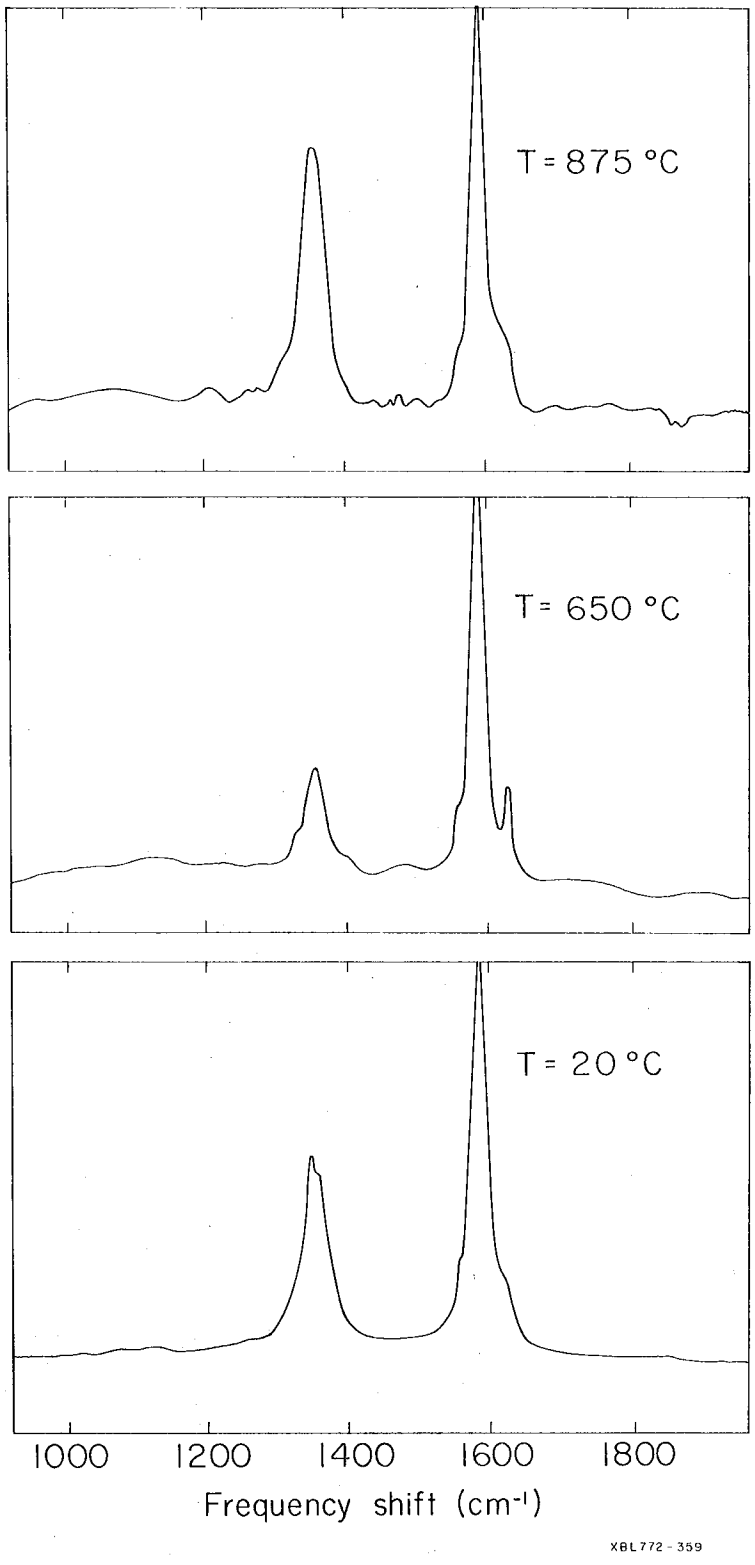

Figure 8. Raman spectra of polycrystalline graphite between 920 and 1950 cm^{-1} as a function of activation temperature.

must be due to changes in surface species. It would be expected that the intensity variation of these modes would be a function of activation temperature if we assume there is competition between two species for a fixed number of sites on the crystallite boundary. This picture is also quite consistent with the observation that the intensity of the 1350 cm^{-1} mode varies inversely with the crystallite size as determined from X-ray data. We are presently involved in trying to establish that these modes are definitely due to surface species. We believe these experiments, in combination with parallel measurements using photoelectron spectroscopy, will help clarify the surface chemical properties of activated carbon.

References

1. H. Rosen and T. Novakov, "Raman scattering and the characterization of atmospheric aerosol particles," Nature 266, 708 (1977).
2. H. Rosen and T. Novakov, "Identification of primary particulate carbon and sulfate species by Raman spectroscopy," Report LBL-5912, Lawrence Berkeley Laboratory, Berkeley, CA 94720; accepted by Atmospheric Environment.
3. J.M. Jaklevic, B.W. Loo, and F.S. Goulding, "Photon induced x-ray fluorescence analysis using energy dispersive detector and dichotomous sampler," Chapter 1 in X-ray Fluorescence Analysis of Environmental Samples, ed. T.G. Dzubay, Ann Arbor, Ann Arbor Science, 1976.
4. M.L. Wright and K.S. Krishnan, Feasibility Study of In-situ Source Monitoring of Particulate Composition by Raman or Fluorescence Scatter, Report EPA-R2-73-219, U.S. Environmental Protection Agency, 1973.

References (contd.)

5. B.W. Loo, J.M. Jaklevic, and F.S. Goulding, "Dichotomous samplers for large-scale monitoring of airborne particulate matter," in Fine Particles; Aerosol Generation, Measurement, Sampling and Analyses, ed. B.Y.H. Liu, New York, Academic, 1976, pp. 311-350.

Determination of Low-Z Elements in Atmospheric Aerosol Particles by Nuclear Reactions

M. Clemenson, S. S. Markowitz, and T. Novakov

Low-Z elements such as carbon, oxygen, nitrogen, and sulfur constitute the major fraction of urban atmospheric aerosol particles, yet there is presently no method available for a rapid and nondestructive analysis of these elements. The X-ray fluorescence technique, an important tool in the determination of heavy element concentrations, is of little use for low-Z elements due to large X-ray absorptive effects and low fluorescence yields. Neutron activation analysis is similarly limited by low reaction cross sections and the lack of suitability of induced radioactivity. Combustion analysis, a useful tool for some low-Z element determinations, is destructive and thus does not allow other analyses to be performed on the same sample. This has led us to the development of a new method for the determination of nitrogen in atmospheric aerosol particles. This method involves the use of protons of sufficient energy to induce the nuclear reaction $^{14}N(p,\alpha)^{11}C$. The radioactive decay of the ^{11}C is followed via its 0.511-MeV annihilation radiation.

A stacked-foil technique was used for irradiation of the aerosol particle samples. A typical stack included a nitrogen standard, the aerosol particle sample to be analyzed, and aluminum beam-energy degraders. The nitrogen standard used in the experiments, melamine ($C_3N_6H_6$), was prepared by vacuum sublimation onto a 0.001-inch thick aluminum foil. The melamine thickness was approximately 0.5 mg/cm^2. The circulating beam energy used in these experiments was generally 16.0 MeV. The proton energy was reduced to 9.2 MeV at the standard and 7.5 MeV at the aerosol particle sample by the use of aluminum foils. The proton energy

at each point in the stack was calculated by the use of known range-energy relationships.[1] The $^{14}N(p,\alpha)^{11}C$ excitation function was determined in separate experiments (Fig. 9). The silver membrane filter was found to be the preferred collection medium because these filters maintain their integrity in the beam while being only slightly activated and contribute very little background at the 511-keV annihilation peak.

The target stacks were irradiated for 1 min at a beam intensity of 1 μA at the LBL 88-inch cyclotron. The decay of the ^{11}C and other positron-emitting nuclides produced in the irradiation of the aerosol particle sample was followed by counting 0.511-MeV annihilation radiation by means of a high resolution Ge(Li) multichannel spectrometer. The decay of the integrated intensity of the 0.511-MeV peak for a typical San Francisco Bay Area aerosol particle sample with a loading of 1 mg/cm^2 is shown in Figure 10. The four major components in this decay curve have been identified as 10.0-min ^{13}N, 20.4-min ^{11}C, 110-min ^{18}F, and 6.5-hr ^{107}Cd. The ^{13}N is produced by the reactions $^{16}O(p,\alpha)^{13}N$ and $^{13}C(p,n)^{13}N$, the ^{18}F is produced by the reaction $^{18}O(p,n)^{18}F$, and the small amount of ^{107}Cd is produced by the $^{107}Ag(p,n)^{107}Cd$ reaction in the silver filter. The dominant component by far is the ^{11}C produced from ^{14}N in the aerosol particle sample. The components can be resolved either by graphical methods or by a more exact computer treatment using the CLSQ program.[2] The count rate at the end of bombardment, A_0, for the ^{11}C component as determined by the computer treatment is then used to calculate the amount of nitrogen in the sample.

Various experiments were carried out to determine the reliability and accuracy of the method. The first experiment involved nebulization of a known amount of $(NH_4)_2SO_4$ onto a silver filter and comparison of the nitrogen determined by activation analysis with the nitrogen content determined by weighing

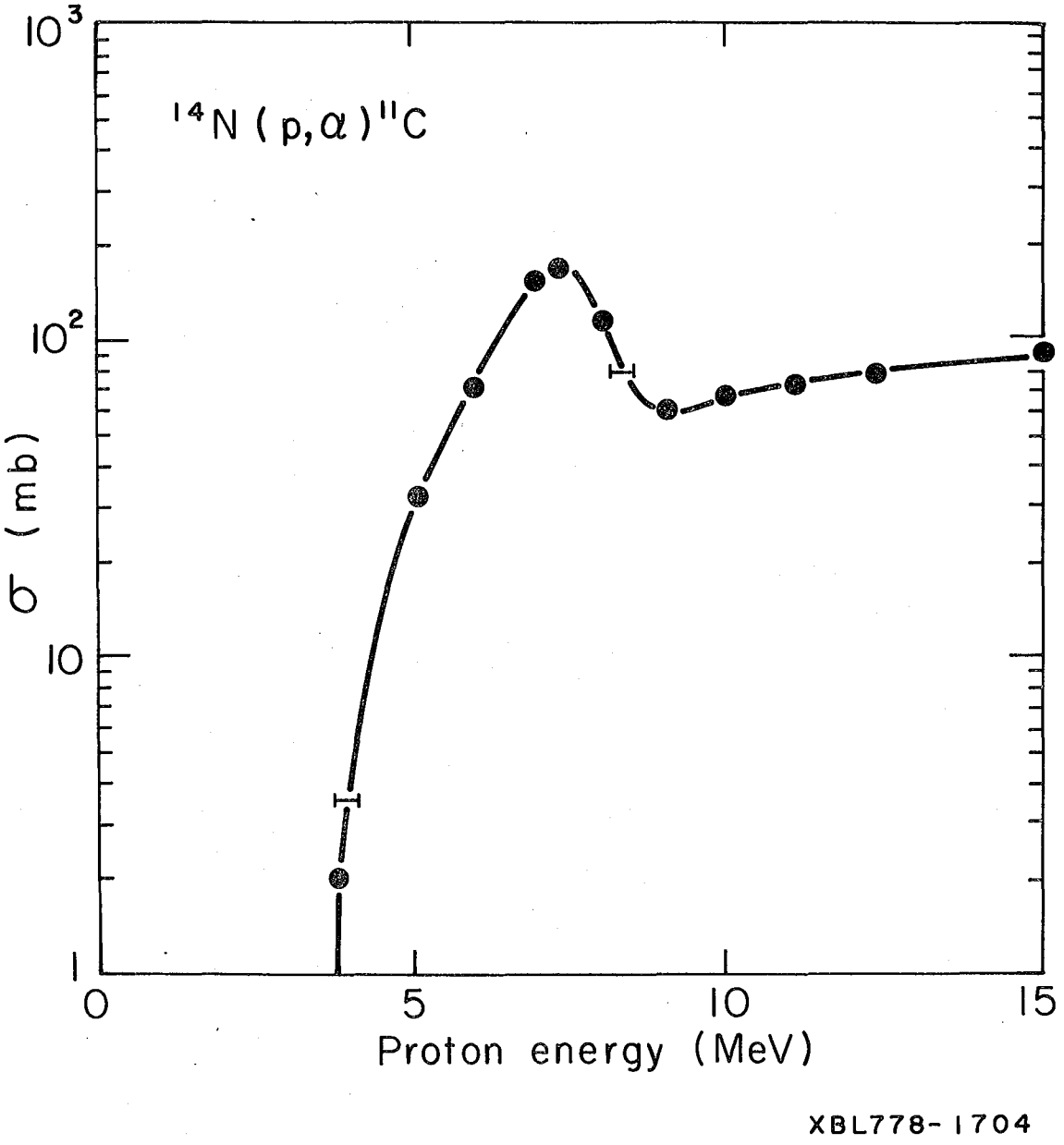

Figure 9. Excitation function for the $^{14}N(\rho,\alpha)^{11}C$ reaction.

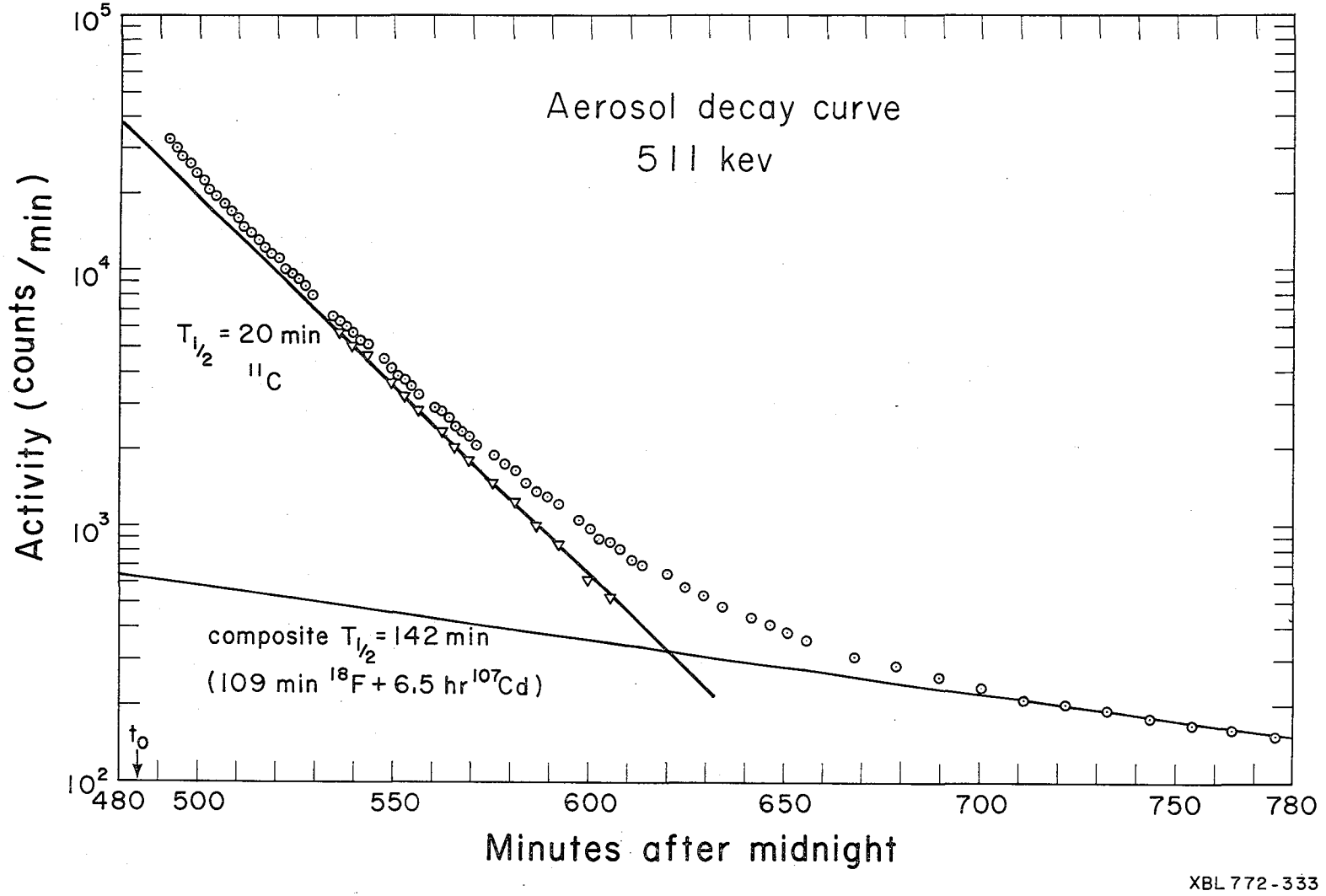

Figure 10. Decay of 511-keV peak from proton irradiation of a typical San Francisco Bay Area aerosol.

the filter (Table II). The next experiments involved the analysis of an unknown

Table II. Summary of experimental results.

Sample	Proton activation analysis	Independent check
$(NH_4)_2SO_4$	69 ± 5 μg/cm^2	70 μg N/cm^2 [known weight $(NH_4)_2SO_4$]
FN1	5.3 ± 0.3%	
FN2	5.4 ± 0.3%	4.3% N (combustion)
FN3	5.4 ± 0.7%	
Ambient samples		
11-5-5	16 ± 2 μg/cm^2	18 μg N/cm^2
11-4/5-2	59 ± 2 μg/cm^2	59 μg N/cm^2 (Combustion
11-5-8	36 ± 5 μg/cm^2	37 μg N/cm^2 of parallel
11-5-11	46 ± 3 μg/cm^2	54 μg N/cm^2 quartz)

nitrogen-containing compound by activation analysis and by combustion analysis. Our analysis was carried out on three separate samples from the same batch to check reproducibility. The results of these experiments are also shown in Table II.

Additional experiments involved the analysis of four aerosol particle samples collected at LBL during an air pollution episode. Parallel quartz filters were sent out for combustion analysis.[3] The close agreement between our results and those determined by combustion analysis is shown in Table II. The results of the time-dependence of the nitrogen content of the atmospheric aerosol particle samples are shown in Section III, p. 95, where results for sulfur, lead, and bromine are also displayed. It is evident that the nitrogen, sulfur, lead, and bromine concentrations "track" one another. Thus our proton activation analysis for relatively low concentrations of total nitrogen in comparatively low-mass samples of atmospheric aerosol particles has been

successfully demonstrated as a practical analysis.

Experiments are presently being performed to develop a new method for sulfur analysis. The first experiments involve determination of the $^{34}S(p,n)^{34m}Cl$ excitation function using targets which have been made by vacuum sublimation of PbS onto 0.001-inch aluminum foils. The proton activation analysis method, which has worked quite well with nitrogen, will be extended in the future to the analysis of other low-Z elements in atmospheric aerosol particles.

References

1. C.F. Williamson, J.P. Boujot, and J. Picard, Tables of Range and Stopping Power of Chemical Elements for Charged Particles of Energy 0.05 to 500 MeV, Report CEA-R 3042, Centre d'Études Nucléaires de Saclay, France, 1966.
2. J.B. Cumming, Applications of Computers to Nuclear and Radiochemistry; ed. G.D. O'Kelly, National Academy of Science-National Research Council, Nuclear Science Series, NAS-NS 3107, 1963, p. 25.
3. We are grateful to C. Spicer, Battelle Memorial Institute, Columbus, Ohio, for the analysis of the quartz filters.

Studies of Carbon Particle Production from Well-defined Flames

R. Toosi, P. Pagni, and T. Novakov

Understanding soot formation phenomena and properties of soot particles produced in flames is of considerable importance from both the industrial and the environmental point of view. Knowledge of the radiation properties of particles formed in flames is important for improving thermal efficiencies of power plants and industrial furnaces. Soot particles are a major source of air pollution in themselves, and they also affect the rate of NO, CO, and hydrocarbon formation.[1] Furthermore, catalytic reaction on suspended soot particulates plays an important role in oxidation of SO_2 to sulfate.[2] Reactions between nitrogen oxides and carbonaceous solids are also of interest for control of NO_x emissions.[3] This suggests that fine particles (about 70 - 100 Å)[4] generated in nonluminous, "clean" flames can be very important in these reactions because of their large surface area.

There is not much information on the properties of these particles because of the many parameters that influence combustion processes. Most of the reports on this subject concern the initiation and characterization of the soot particles within the flame, or the soot emitted by flames as carbon black. This characterization was usually done by measuring the amount of scattered light or by probing the gases and analyzing deposits with the electron microscope.[5] These techniques do not give much information on the properties of soot particles from the "nonsooty" flames, and the question of what happens to these nuclei after they leave the flame remains unanswered.

A water-cooled porous-plate flat-flame burner was used in the study of a premixed acetylene-air flame. Figure 11 shows a schematic of the experimental

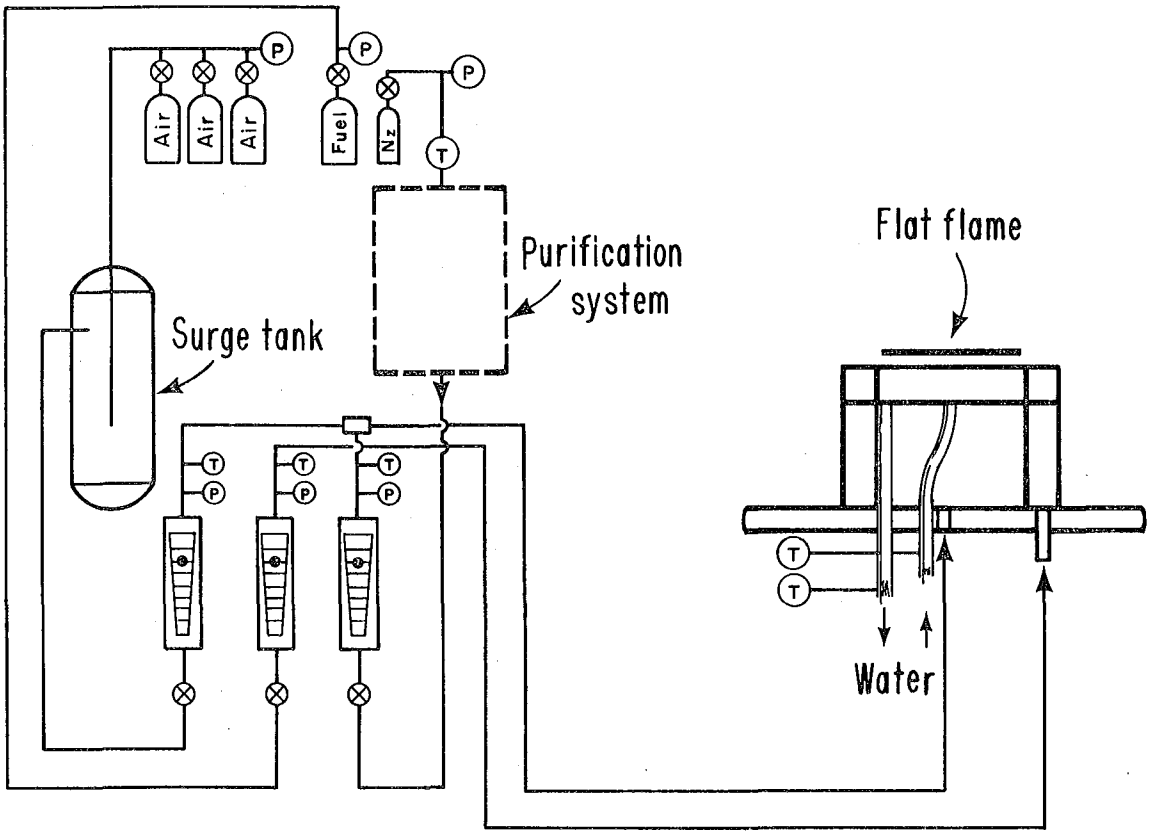

Figure 11. Schematic of the experimental setup. A mixture of dry purified air and acetylene is metered and then burned, producing a flat flame. Part of the combustion product is sampled at different locations and diluted before analysis.

setup. The burner is located in a stainless steel combustion chamber which prevents entrainment of combustion products with dirty laboratory air. A sheath of nitrogen gas around the burner minimizes the mixing of fresh gases with old combustion products. Part of the burned gases is probed and then diluted with clean air used for different gas and solid phase analyses. Flames obtained in this burner are stable and well characterized for a large range of combustion parameters. Acetylene was used in this study because its flammability limits are wide (2.5 - 80% acetylene in an acetylene-air mixture)[6] and the flames are very stable. The acetylene was purified and metered before mixing with filtered dry compressed air. Perfectly flat flames were obtained for a range of equivalence ratio (ϕ) of 0.7 to 1.4. Flames richer than this tend to become polyhedral. At ϕ = 1.8, the flame becomes luminous and carbon particles are detectable to the eye. Flame temperature was measured using a 0.0076-cm diameter Pt-Pt, 10% Rh thermocouple. The maximum flame temperature was 1794°K for a stoichiometric mixture (ϕ = 1.0) at a flame velocity of 21 cm/sec. Flame temperature remained uniform to ± 1% of maximum temperature except at the very edges where mixing with the cool ambient air occurs. We measured heat losses to the burner for different flow rates and equivalence ratios and calculated adiabatic flame temperature and flame velocity by extrapolating data to zero heat loss. Maximum adiabatic flame velocity of 135 cm/sec at ϕ = 1.0 was found. Assuming flow is controlled by a single overall reaction obeying the simple Arrhenius rate expression, we obtained an activation energy of E = 48 ± 10 kcal/°K (Fig. 12). Experiments were repeated for total flow ratios of 10-35 liters/min. Increasing the total flow rate increases the distance of the flame relative to the burner surface. Heat removal becomes less efficient and the flame becomes more adiabatic.

Elementary studies of number and size distribution were made using an

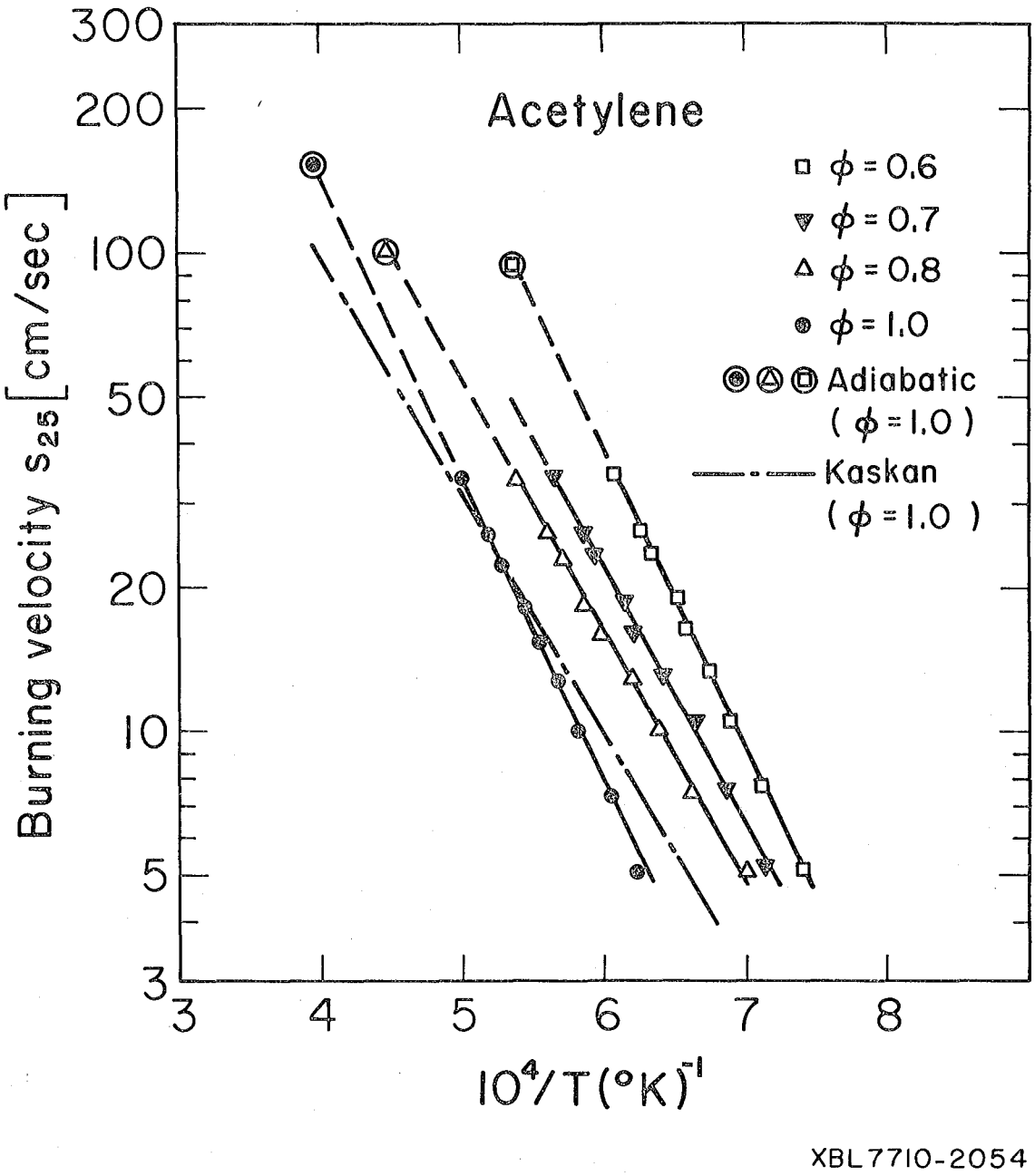

Figure 12. Flame velocity of the flat acetylene flame S_{25} (normalized to 25°C unburned gas) as a function of inverse temperature. An Arrhenius-type equation $S_{25}^2 = ke^{-E/RT}$ when E = 58 ± 10 kcal/°K fits the data. Adiabatic flame velocities are obtained by extrapolating the data to equilibrium adiabatic flame temperature.

Electrical Aerosol for Mobility Analyzer (EASA) and a Condensation Nuclei Counter (CNC). Based on these studies, we detected particles of 50 - 200 Å and concentrations of 10^8 - 10^{12} particles/cc. We are also investigating the effects of humidity and other combustion parameters on the particle size distribution using X-ray photoelectron spectrometry to study the surface chemistry of carbon deposits.

References

1. H.C. Perkins, Air Pollution, New York, McGraw-Hill, 1974.
2. T. Novakov, S.-G. Chang, and A.B. Harker, "Sulfates as pollution particulates," Science 186, 259 (1974).
3. H.W. Edwards, "Reduction of nitric oxides by graphite," abs. pap., American Chemical Society, 1973, p. 60.
4. K.T. Whitby, R.B. Husar, and B.Y.H. Liu, "The aerosol size distribution of Los Angeles smog," J. Colloid and Interface Sci. 39, 177 (1972).
5. R. Toossi and P.J. Pagni, A Review of Combustion Generated Carbon Particles, Report UCB-FRG-WP-75-8, Mechanical Engineering Dept., Unversity of California, Berkeley, CA 94720, 1975.
6. A. Williams and D.B. Smith, "The combustion and oxidation of acetylene," J. Chem. Rev. 70, 267 (1970).

SECTION II

ATMOSPHERIC CHEMISTRY

Catalytic Oxidation of SO_2 on Carbon in Aqueous Suspension

S.-G. Chang, R. Brodzinsky, S. S. Markowitz, and T. Novakov

Atmospheric sulfate, which is a major constituent in ambient aerosol particles, is presumably formed by the oxidation of SO_2. The dominant mechanisms responsible for this transformation have not presently been established. One set of mechanisms which is thought to be important involves the dissolution of SO_2 in water droplets. When liquid water is present, as in clouds, fog, and plumes, the atmospheric SO_2 can dissolve in the droplets[1] and be oxidized by dissolved O_2 to sulfate. This reaction is slow, except in the presence of a catalyst, such as the metal ions Mn^{2+}, Fe^{3+}, and Cu^{+2},[2-7] or ammonia.[2,8,9] Concentrations of these catalysts in the atmosphere, however, are small.

A major primary pollutant is the soot produced from the incomplete combustion of fossil fuel. These soot particles not only contribute to the ambient particulate loading, but, as we have previously suggested,[10] are an efficient catalyst for the oxidation of SO_2 to sulfate in humid air. This behavior is similar to that of activated carbon, whose catalytic properties are well known. In our previous experiments, it was shown that the soot-catalyzed oxidation of SO_2 is more efficient when prehumidified, rather than dry, air is used to dilute the SO_2. However, the specific role of water was not made clear in these experiments. The effect of liquid water on the soot-catalyzed reaction is important because in plumes liquid water may condense on the soot particles, and the soot may also encounter clouds and fog during their transport through the atmosphere.

The purpose of the research described here is to investigate the oxidation of SO_2 in an aqueous suspension of soot particles. The reaction was studied in systems containing various concentrations of sulfurous acid and suspended carbonaceous particles. Soots that were produced by the combustion of acetylene and natural gas, as well as that produced from a diesel engine, were used in this study and were found to be extremely good catalysts. The results obtained with these combustion-generated soots are essentially reproduced by suspensions of similar concentrations of activated carbon (Nuchar).[11] Since it is difficult to reproducibly prepare soot suspensions, suspensions of Nuchar were used as a model system. The majority of results reported are therefore obtained using the model system. The range of carbon concentrations used in the suspensions were from 0.004% to 0.63% by weight, which corresponds to the concentrations of carbon expected in water droplets in the open atmosphere and in plumes.

In this paper we show that the oxidation of sulfurous acid (H_2SO_3) to sulfuric acid is catalyzed by soot. This reaction appears to occur in two steps, an initial rapid consumption of H_2SO_3 followed by a slower process. The rate of the first process is too fast to follow. The rate of the second process is first order with respect to the carbon concentration and is independent of the H_2SO_3 concentration. The overall reaction is also shown to be independent of pH.

A 6% H_2SO_3 solution (Baker & Adamson reagent grade) was mixed with distilled H_2O to a desired initial concentration in a 200-ml volume. This solution was contained in a 250-ml Erlenmeyer flask and was stirred with a Teflon-coated magnetic stirrer. Varying weights of Nuchar C-190 were added to this solution, and the concentration of H_2SO_3 (or $SO_2 \cdot H_2O$) was monitored by classic iodometric titrations during the course of the reaction. At convenient time intervals, 4- or 10-ml aliquots were removed and filtered in a sintered glass funnel. A known excess of I_2 was added and backtitrated with

1.00×10^{-3} M $Na_2S_2O_3$ with a starch indicator. All runs were done at room temperature ($\sim$ 20°C) and were open to the air. The pH of the reaction mixture was measured using a Beckman 4500 digital pH meter with a probe combination electrode (Beckman #39013). Each experiment lasted approximately 30 min to 1 hr.

Figures 13 and 14 illustrate some of the specific features of the oxidation of H_2SO_3 by dissolved oxygen in aqueous suspensions of Nuchar. In Figure 13 the concentration of H_2SO_3 is plotted against reaction time for different concentrations of Nuchar and a constant initial H_2SO_3 concentration. Figure 14 shows similar plots for a constant (0.16%) Nuchar concentration and varying initial H_2SO_3 concentrations. It is apparent from these data that this is a two-step process. The rate of the initial disappearance of H_2SO_3 is so fast that it could not be followed by the analytical technique employed in this investigation. The second process is manifested by a much slower linear reduction in H_2SO_3 concentration.

The amount of H_2SO_3 consumed, at a constant temperature, by the rapid first-step process is linearly proportional to the concentration of Nuchar for the two initial H_2SO_3 concentrations (6.56×10^{-4} and 8.85×10^{-4} M) studied (Fig. 15). The relationship between the magnitude of the initial H_2SO_3 drop and the initial H_2SO_3 concentration (Fig. 16) appears to resemble the adsorption isotherm of type I after the classification given by Brunnauer, Emmett, and Teller.[12]

Referring now to the slower second process, we note that the data shown in Figure 17 indicate a linear relationship between the reaction half-life and the reciprocal of the Nuchar concentration. This behavior suggests a first order reaction with respect to the carbon catalyst concentration under the conditions of this experiment (H_2SO_3 concentration = 8.84×10^{-4} M; 20°C). The reaction rate of the slow process appears to be zeroth order with respect to the H_2SO_3

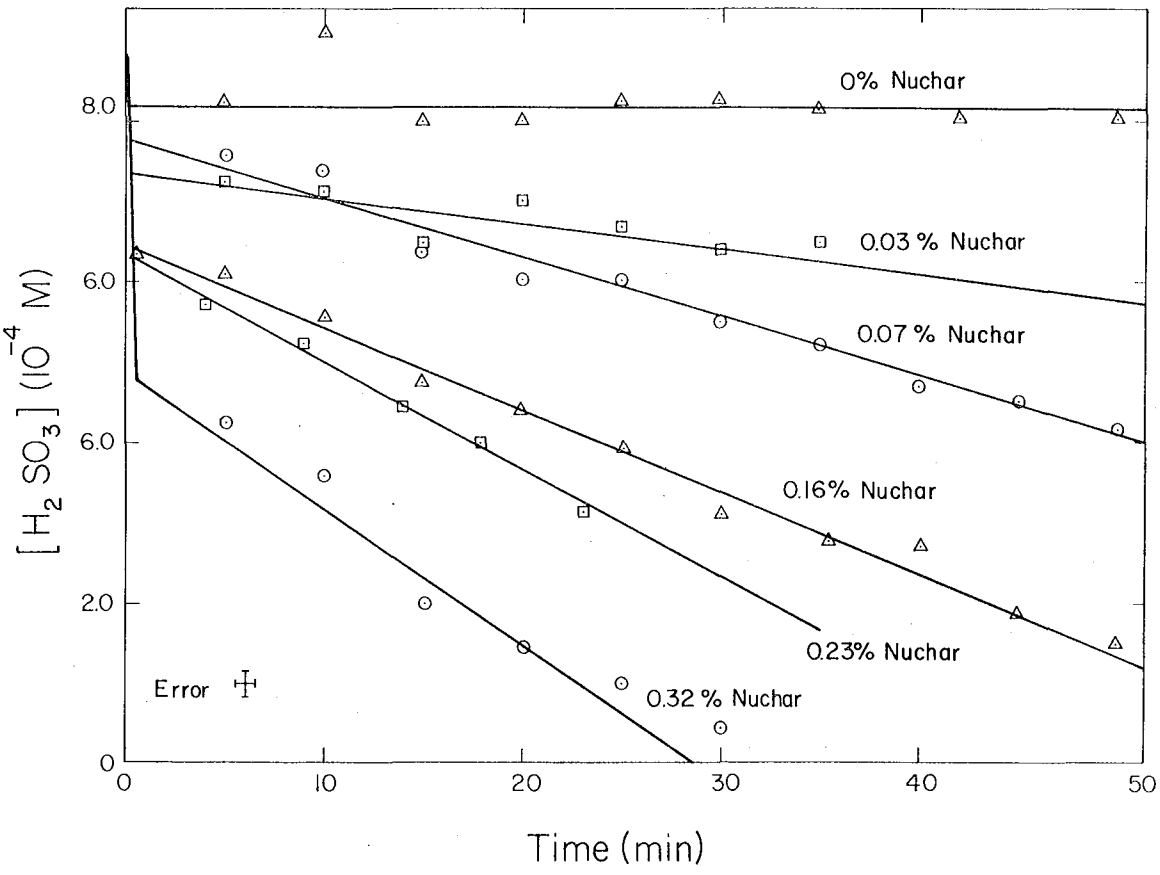

Figure 13. H_2SO_3 concentration versus time for various Nuchar concentrations. The initial H_2SO_3 concentration was 8.85×10^{-4} M.

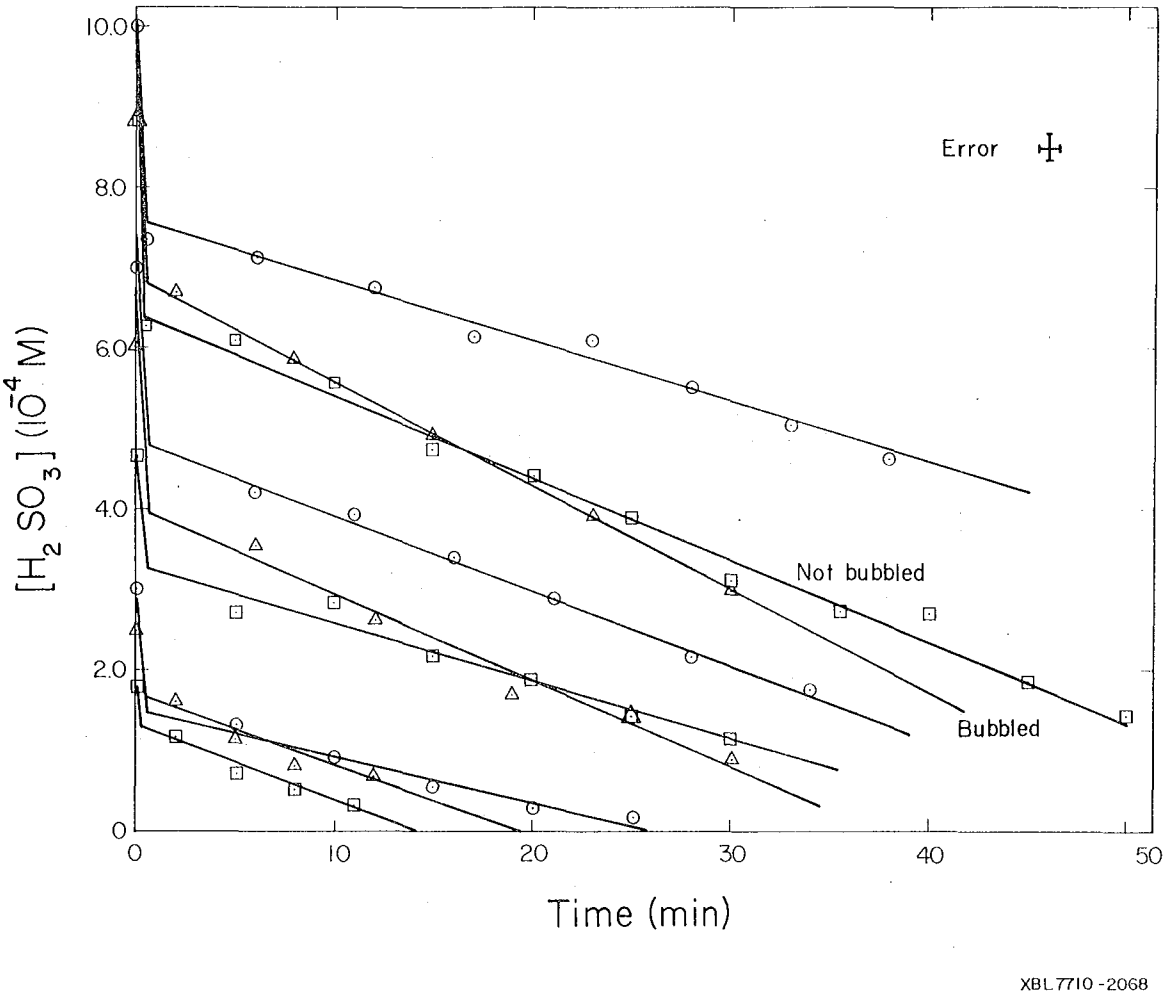

Figure 14. H_2SO_3 concentration vs. time for various initial concentrations of H_2SO_3 + a fixed Nuchar concentration of 0.16% by weight.

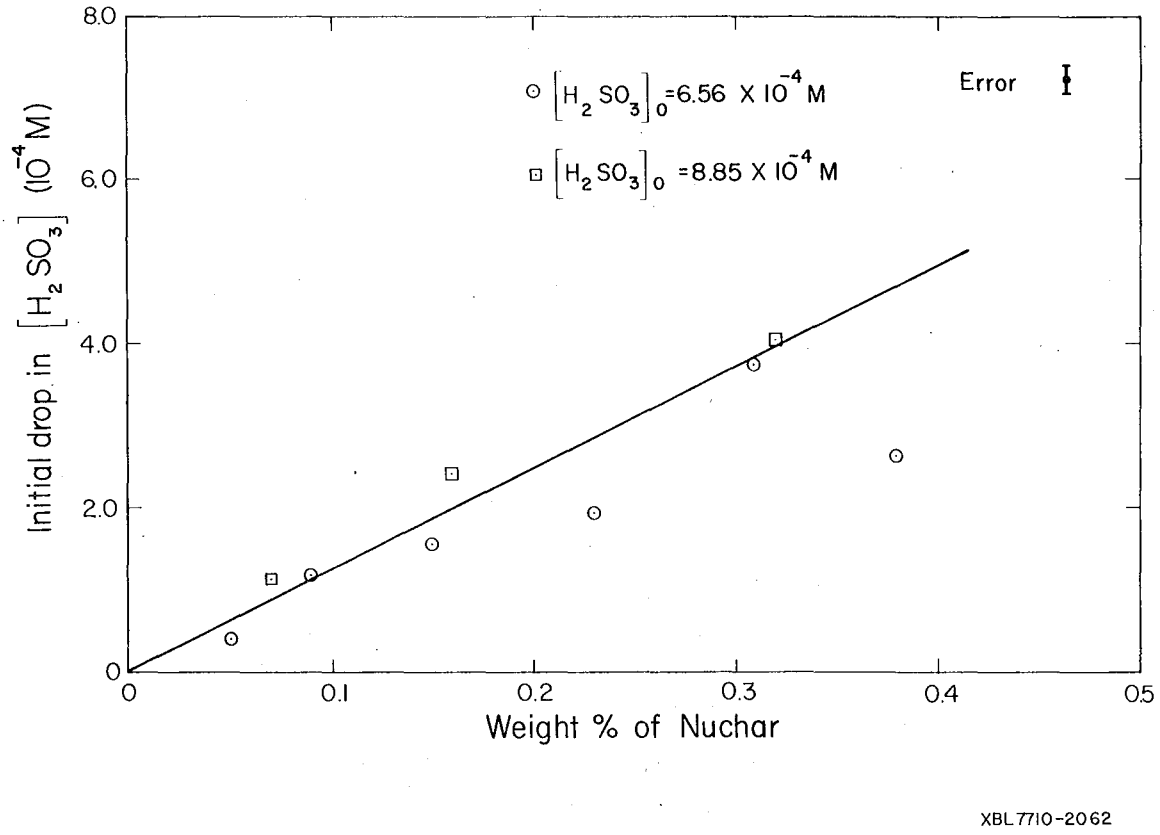

Figure 15. Drop in the H_2SO_3 concentration by rapid consumption process for various concentrations of Nuchar.

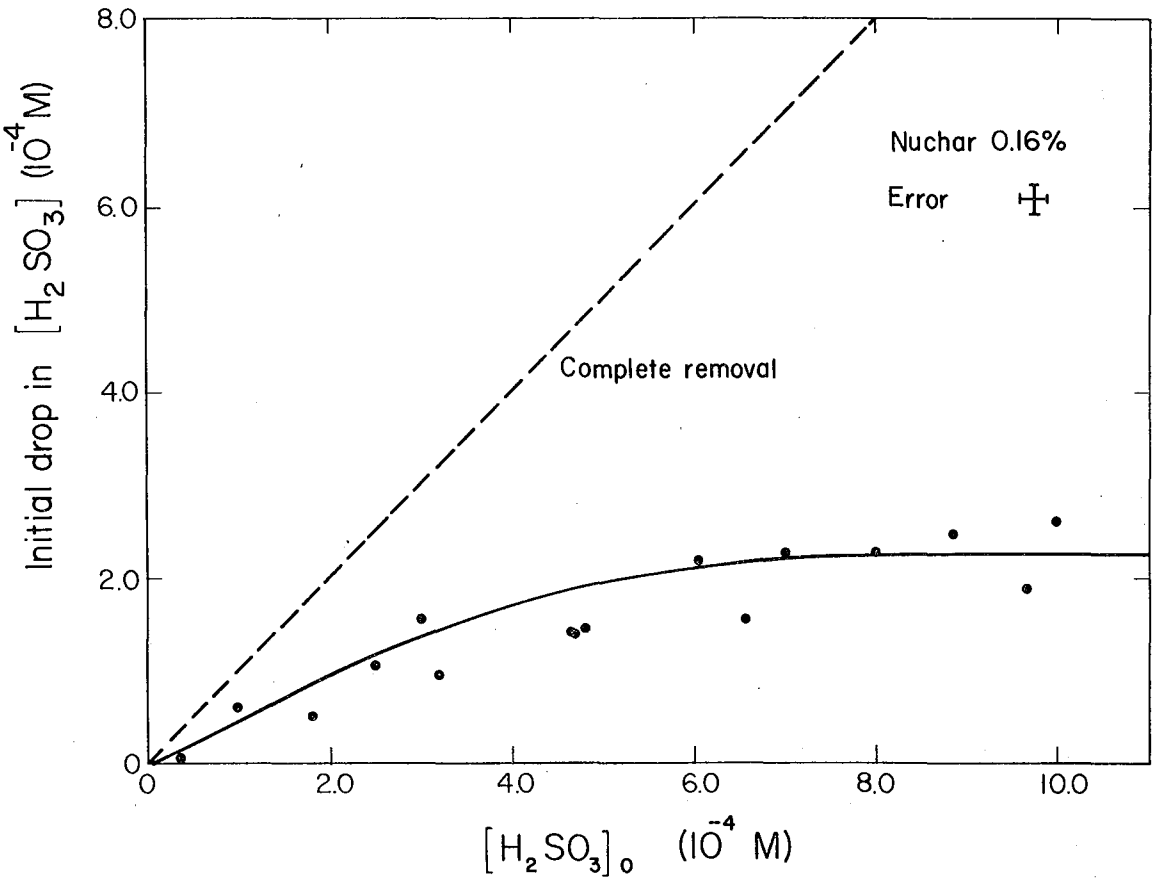

XBL7710-2063

Figure 16. Drop in the H_2SO_3 concentration by rapid consumption process for various initial concentrations of H_2SO_3 with Nuchar = 0.16% by weight.

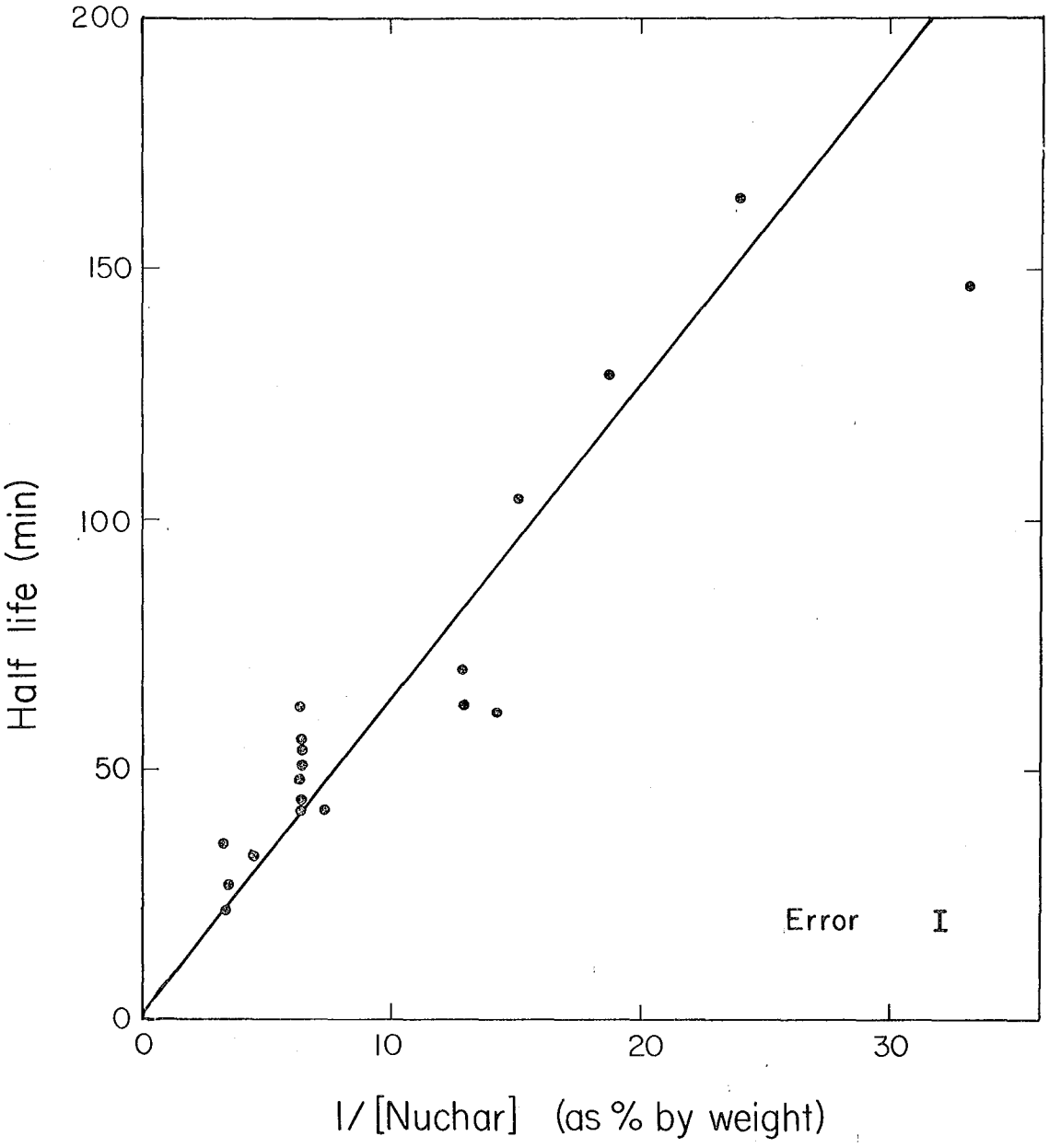

XBL7710-2067

Figure 17. Reaction half-life vs. reciprocal of Nuchar concentration. Plot shows first order dependence with respect to Nuchar.

concentration because of the linear relationship between the H_2SO_3 concentration and the reaction time, as shown in Figures 13 and 14. Also a straight line passing through the origin was obtained by plotting the reaction half-life against the initial H_2SO_3 concentration (Fig. 18).

In order to assess the dependence of the SO_2 oxidation reaction on pH, we have attempted to determine the reaction rates in buffered solutions. Sodium citrate-HCl and potassium phthalate-HCl buffer solutions were used for the pH range between 4.4 and 6.0, and between 3.1 and 4.0, respectively. However, no conclusive results could be obtained from these experiments. The data seem to indicate that these buffer reagents adsorb on the surface of the Nuchar and therefore change its catalytic property.

Because of this difficulty, experiments were performed in which a known volume of 0.2 M H_2SO_4 was mixed into the sulfurous acid solution before adding Nuchar. The initial concentration of H_2SO_4 was varied while the Nuchar and sulfurous acid concentrations were kept constant. The results, represented in Figure 19, demonstrate that the reaction rate essentially does not depend on the initial pH of the solution. Note also that with no Nuchar present, the sulfurous acid concentration was not affected during the time interval of this experiment by the addition of H_2SO_4. The pH in these experiments ranged from 1.45 to 2.9. The carbon particle-catalyzed reaction therefore differs from the metal ion-catalyzed reaction in not being dependent on the pH of the aqueous solution (in the pH range between 1.45 and 2.9). We have thus concluded that the reaction itself is independent of pH.

In a separate series of experiments, we have examined the role of dissolved oxygen as well as possible impurities associated with the activated carbon on the behavior of the reaction. It is conceivable that the initial rapid consumption of H_2SO_3 could be due to the depletion in the amount of dissolved oxygen in the solution. The second slower rate of consumption would then be

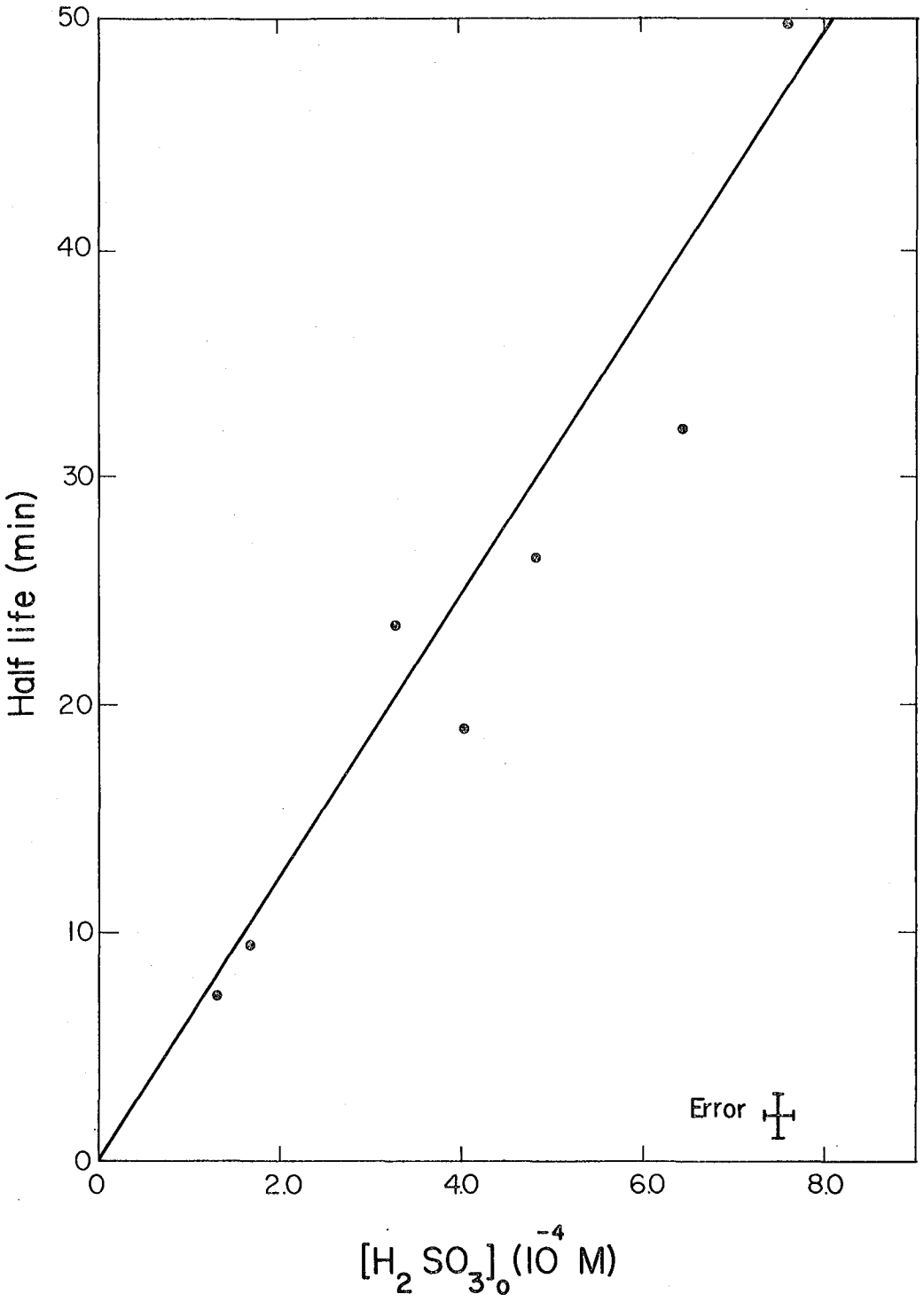

Figure 18. Reaction half-life versus initial H_2SO_3 concentration. Plot shows zeroth order dependence with respect to H_2SO_3.

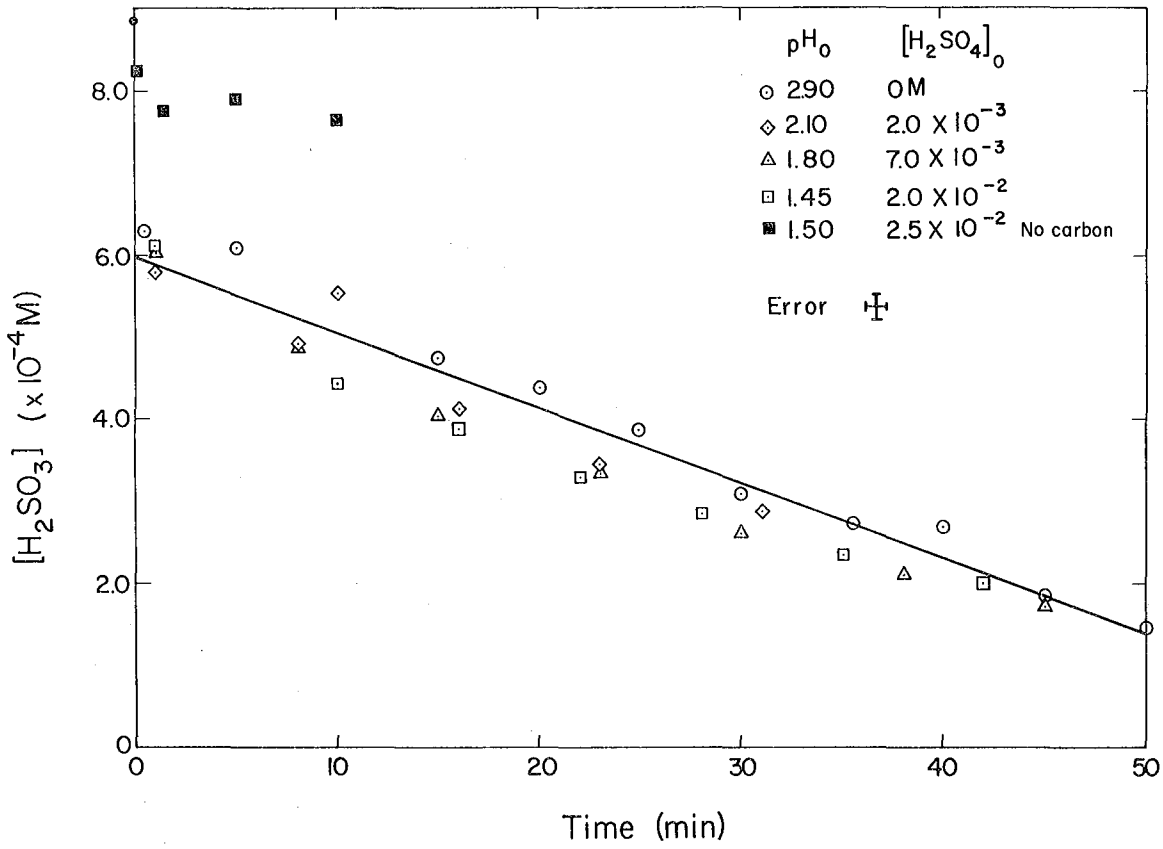

Figure 19. H_2SO_3 concentration vs. time at a Nuchar concentration of 0.16% by weight at various pH's and H_2SO_4 concentrations. The initial H_2SO_3 concentration was 8.85×10^{-4} M.

limited by the rate of diffusion of the oxygen into the solution. This hypothesis was ruled out by noting that the behavior of the reaction was not affected by bubbling air into the solution (Fig. 14). We have also demonstrated that the consumption of H_2SO_3 is not due to reactions involving impurities in Nuchar. This was done by reacting three samples of Nuchar with the H_2SO_3 and allowing the reaction to go to completion (total oxidation of H_2SO_3). The samples were decanted. One was placed in a new solution of sulfurous acid while still wet, another was air dried and placed into solution, and the third was oven dried. All three again exhibited the same initial rapid drop of H_2SO_3 and the same overall catalytic behavior. In another experiment, the possibility that a small Fe_2O_3 impurity in the Nuchar was responsible for the oxidation was tested. For an Fe_2O_3 concentration comparable to the Nuchar concentration used in the previous experiments, no significant oxidation was observed over a 30-minute time interval.

We have determined the concentration of sulfate using the barium chloranilate method at the end of a reaction. It was found that there was a mass balance between the sulfurous acid consumed and the sulfuric acid produced. Therefore oxidation of sulfurous acid definitely occurs in the solution.

The similarity between combustion-produced soot particles and Nuchar in the oxidation of SO_2 in an aqueous suspension was also determined. Soot from an acetylene and a natural gas flame was collected by impinging the combustion effluent into distilled water. The rate of disappearance of sulfurous acid in this aqueous soot suspension is depicted in Figure 20. Similar results were also obtained for diesel exhaust soot. These results show that the reaction rate is obviously very fast even for the very small concentrations of the combustion-generated soots used in these experiments.

Neytzell de Wilde and Taverner[13] have studied the rate of oxidation of sulfurous acid catalyzed by Mn^{+2} and Fe^{+3} in aqueous solution under conditions

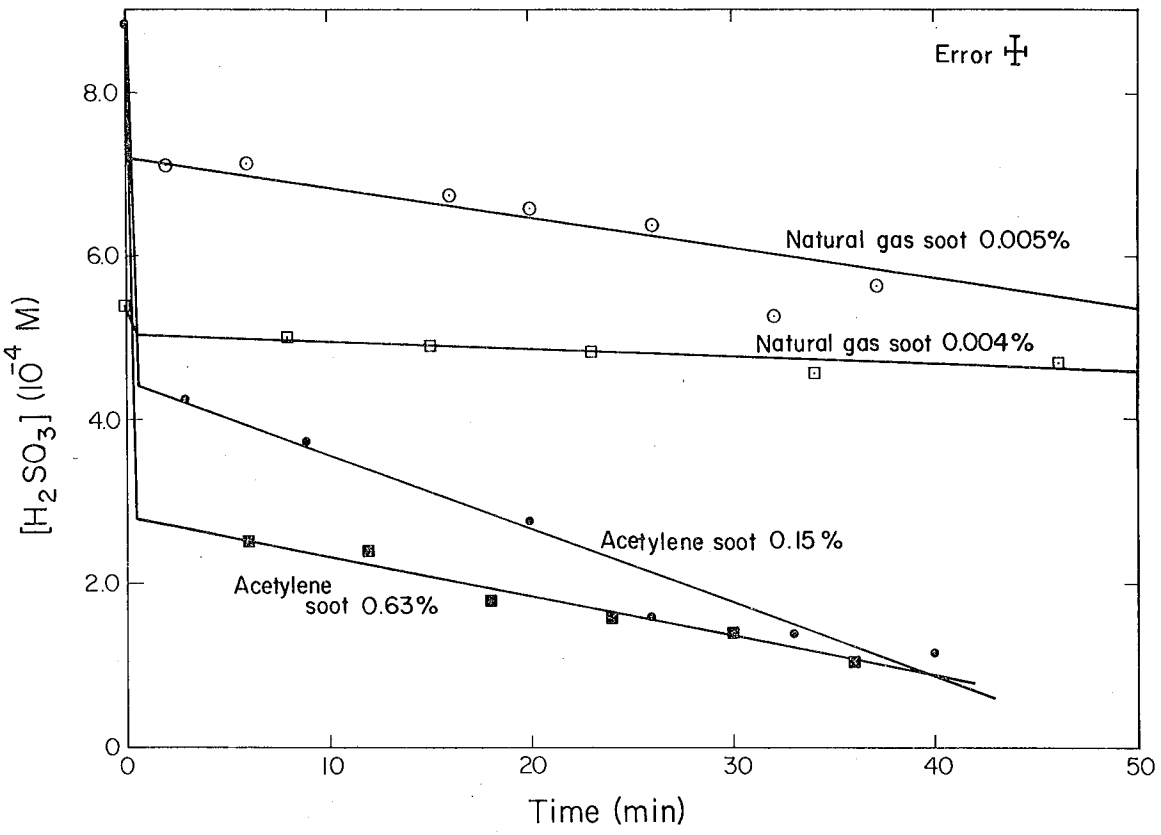

XBL7710-2065

Figure 20. H_2SO_3 concentration vs. time for acetylene and natural gas soot suspensions.

similar to those used in this study. The rate is about two orders of magnitude faster for Mn^{+2} or Fe^{+3} than for Nuchar for the same mass concentration of catalysts. However, since the concentration of soot in the atmosphere easily exceeds the concentrations of these transition metals by several orders of magnitude, the carbon mechanism could be more important than those involving transition metals.

References

1. H.F. Johnstone and P.W. Leppla, "The solubility of sulfur dioxide at low partial pressures," J. Amer. Chem. Soc. 56, 2233 (1934).
2. C. Junge and T.G. Ryan, "Study of the SO_2 oxidation in solution and its role in atmospheric chemistry," Quart. J. Royal Meteor. Soc. 84, 46 (1958).
3. H.F. Johnstone and D.R. Coughanowr, "Absorption of sulfur dioxide from air," Ind. Eng. Chem. 50, 972 (1958).
4. M.J. Matteson, W. Stöber, and H. Luther, "Kinetics of the oxidation of sulfur dioxide by aerosols of manganese sulfate," Ind. Eng. Chem. 8, 677 (1969).
5. J. Freiberg, "The mechanism of iron catalyzed oxidation of SO_2 in oxygenated solutions," Atmos. Environ. 9, 661 (1975).
6. J. Freiberg, "Effects of relative humidity and temperature on iron-catalyzed oxidation of SO_2 in atmospheric aerosols," Environ. Sci. Tech. 8, 731 (1974).
7. J. Freiberg, "The iron catalyzed oxidation of SO_2 to acid sulfate mist in dispersing plumes," Atmos. Environ. 10, 121 (1976).
8. W.D. Scott and P.V. Hobbs, "The formation of sulfate in water droplets," J. Atmos. Sci. 24, 54 (1967).

References (contd.)

9. J.M. Miller and R.G. de Pena, "Contribution of scavenged sulfur dioxide to the sulfate content of rain water," J. Geophys. Research 77, 5905 (1972).

10. T. Novakov and S.G. Chang, "Catalytic oxidation of SO_2 on carbon particles," AIChE Symposium Series 72, 255 (1975).

11. For previous works related to this subject, see M. Hartman and R.W. Coughlin, "Oxidation of SO_2 in a trickle-bed reactor packed with carbon," Chem. Eng. Sci. 27, 867 (1972) and references therein.

12. S. Brunauer, P.H. Emmett, and E. Teller, "Adsorption of gases in multi-molecular layers," J. Amer. Chem. Soc. 60, 309 (1938).

13. F.G. Neytzell de Wilde and L. Taverner, "Experiments relating to the possible production of an oxidizing acid leach liquor by autooxidation for the extraction of uranium," Proc. 2nd UN International Conf. on the Peaceful Uses of Atomic Energy 3, 303 (1958).

Identification of Surface Nitrogen Complexes on Graphite Particle Surfaces

S.-G. Chang and T. Novakov

Soot particles resulting from incomplete combustion of fossil fuel are a major constituent of airborne particulate matter (see Section I, p. 18). These carbon particles often contain surface nitrogen species,[1,2] which appear to be one of the principal chemical forms of nitrogen in airborne particulate samples. In order to have a better understanding of these species, we have studied the interaction of graphite particles with ammonia, using Fourier transform infrared and X-ray photoelectron spectroscopy. To help in assigning vibrational frequencies, infrared spectra of graphite particles after reaction with deuterated ammonia, air, and xenon have also been obtained.

The application of optical spectroscopy to study the structure of surface species on graphite is difficult because of graphite's high absorption coefficient.[3] Friedel et al. have successfully obtained infrared transmission spectra of graphite[4] and activated carbon[5] after extensive grinding. We have modified their grinding technique in this experiment so that graphite particles can be ground at room temperature in ammonia in the absence of air. The concentration of nitrogen with respect to carbon is determined by means of X-ray photoelectron spectroscopy. Samples were also prepared by grinding graphite in deuterated ammonia, air, and xenon. After grinding, the carbon particles were thoroughly mixed with KBr powder, pressed into pellets, and used for Fourier-transform infrared analysis.

Grinding of graphite reduces particle sizes and creates fresh surfaces. Surface carbon atoms of graphite particles show a strong chemical reactivity

because of unsaturation in valency. This is reflected in the appearance of structures in infrared and XPS spectra. Figure 21 shows the infrared spectrum between 500 and 4000 cm^{-1} after extensive grinding of graphite for about 100 hr. Graphite particles ground in Xe, air, NH_3, and ND_3 are respectively shown in Figures 21a, 21b, 21c, and 21e. Figures 21d and 21f have 2X expansions along the ordinate of 21c and 21e respectively, and 21g is the spectrum of the sample shown in 21e after heat treatment in vacuum at 1000°C.

The infrared results suggest the occurrence of dissociative chemisorption of NH_3 on graphite particle surfaces. In Figures 21c and 21d, there is a broad absorption band between 3000 and 3600 cm^{-1} which could be ascribed to N-H stretching. The assignment among primary amines, secondary amines, and/or imines is impossible, however. These N-H stretching vibrations should shift to near 2500 cm^{-1} in the case of deuteration, as observed in Figures 21e and 21f.

The C-N stretching mode vibrates at approximately 1200 cm^{-1} and appears in both graphite-NH_3 and graphite-ND_3 samples. We therefore tentatively assign this band to the C-N stretching arising from tertiary amines. A weak absorption band at 1340 cm^{-1} could be due to stretching of the phenyl carbon-nitrogen bond in the aromatic amines with the nitrogen directly on the ring.

Surface nitrogen groups indicating the dissociation of more than one bond in a molecule of ammonia are also detected. An absorption band between 1600 and 1700 cm^{-1} could be ascribed to imines (C=N), a weak band at 2300 cm^{-1} to nitrile (C≡N), and one at 2180 cm^{-1} to isocyanide ($-N^{+}\equiv C^{-}$).

Evidence of the dissociative chemisorption of ammonia on graphite particle surfaces is also supported by the appearance of the C-D stretching band at 2050 cm^{-1}. The assignment of the C-H stretching is ambiguous because the C-H stretching is near 2900 cm^{-1} where a vibrational band appears on both graphite-NH_3 and graphite-ND_3 samples. This band could be the overtone and/or combination

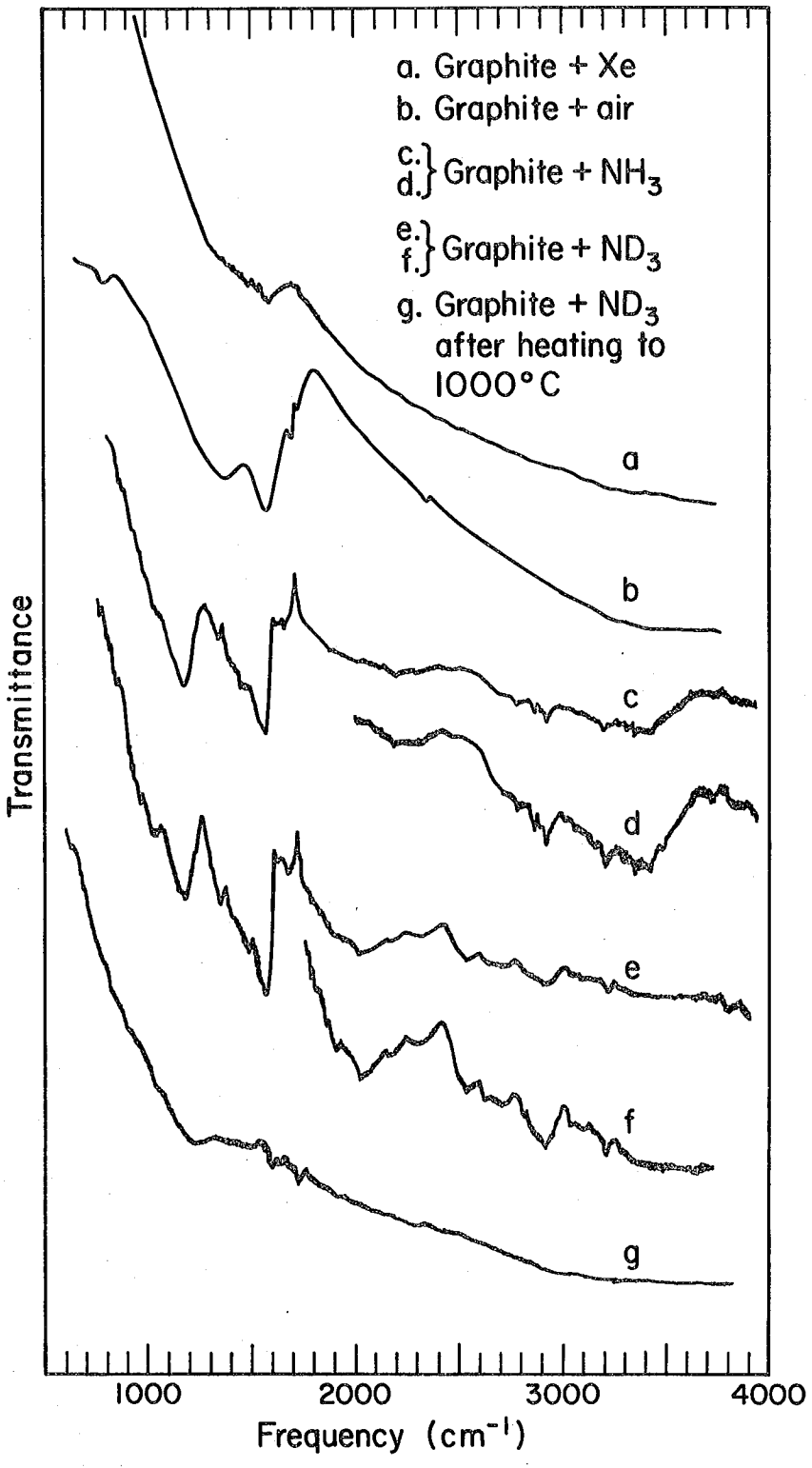

Figure 21. Infrared spectrum between 500 and 4000 cm^{-1} of graphite particles ground with various gases.

bands resulting from the strong absorption band between 1300 and 1600 cm^{-1}. There is also a band, possibly of the same nature, at 2700 cm^{-1} in both samples. The assignment of a strong absorption band at 1580 cm^{-1}, together with a shoulder at 1450 cm^{-1} in both samples, is under way. Graphite ground in Xe reveals a weak absorption band at 1580 cm^{-1}; six absorption bands are observed for graphite ground in air (Fig. 21). The dominant features are two strong absorption bands at about 1580 and 1380 cm^{-1}. Smith et al.[6] did not detect any infrared absorption band for charcoal ground in nitrogen. We therefore suggest that the weak band at 1580 cm^{-1} observed in the graphite-Xe sample is produced by exposure of the graphite powder to air during either the preparation of the KBr pellet or the grinding process because of leakage into the grinding vial. The interpretation of the band at 1580 cm^{-1}, which always occurs as a result of the interaction of oxygen with carbon particles, is uncertain. This band has been attributed to a vibration mode of a carbonyl group by Smith et al.[6] and others. Friedel et al.[7] did not observe a frequency shift due to the isotope effect, however. We observed a strong absorption band at about the same frequency when graphite interacts with ammonia as mentioned earlier, although the band shape is slightly different from that observed when graphite interacts with oxygen. On this basis, we tentatively suggest that the band at 1580 cm^{-1} could be a normal vibration mode of the aromatic ring, but it is always weak and difficult to detect unless it is made stronger by external conjugation of a double bond (such as C=O or C=N) with the aromatic ring in analogy to what has been observed in aromatic hydrocarbons.[8] Based on the same reasoning, a shoulder at 1450 cm^{-1} in the infrared spectrum of the graphite-NH_3 sample could also be due to one of the characteristic skeletal in-plane stretching modes of the aromatic structure. There is a broad band, possibly of the same nature, at 1380 cm^{-1} in the graphite-air sample. A band at 1380 cm^{-1} also appears in the Raman spectrum of amorphous

and polycrystalline graphitic carbon but does not appear in single crystals of graphite. The origin of this band has been discussed by Tuinstra and Koenig,[9] Friedel and Carlson,[4] and Nakamizo et al.[10]

In addition to the two strong absorption bands at 1580 and 1380 cm^{-1} in the infrared spectrum of the graphite specimen ground in air, four weak bands at 800, 1680, 1720, and 2320 cm^{-1} are also observed (Fig. 21b). The bands at 800 and 2320 cm^{-1} are practically the same vibrational modes as those found by Friedel and Carlson.[4] However, we have assigned the band at 2320 cm^{-1} to the C≡C vibrational band rather than the combination band resulting from the 800 and 1380 cm^{-1} bands as suggested by Friedel and Carlson. The sum of 800 and 1380 cm^{-1}, 2180 cm^{-1}, is too far to be the observed 2320 cm^{-1}. The origin of the band at 800 cm^{-1} is still uncertain. We have assigned two new bands at 1680 and 1720 cm^{-1} to ketonic carbonyl vibrations.

We have also taken X-ray photoelectron spectra of the nitrogen (1s) region and the carbon (1s) region of the graphite-NH_3 sample. The marked asymmetry together with the broad width of the XPS N(1s) peak compared with the C(1s) peak support the infrared results which indicate more than one type of surface nitrogen species. These surface nitrogen complexes are thermally stable at least up to 350°C. However, after heating to 1000°C, they are removed from the graphite surface.

References

1. T. Novakov, P.K. Mueller, A.E. Alcocer, and J.W. Otvos, "Chemical composition of photochemical smog aerosols by particle size and time of day; chemical states of sulfur and nitrogen by photoelectron spectroscopy," J. Colloid Interface Sci. 39, 225 (1972).

References (contd.)

2. S.G. Chang and T. Novakov, "Formation of pollution particulate nitrogen compounds by NO-soot and NH_3-soot gas-particle surface reactions," Atmos. Environ. 9, 495 (1975).

3. P.J. Foster and C.R. Howarth, "Optical constants of carbons and coals in the infrared," Carbon 6, 719 (1968).

4. R.A. Friedel and G.L. Carlson, "Infrared spectra of ground graphite," J. Phys. Chem. 75, 1149 (1971).

5. R.A. Friedel and L.J.E. Hofer, "Spectral characterization of activated carbon," J. Phys. Chem. 74, 2921 (1970).

6. D.M. Smith, J.J. Griffin, and E.D. Goldberg, "Spectrometric method for the quantitative determination of elemental carbon," Anal. Chem. 47, 233 (1975).

7. R.A. Friedel, R.A. Durie, and Y. Shewchyk, "The infrared spectra of oxygen-18 labelled chars," Carbon 5, 559 (1967).

8. L.J. Bellamy, "The infra-red spectra of complex molecules," New York, John Wiley and Sons, 1966.

9. F. Tuinstra and J.L. Koenig, "Raman spectrum of graphite," J. Chem. Phys. 53, 1126 (1970).

10. M. Nakamizo, R. Kammereck, and P.L. Walker, Jr., "Laser Raman studies on carbon," Carbon 12, 259 (1974).

A Plume Model for the Soot-catalyzed Oxidation of SO_2

R. Toossi, S.-G. Chang, P. Pagni, and T. Novakov

Theoretical prediction of the spatial distribution of pollutant concentrations emitted by sources such as power plant stacks is important in environmental impact studies. This prediction is especially important in regions close to the stack where the plume is hot and experimental measurements are difficult to carry out. Much work has been done on the dispersion of pollutants; however, chemical reactions are usually neglected, so current models do not generally give information on the secondary pollutants formed inside the plume.

Gaseous reactions have recently been taken into consideration in a few photochemical smog models.[1] Freiberg[2] has recently studied the iron-catalyzed oxidation of SO_2 in water droplets in a dispersing plume. We have developed a model describing the catalytic oxidation of SO_2 to sulfuric acid on soot particles in a coal-fire dispersing stack plume when condensation of H_2O does not occur during the adiabatic expansion and transport of the plume.

Yamamoto et al.[3-5] have investigated the catalytic oxidation of SO_2 on activated carbon in the presence of O_2 and H_2O vapor. The experiments were carried out so that the conditions simulate those in the scrubbing process where the temperature and the concentration of SO_2 and H_2O are much higher and the concentration of O_2 is lower than the concentrations in plumes and in the ambient atmosphere. The rate of reaction was found to be first order with respect to SO_2, provided the concentration of SO_2 was less than 0.01%, and depended on the square root of the concentration of O_2 and H_2O vapor. The activation energy was found to vary from -4 to -7 kcal/mole between 70 and 150°C, depending on the origin of the activated carbon. Even though the catalytic

activity of carbon particles is not yet well understood, we do know that it depends on the surface chemical and physical compositions of the particles. The effect of the physical properties of activated carbon, such as surface area and micro- and macropore volumes, on the rate of oxidation of SO_2 was also investigated by Yamamoto et al.[3-5] Initially the reaction occurs on the surface of both micropores and macropores, and the rate is constant for a given activated carbon until the amount of accumulated H_2SO_4 reaches about 10 wt % of the carbon. Beyond that amount, the rate gradually decreases with the reaction time until the micropore volume is filled up by H_2SO_4. The reaction continues only on the macropores with a constant, but much slower, rate than initially.

According to the results given by Yamamoto et al.,[3-5] a rate expression until the amount of H_2SO_4 formed reaches 10 wt % of the carbon can be written as follows:

$$\frac{d(H_2SO_4)}{dt} = -\frac{98}{64}\frac{d(SO_2)}{dt} = W\, C_{SO_2}\, C_{O_2}^{0.5}\, C_{H_2O}^{0.5}\, (k_1 + k_2) e^{-E_a/RT} \qquad (1)$$

where W, C_{SO_2}, C_{O_2}, and C_{H_2O} are the concentrations of carbon, SO_2, O_2, and H_2O vapor; k_1 and k_2 are the rate constants on the surface of the micro- and macropores respectively; and E_a is the activation energy. The reaction rate of the coal base-activated carbon obtained by Yamamoto et al. was used in our plume modeling. This specific carbon has the following physical properties: micropore volume — 0.4 ml/g; micropore radius — 7.4 Å; macropore volume — 0.40 ml/g; macropore radius — 2.2 μ; BET surface area — 894 m^2/g; and particle diameter — 0.25 mm. Although the reaction was studied between 70 and 150°C, we assume that the activation energy determined is still valid at ambient temperatures and that the rate at such temperatures can be obtained by extrapolation.

Based on these results, we suggest a physical model for the prediction of the rate of conversion of SO_2 on soot particles emitted from a single stack in the laminar cross wind.

Our present plume model is an extension of the work of Hoult, Fay, and Fourney[6] to include chemical reactions in the plume. We assume velocity, density, and pollutant concentration profiles are similar at all sections normal to the plume. Atmospheric turbulence is assumed to be much smaller than turbulence generated by the plume. Geometry and coordinate systems chosen are shown in Figure 22. A cross section of the plume at a direction normal to plume trajectory is a circle of diameter 2b. The relationshp between such a coordinate system and the Cartesian system is given by

$$z = \int_0^s \sin\theta \, ds$$

$$x = \int_0^s \cos\theta \, ds$$

Conservations of mass, momentum (in $\bar{r}$ and in θ direction), energy, and N species present constitute (N+4) differential equations which can be solved to obtain density, velocity, radius, angle of plume, and concentrations of the N species present. Initial conditions are determined at the stack exit.

As a special case, it is assumed that all the profiles are top hats. This reduces the equations to a set of ordinary differential equations which are then nondimensionalized and integrated. Nondimensionalization was made with respect to two characteristic length scales — ℓ_b, the buoyancy length scale, and ℓ_m, the momentum length scale — and a characteristic time scale ω^{-1}, which is the characteristic time for oscillation of a plume about its equilibrium position in the atmosphere. A detailed mathematical formulation and derivation and the method of computation will be given in another LBL report.

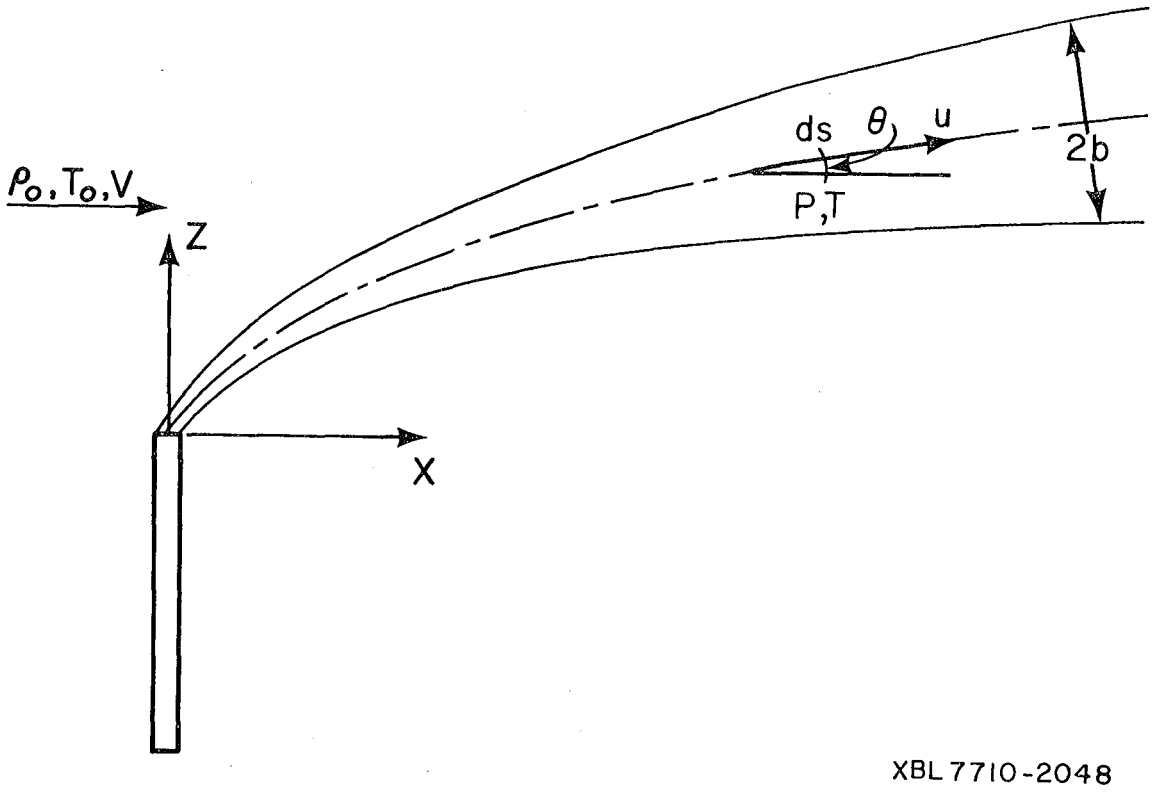

Figure 22. Coordinate system, P, T, and u are the potential density, absolute temperature, and velocity; b is half the plume diameter, and V is wind velocity.

Conservation of chemical species j can be written as

$$\frac{d}{ds} \int C_j u dA = \varepsilon C_{j,\infty} + \int w_j'' \, dA$$

where C_j is the concentration at any point inside the plume, $C_{j,\infty}$ is the background ambient concentration, ε is the entrainment rate, and w_j'' is the rate of production of the species j in the model

$$w''_{H_2O} = w''_{carbon} = 0$$

$$w''_{SO_2} = -\frac{64}{98} w''_{H_2SO_4}$$

where $w''_{H_2SO_4}$ is given by Eq. 1 for the gas phase reaction.

The example summarized below has been worked out using data given by Carpenter[7] for a TVA coal-fired power plant:

Velocity at the stack exit = 10 m/sec

Wind velocity = 3 m/sec

Stack diameter = 8.2 m

Temperature excess at the stack = 95°C

Flux of SO_2 emissions = 1500 g/sec

The centerline plume trajectory, temperature, and horizontal velocity are plotted in Figures 23 and 24 as the plume travels downwind. Maximum plume rise occurs at distance $x = \pi \ell_b S$, where S is the stratification parameter defined as the ratio of flow time for an element of plume to reach its final height, to the flow time required for the plume to be bent over appreciably in a cross wind.

Nondimensional concentration of soot particles and sulfur dioxide as a function of nondimensional distance from the stack is plotted in Figure 25. At distances far enough downstream, the concentrations approach those of ambient

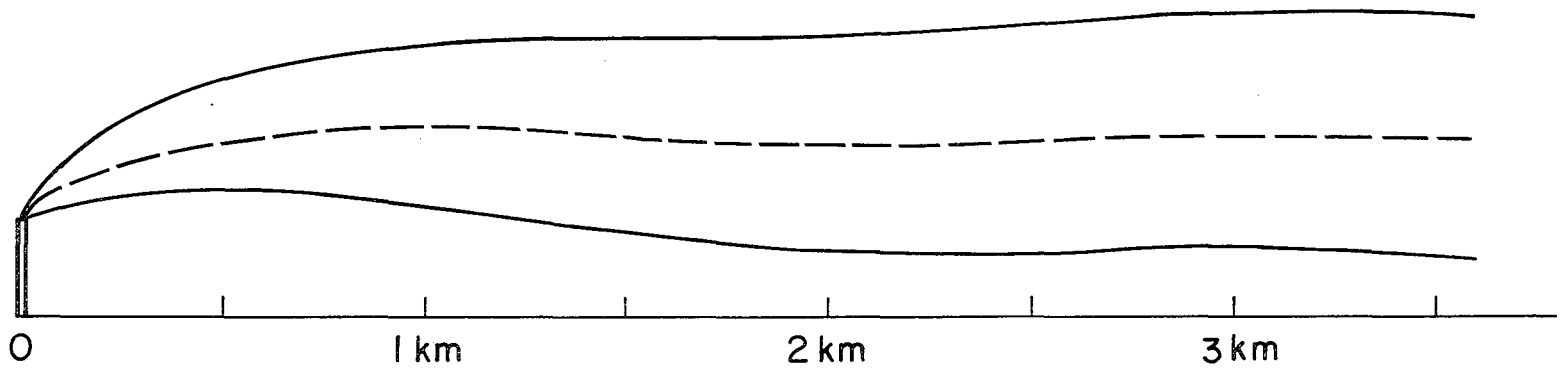

XBL7710-2155

Figure 23. Plume trajectory. The dotted line is the centerline. Note the periodic nature of the plume due to the stratification. The plume eventually stabilizes at its maximum rise.

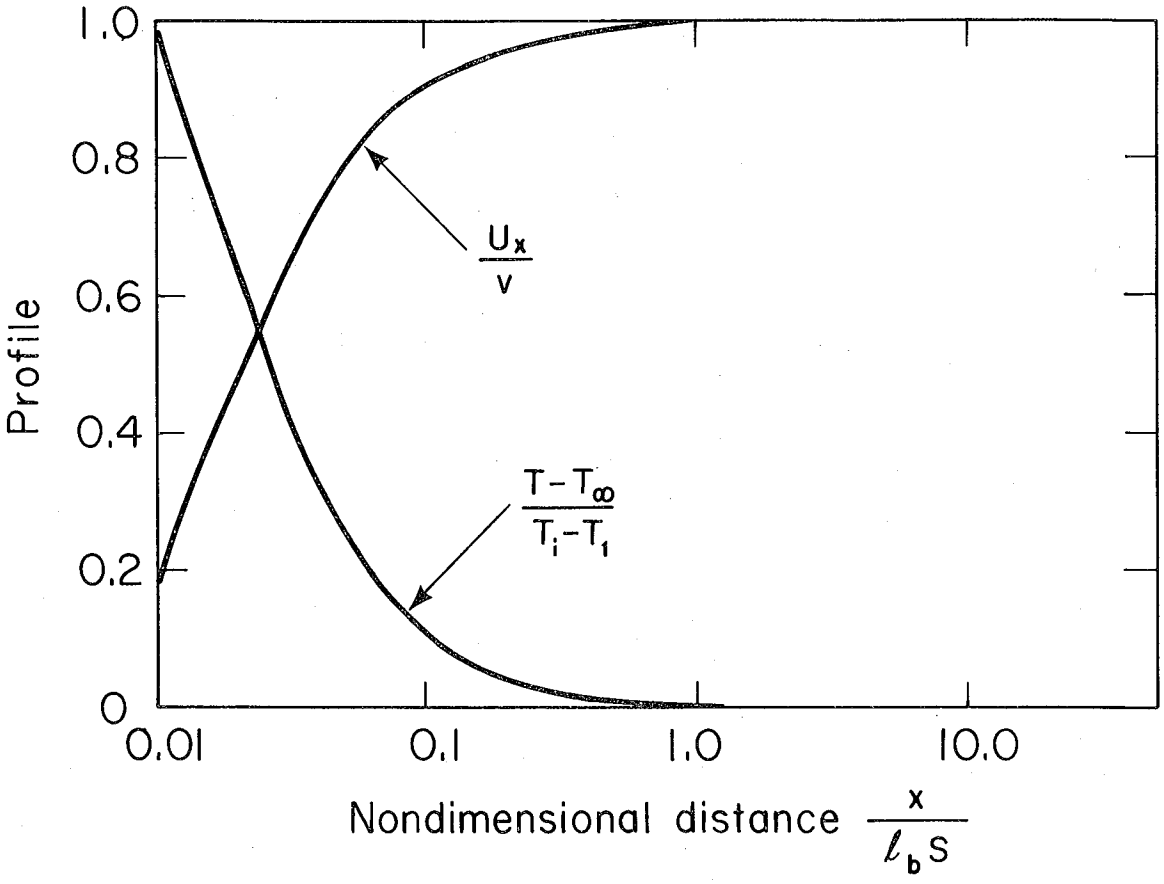

XBL7710-2060

Figure 24. Dimensionless temperature and velocity distribution inside the plume as a function of distance downstream from the stack. U_x is the component of velocity in the horizontal x direction.

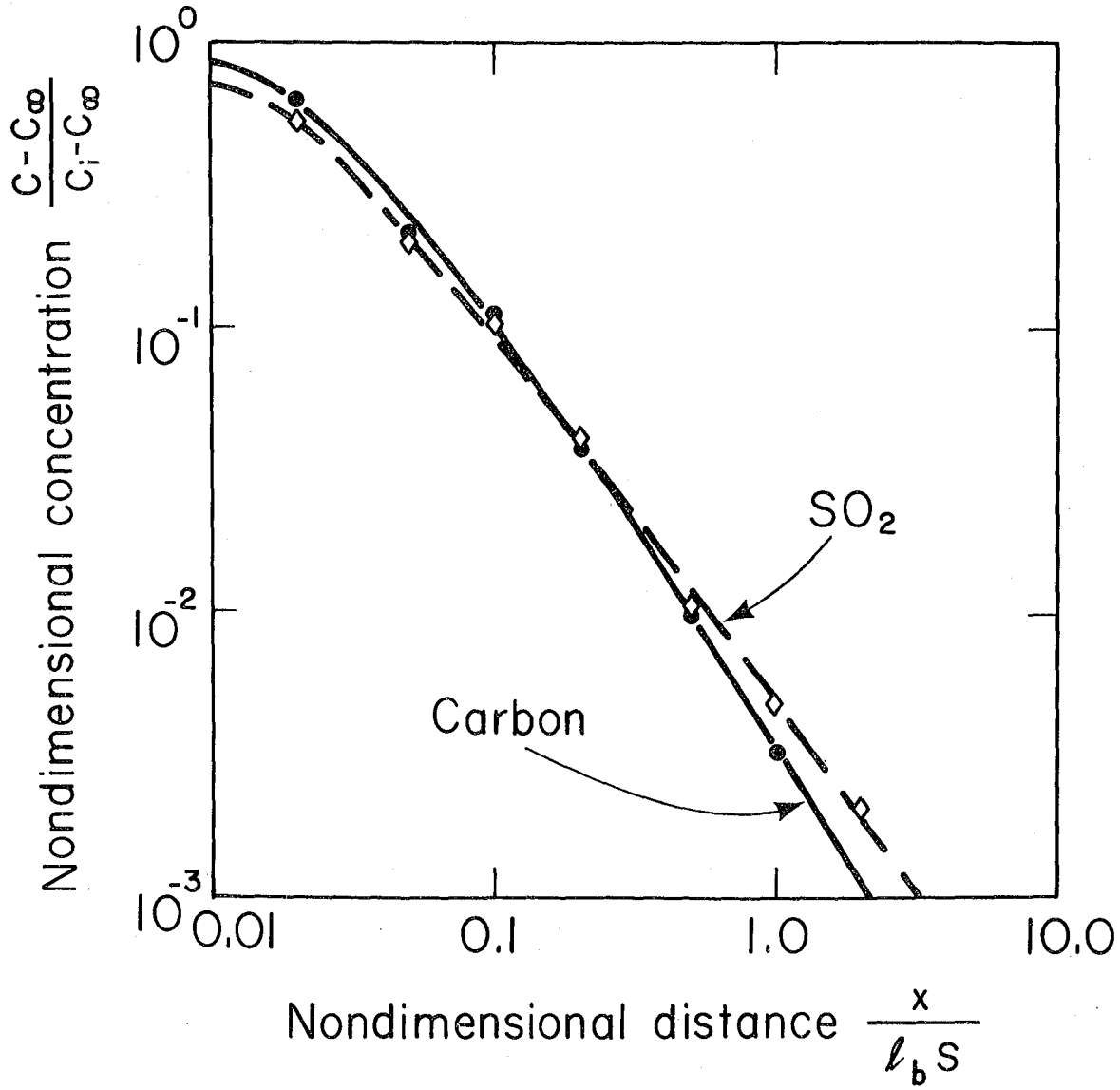

XBL 7710-10243

Figure 25. Nondimensional concentration of different species vs. distance traveled downstream from the stack. Ambient concentrations are: $C_{SO_2,\infty}$ = 8·E-05 g/m^3 ; $C_{carbon,\infty}$ = 2·E-05 g/m^3; $C_{H_2O,\infty}$ = 10.4 g/m^3 (80% RH).

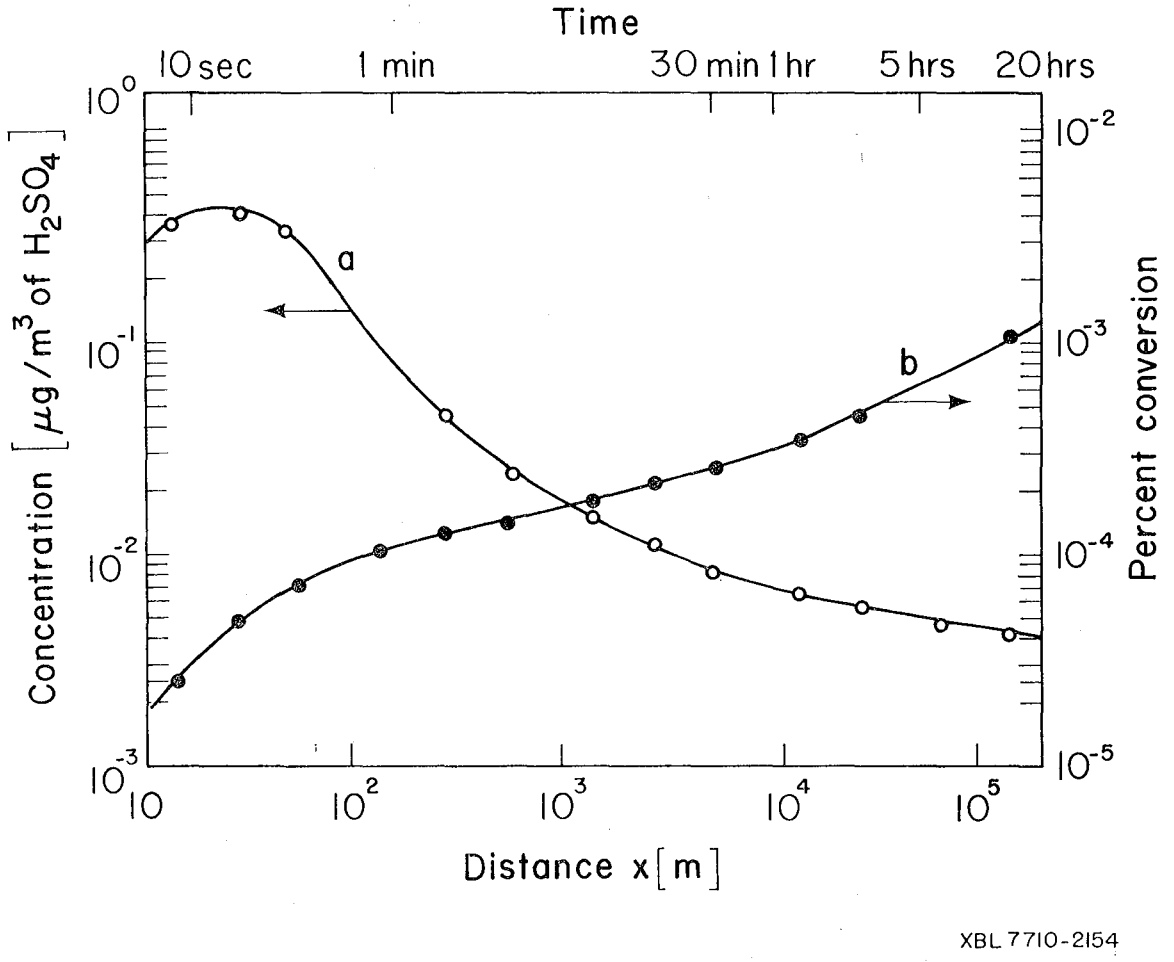

Figure 26. a) Mass of sulfuric acid formed. b) Precent of total conversion. The time of transport to a certain distance is given in a different scale at the top of the figure.

conditions. The ambient SO_2 concentration is above the carbon particulate concentration in this example. A similar plot can be drawn for the concentration of sulfuric acid formed, based on the Yamamoto mechanism (Fig. 26).

Our results show that although total conversion of SO_2 increases with time, the concentration of H_2SO_4 reaches a maximum in the plume only a short distance downstream from the stack. The rate of oxidation of SO_2 on carbon particles is slow when relative humidity is low and there is no water condensation on the surface of the carbon particles. We have recently studied catalytic oxidation of SO_2 on soot particles in aqueous suspension (see pp. 42-56). The results indicate that the rate under these conditions is very fast. A complete rate expression in an aqueous system will be derived. We will calculate the conversion of SO_2 to H_2SO_4 in a plume, including both SO_2-air-soot-H_2O vapor, and SO_2-air-soot-H_2O liquid mechanisms.

References

1. a) S.D. Reynolds, P.M. Roth, and J.H. Seinfeld, "Mathematical modeling of photochemical air pollution—I. Formulation of the model," Atmos. Environ. 7, 1033 (1973).

   b) P.M. Roth, P.J.W. Roberts, and M.-K.Liu, "Mathematical modeling of photochemical air pollution—II. A model and inventory of pollutant emissions," Atmos. Environ. 8, 97 (1974).

   c) S.D. Reynolds, M.-K. Liu, T.A. Hecht, P.M. Roth, and J.H. Seinfeld, "Mathematical modeling of photochemical air pollution—III. Evaluation of the model," Atmos. Environ. 8, 563 (1974).

2. J. Freiberg, "The iron catalyzed oxidation of SO_2 to acid sulphate mist in dispersing plumes," Atmos. Environ. 10, 121 (1976).

References (contd.)

3. K. Yamamoto, M. Seki, and K. Kawazoe, "Rate of oxidation of sulfur dioxide on activated carbon surfaces," Nihon Kagaku Kaishi 6, 1046 (1972).

4. I. Sugiyama, K. Kawazoe, and K. Yamamoto, "Effect of particle size of the activated carbon pellets on the rate of sulfur dioxide oxidation," Nihon Kagaku Kaishi 6, 1052 (1972).

5. K. Yamamoto, M. Seki, and K. Kawazoe, "Effect of sulfuric acid accumulation on the rate of sulfur dioxide oxidation on activated carbon surface," Nihon Kagaku Kaishi 7, 1268 (1973).

6. D.P. Hoult, J.A. Fay, and L.J. Forney, "A theory of plume rise compared with field observations," Jour. APCA 19:8, 585 (1969).

7. S.B. Carpenter, et al., "Full-scale study of plume rise at large coal-fired electric generating stations," Jour. APCA 18:7, 458 (1968).

Photodecomposition of Lead Bromochloride

S.-G. Chang, R. L. Dod, R. D. Giauque, and T. Novakov

Most lead in the atmosphere, especially in urban areas, originates from combustion of gasoline containing antiknock additives. The dominant chemical form of lead in automobile exhaust is lead bromochloride.[1] Field experiments indicate that the halogen-to-lead ratio decreases with aerosol age,[2-5] presumably as the result of photodecomposition. Pierrard[6] has studied the photodecomposition of PbBrCl in carbon tetrachloride. However, the absorption spectrum, molar extinction coefficients, and quantum efficiencies for this process have not been reported previously. We have obtained this information by means of uv-visible, X-ray photoelectron, and X-ray fluorescence spectroscopy.

Vacuum-evaporated PbBrCl films were used throughout this study. The films were deposited in a Varian vacuum vapor deposition chamber ($\sim 10^{-5}$ torr) onto quartz substrates for absorption spectrum measurements, and aluminum substrates for quantum efficiency studies. The thickness of the PbBrCl deposits was measured with a Varian interference microscope.

The absorption spectra were obtained with a Cary 118 recording spectrophotometer. Figure 27 shows the absorption spectra between 700 and 300 nm of PbBrCl (dashed line), PbBrCl irradiated with natural sunlight (dotted line), and PbBrCl irradiated with a 200-W mercury arc after being exposed to natural sunlight for 2 hr (solid line). The PbBrCl film was darker after arc irradiation. This is presumably due to the formation of PbO species which are highly absorbing in the visible spectral region. The thickness of the vacuum-evaporated PbBrCl film was 196.5 ± 6.7 nm. Assuming a value of 6 g/cm^3 for the density of the PbBrCl film (based on the unit cell volume given by Calingaert

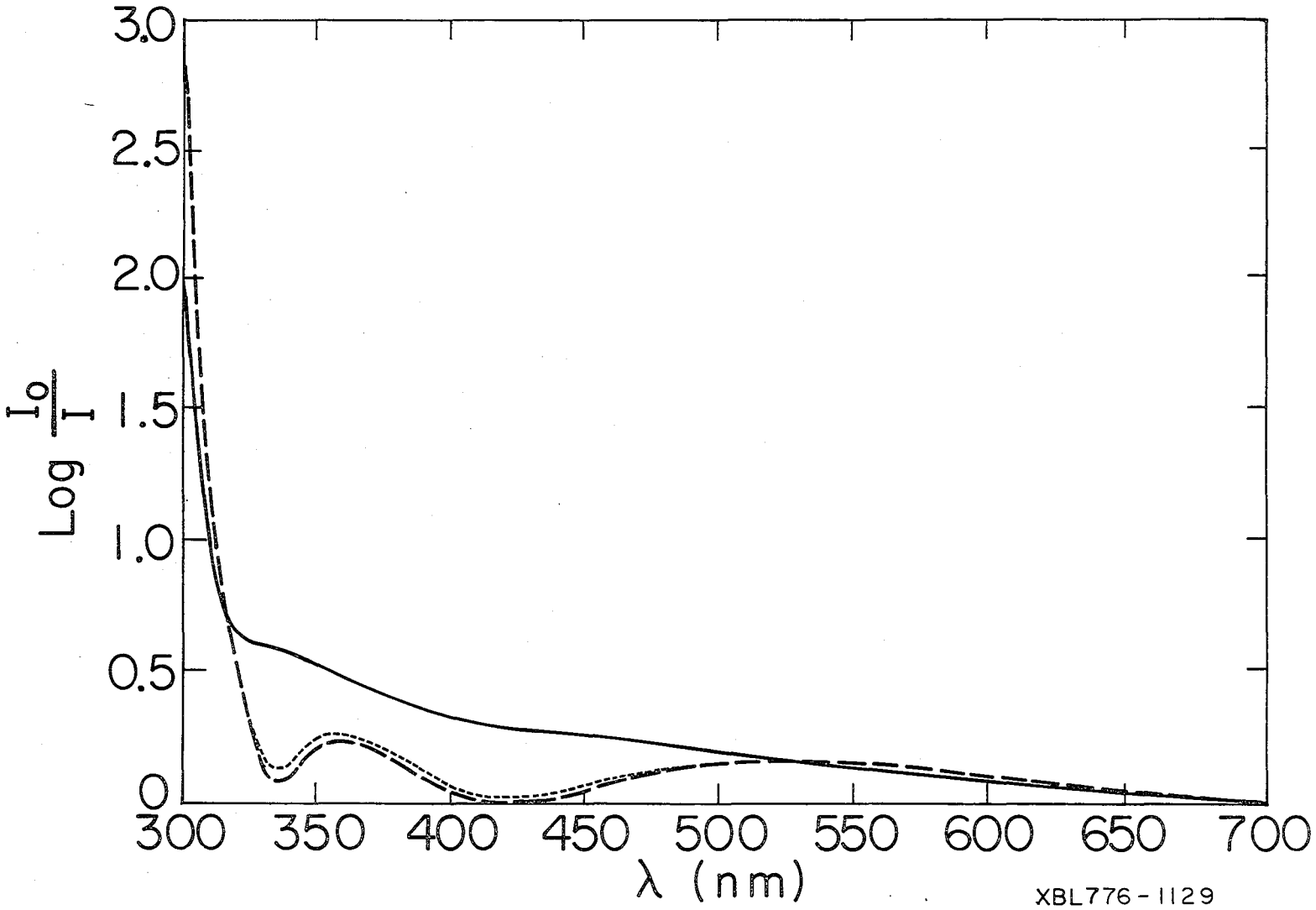

Figure 27. – – – – Absorption spectrum of PbBrCl thin film at 20°C.
------- Absorption spectrum of PbBrCl after a 1-hr exposure in air to natural sunlight at 20°C at a level of 95 mW/cm^2.
——— Absorption spectra of PbBrCl after a 2-hr additional irradiation by a 200-W mercury arc at a level of 20 mW/cm^2.

et al.[7]), the molar extinction coefficients of PbBrCl at 525, 475, 350, and 300 nm were calculated to be 9.66 x 10^2, 7.06 x 10^2, 1.20 x 10^3, and 1.82 x 10^4 ℓ/mole-cm.

The rate of photodecomposition was studied at 525, 475, 350, and 300 nm. Figure 28 illustrates the use of XPS in monitoring the changes in concentrations of the various species during the course of the PbBrCl photodissociation. The binding energies of the electrons of PbBrCl are: $Cl(2p_{1/2,3/2})$ – 199.4, 197.9 eV; $Pb(4f_{5/2,7/2})$ – 143.7, 138.8 eV; and Br $(3d_{3/2,5/2})$ – 69.4, 68.6 eV. After a 5-min in-vacuo irradiation of PbBrCl by the 200-W mercury arc, $4f_{5/2,7/2}$ peaks corresponding to metallic lead appear at binding energies of 141.5 and 136.6 eV.[8] The intensity of these metallic lead peaks grows as the irradiation time increases (Fig. 28).

If the metallic lead formed during photolysis is oxidized to PbO, then its XPS lines, which are only slightly shifted from the PbBrCl peaks, can interfere with the determination of both the metal and the halide peak intensities. This was not found to be a problem, however, because the rate of oxidation of metallic lead to PbO is slow at the pressures maintained in the XPS sample chamber ($\leq 10^{-8}$ torr). For example, the intensity of metallic lead decreased by only $\sim$ 10% when the sample irradiated for 140 min was left in the vacuum chamber for 40 hr. Lead can be oxidized quickly, however, when it is exposed to ambient air. This is shown in Figure 28 for a sample exposed to air for 10 min.

Figure 29 shows the results of irradiation at 300 nm, with a photon flux of 5.05 x 10^{13} photons/cm^2 sec. Similar results were obtained at 350 nm. The rate of production of metallic lead is initially fast but approaches saturation with continued irradiation. We did not detect the appearance of the metallic lead photoelectron peaks when the sample was irradiated at 525 or 475 nm.

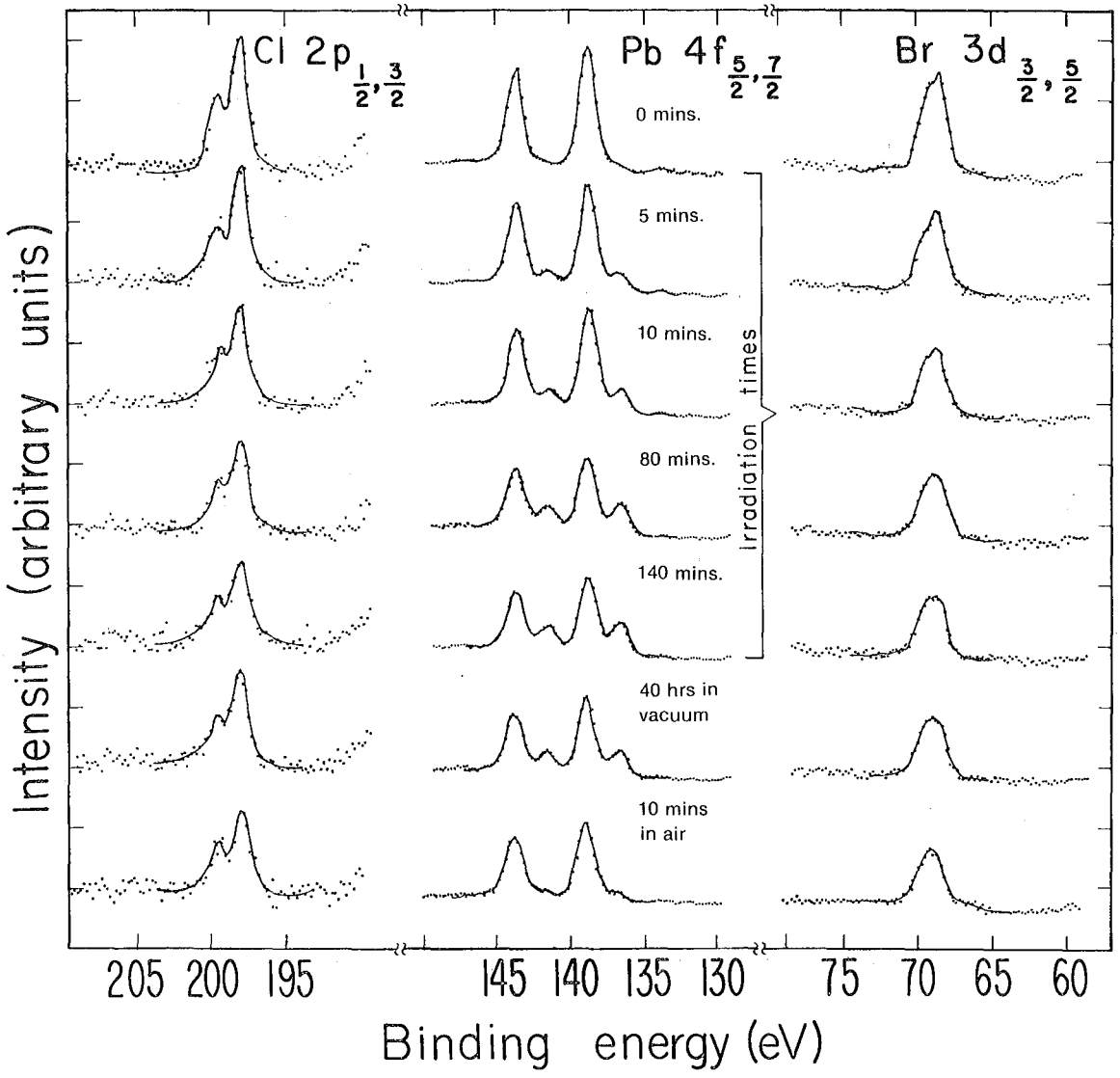

XBL776-1130

Figure 28. XPS spectra of PbBrCl showing changes in intensity of reactant and product peaks with increasing irradiation.

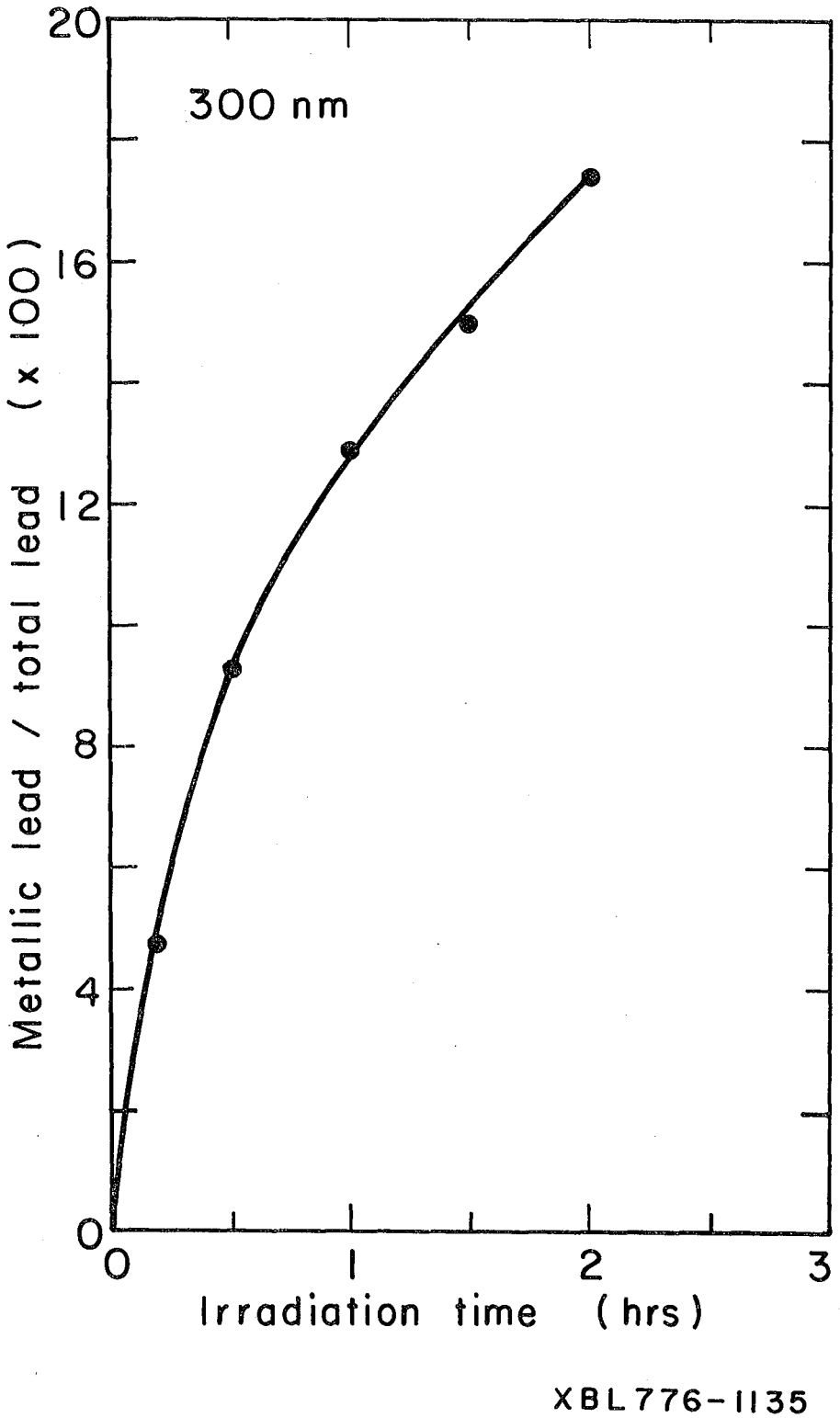

Figure 29. Ratio of metallic lead to total lead as a function of the irradiation time during the course of irradiation of PbBrCl at 300 nm.

Angularly resolved XPS measurements[9] were performed to find the extent to which the PbBrCl photolysis was confined to the sample surface. For a sample irradiated by the mercury arc for about 4 hr, there is a marked increase in the relative intensity of metallic lead to lead halide when the photoelectron escape angle is low (Fig. 30). This increase implies a higher concentration of metallic lead on the surface of the film than in the bulk. The mean free path of electrons in metallic lead[10] is about 2.0 nm at a kinetic energy of 1350 eV. We have calculated the mean free path of electrons in PbBrCl to be about 2.5 nm, using the formula given by Penn.[10] Therefore the ratios of metallic lead to total lead concentrations (Figs. 29, 30) represent only a thin surface layer, not the entire PbBrCl film ($\sim$ 200 nm thick). However, we can calculate the bulk lead-to-lead-halide ratio for the entire sample by using the Beer-Lambert Equation and the molar extinction coefficients reported earlier. This is done by multiplying the lead-to-lead-halide ratio (for the sample surface) determined from XPS by the factor $(I_0-I_3)\ell_1\cos(90-\theta)/[(I_0-I_1) + (I_2-I_3)]\ell_2$. I_0 is the intensity of the radiation incident on the surface of the PbBrCl film; I_1 is the intensity of the radiation after penetrating a distance $\ell_1\cos(90-\theta)$, where ℓ_1 is the electron mean free path and θ is the photoelectron escape angle; I_2 is the intensity of the radiation that reaches the surface layer after it penetrates the entire thickness of the film (ℓ_2) and after it reflects from the aluminum backing; and I_3 is the intensity of the radiation as it emerges from the surface of the sample. From this ratio and from the X-ray fluorescence results, we can calculate the amount of halogen lost as a function of the irradiation time. The quantum efficiency can then be calculated according to the following equation:

$$\phi_\lambda = \frac{\Delta}{Jt(I_0-I_3)/I_0}$$

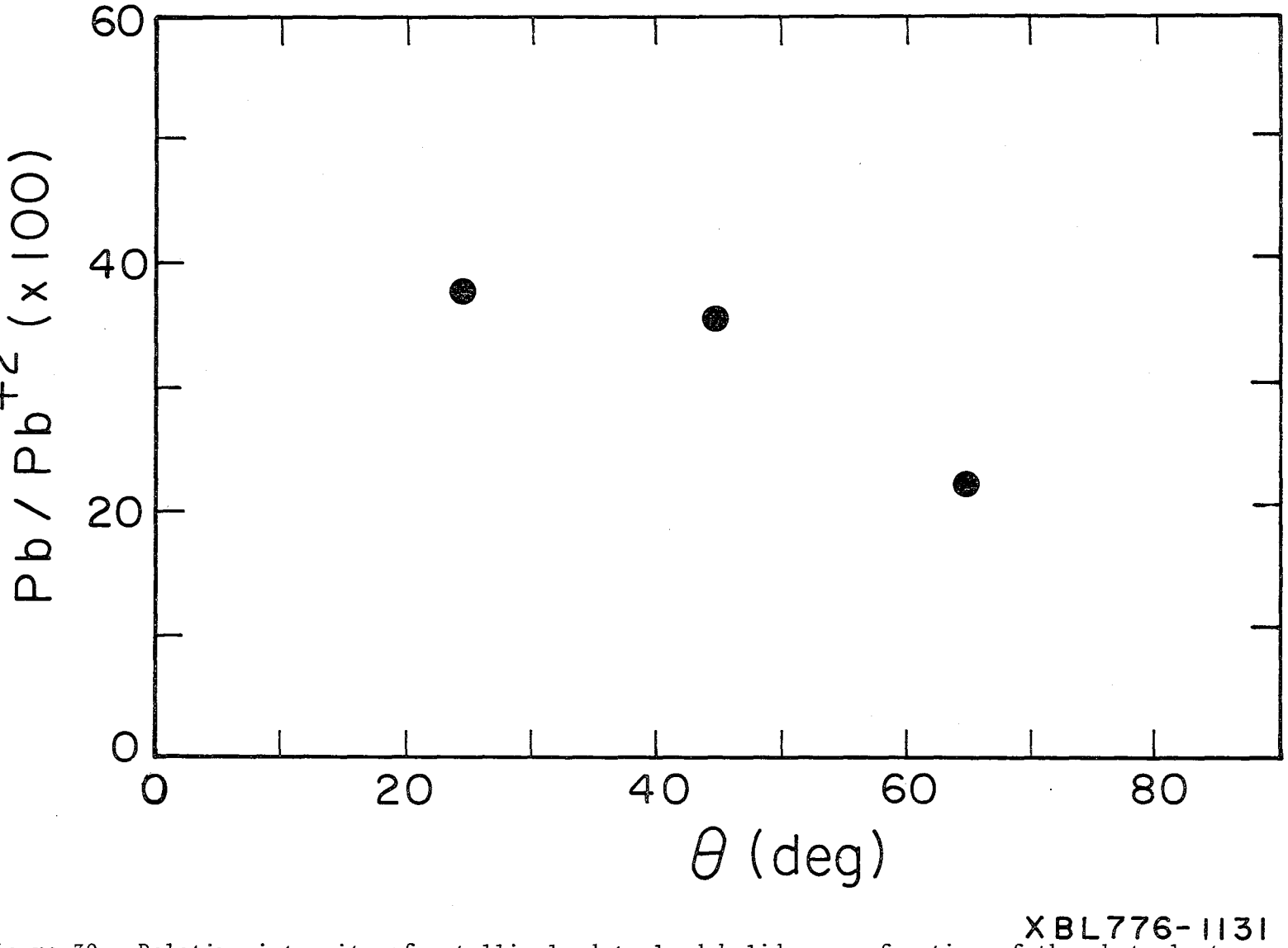

Figure 30. Relative intensity of metallic lead to lead halide as a function of the photoelectron escape angle.

where ϕ_λ is the quantum efficiency at wavelength λ, Δ is the amount of bromine or chlorine lost in number of atoms per square centimeter during the irradiation time t (in seconds), and J is the photon flux in number of photons per second-square centimeter. We have calculated the quantum efficiencies at 350 and 300 nm for chlorine and bromine when the irradiation time (t) approaches zero. The results are listed in Table III. The quantum efficiencies at 525 and 475 nm are negligible because no obvious photolysis of PbBrCl was observed at these wavelengths.

Table III. Quantum efficiencies for the production of bromine and chlorine during the photodissociation of PbBrCl.

Wavelength (nm)	Photon flux (photons/cm^2 sec)	Film thickness (nm)	Total irradiation time (hr)	Δ_{Br}[a] (μg/cm^2)	Δ_{Cl}[b] (μg/cm^2)	ϕ_{Br}	ϕ_{Cl}
350	5.85×10^{13}	179	9.5	1.72	0.55	0.038	0.027
300	2.5×10^{13}	179	2	2.30	0.90	0.35	0.31

[a] Δ_{Br} = loss of bromine after irradiation

[b] Δ_{Cl} = loss of chlorine after irradiation

References

1. D.A. Hirschler, L.F. Gilbert, F.W. Lamb, and L.M. Niebylskr, "Lead compounds in automobile exhaust gas," Ind. Eng. Chem. 49, 1131 (1957).

2. R.L. Lininger, R.A. Duce, J.W. Winchester, and W.R. Matson, "Chlorine, bromine, iodine, and lead in aerosols from Cambridge, Massachusetts," J. Geophys. Res. 71, 2457 (1966).

3. E.L. Jernigan, B.J. Ray, and R.A. Duce, "Lead and bromine in atmospheric particulate matter on Oahu, Hawaii," Atmos. Environ. 5, 881 (1971).

References (contd.)

4. J.A. Robbins and F.L. Snitz, "Bromine and chlorine loss from lead halide automobile exhaust particulates," Environ. Sci. Technol. 6, 164 (1972).

5. California Air Environment (University of California) 6, 5 (1977).

6. J.M. Pierrard, "Photochemical decomposition of lead halides from automobile exhaust," Environ. Sci. Technol. 3, 48 (1969).

7. G. Calingaert, F.W. Lamb, and F. Meyer, "The lead chloride-lead bromide system," J. Am. Chem. Soc. 71, 3709 (1949).

8. K.S. Kim, T.J. O'Leary, and N. Winograd, "X-ray photoelectron spectra of lead oxides," Anal. Chem. 45, 2214 (1973).

9. C.S. Fadley, R.J. Baird, W. Siekhaus, T. Novakov, and S.Å.L. Bergström, "Surface analysis and angular distributions in X-ray photoelectron spectroscopy," J. Electron Spectroscopy 4, 93 (1974).

10. D.R. Penn, "Quantitative chemical analysis by ESCA," J. Electron Spectroscopy 9, 29 (1976).

Heterogeneous Reactions of Polynuclear Aromatic Hydrocarbons and Soot Extracts with NO_2

L. Gundel, S.-G. Chang, and T. Novakov

Polycyclic aromatic hydrocarbons (PAH) can be produced directly from the combustion of fossil fuel and are always associated with soot particles.[1] Many PAH are known to be carcinogenic. Also, PAH may undergo chemical modification as a result of irradiation by sunlight[2] or by reaction with pollutant gases[3] to produce modified forms which may have enhanced health-hazard potential. We have begun a study of the reactions of selected PAH with NO_2 in order to assess their influence on the fate of PAH in ambient carbonaceous particulate material.

Heterogeneous reactions of PAH with NO_2 have not been investigated extensively before this study. However, their reactions with HNO_3 in solution produce nitro-substituted compounds and quinones.[4] Anthracene and perylene were chosen as prototypes for this work because of their availability, occurrence in particulate extracts,[5] and reactivity toward nitration in solution.[4] Finely ground hydrocarbon samples ($\sim$ 0.3 g) were exposed to 25-100 torr NO_2 in a light-tight, evacuated, stainless steel reaction vessel at room temperature. For both anthracene and perylene, the pressure dropped continuously and stabilized after 1/2-hr exposure to NO_2. Not much change in pressure was observed with longer monitoring (12-24 hr). NO was produced during the reaction and was observed as a blue condensation product after the reaction. Column chromatography, with neutral alumina as the stationary phase and toluene as eluent, was used to separate the hydrocarbon products from the starting material and from each other. These fractions were crystallized by evaporation from a toluene solution. Infrared spectra of the separated hydrocarbons in KBr pellets were recorded on a Perkin-

Elmer 621 grating spectrometer and are shown in Figures 31 and 32. Experiments were also performed to test the effects of water vapor on the NO_2-anthracene reaction and of humid air on the NO_2-perylene reaction. Table IV summarizes the experimental conditions and the assignments for the various spectral features observed in all experiments.

Characteristic nitro aromatic absorptions appear in all reaction products for 30-min and longer exposures to NO_2. These occur in the regions 1515 ± 8 cm^{-1} (asymmetric C-NO_2 stretch) and 1350 ± 13 cm^{-1} (symmetric C-NO_2 stretch). Strong aromatic nitro absorptions are also observed in kerosene soot benzene extract solids exposed to NO_2 for 24 hours. Out-of-phase C-H wagging vibrations of PAH (900-700 cm^{-1}) show absorption frequencies which are characteristic of both the number of adjacent hydrogen atoms per ring and ring substitution.[6] Polar substituents usually introduce new C-H wagging vibrations, and this effect is particularly noticeable in the nitroperylene product, Figure 32c.

Comparison with published spectra[7] shows that the anthracene reaction product is 9-nitroanthracene, whether or not water vapor is present with NO_2. For perylene the reaction products are the same when perylene reacts with NO_2 alone or in the presence of humid air. The major nitroperylene product has a melting point range (207-210°C in argon) close to that of 3-nitroperylene (210-212°C),[8] compared with 277-279°C for perylene. However, elemental analysis and the severe disruption of the C-H wag absorption modes indicate that the compound may have more than one nitro group per molecule. The minor perylene reaction product contains nitrogen and has column behavior similar to that of 1-nitroperylene,[7] but this identification has not been confirmed. 3-nitroperylene is the only nitro product formed in the classical nitration of perylene in acetic anhydride with nitric acid,[9] which is consistent with molecular orbital calculations for the 3 position as that of highest electron density,[4b,10] and

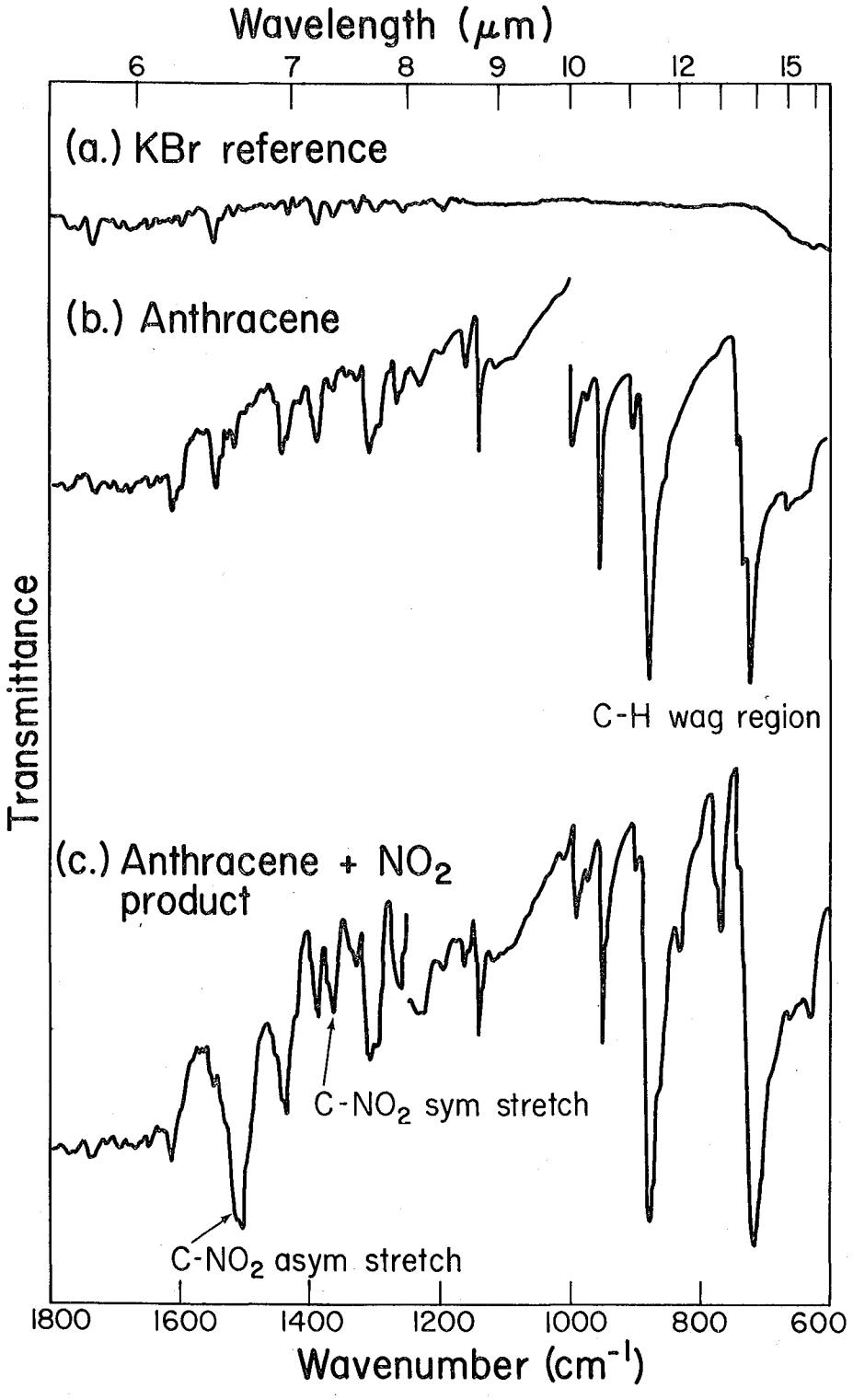

XBL 7710-2093

Figure 31. Infrared absorption spectra in KBr: (a) KBr reference; (b) anthracene; (c) anthracene + NO_2 reaction product (9-nitroanthracene).

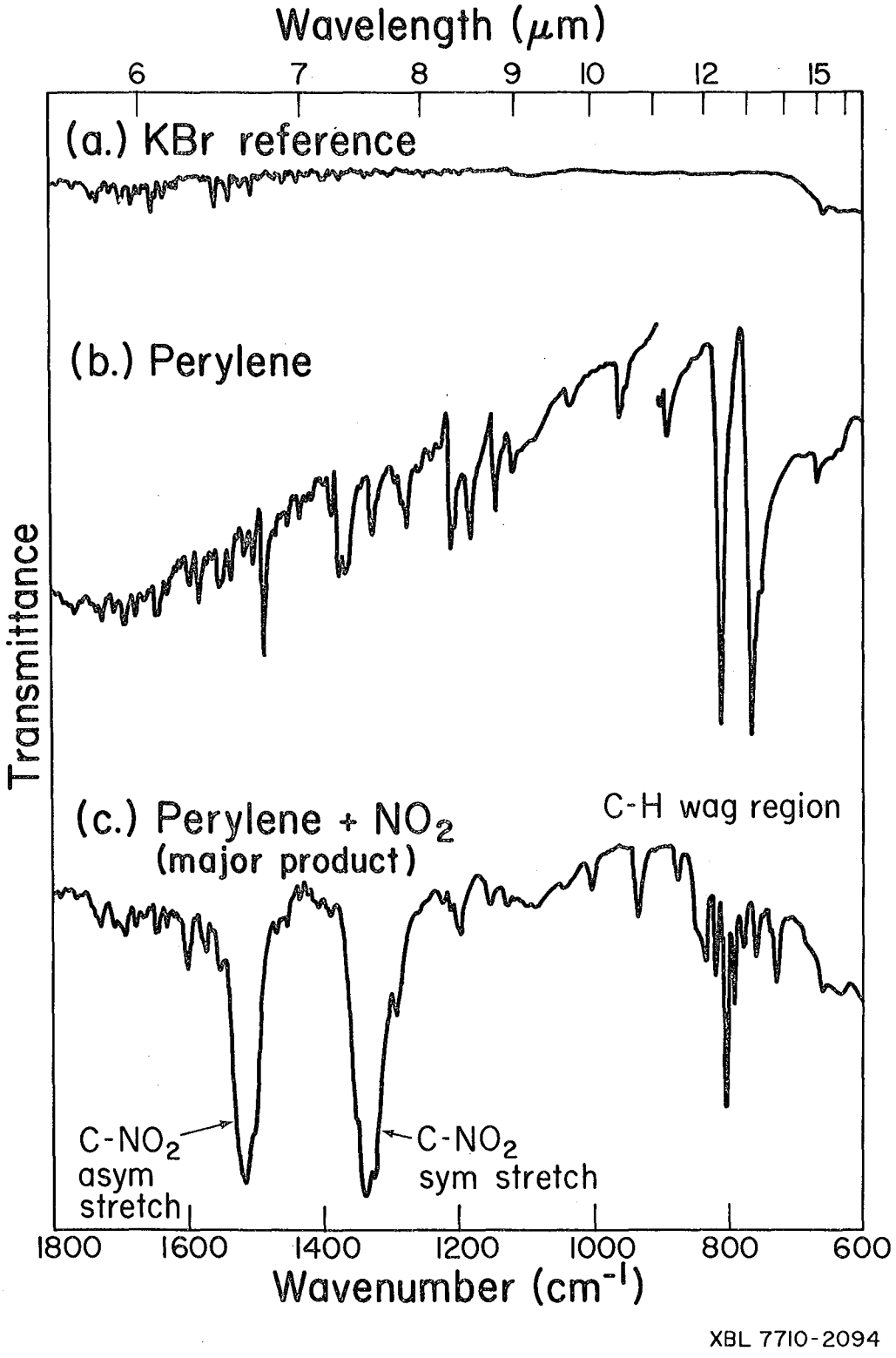

Figure 32. Infrared absorption spectra in KBr: (a) KBr reference; (b) perylene; (c) perylene + NO_2 major reaction product (3-nitroperylene).

Table IV. Summary of experimental conditions and results.

Reactants[a]	Products (30-min exposure)	Estimated yield[b]	C-NO_2 asym str (cm^{-1})	C-NO_2 sym str (cm^{-1})	Aromatic C-H wag[c]
Anthracene(white) + NO_2	9-nitroanthracene(orange) (Figure 1)	10%	1508(m)	1363(w)	p879(s),832(w), 768(m),p719(s)
Anthracene + NO_2 + H_2O	9-nitroanthracene	Not available	1510(m)	1363(w)	p878(s),833(w), 770(m),p720(s)
Perylene(orange) + NO_2	3-nitroperylene(bright red) (Figure 2)	7-10%	1517(s)[d]	1339(s)[d]	836(w),820(w), p808(m),791(w), 778(w),p760(w), 730(w)[d]
	1-nitroperylene(?)(dark red)	≤ 5%	—[e]	—[e]	p810(s),p764(s)
Perylene + NO_2 + H_2O + air	3-nitroperylene	10%	1520(s)	1340(s)	See above
	1-nitroperylene(?)	≤ 5%	—[f]	—[f]	—[f]
Kerosene soot(benzene extract) + NO_2(dk brown)	Aromatic nitro compounds (dark red)(24-hr exposure)	Not available	1523(s)[g]	1338(s)[g]	898(w),798(m)

[a]Typical initial conditions: 2.0×10^{-3} mole PAH, 3×10^{-3} mole NO_2 (4×10^{-4} mole H_2O, air to ambient pressure).

[b]Mole percent, based on mass of separated reaction products, identified as listed.

[c]C-H wag frequencies of parent PAH are preceded by p. Intensities are indicated as s—strong, m—medium, and w—weak.

[d]The strength of nitro absorptions and disruption of C-H wag pattern suggests more than one nitro group per molecule.

[e]Apart from a strong absorption at 1452 cm^{-1}, the spectrum is identical to that of unreacted perylene.

[f]No spectra available.

[g]Broad.

thus most susceptible to electrophilic attack by NO_2^+, the known nitrating agent in solution.[4a] The radical NO_2 is expected to show similar electrophilic character in attack on aromatic molecules.[11]

The infrared spectra, melting point, and isolation of NO as a reaction product indicate that the overall stoichiometry of the reaction of solid perylene with NO_2 gas is

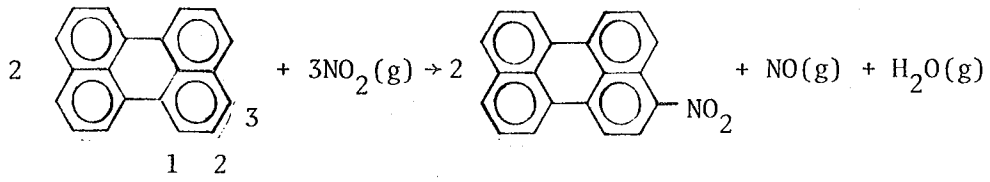

High-resolution NMR spectra of these products will be obtained to confirm this interpretation.

These results suggest that reactions of PAH with NO_2 may occur in stagnant polluted atmospheres, under nonphotochemical conditions. Nitro PAH may have enhanced toxicity compared with PAH.[3] Nitro PAH are readily reduced to amines,[11] since the nitro group activates PAH toward reaction with electron-rich nucleophiles such as NH_3. The nitro group also influences the photochemical behavior of these compounds,[12] and could affect the fate of particulate PAH. To assess the relative importance of these reactions in source and ambient particulate chemistry, we plan to measure reaction rates and to investigate reactions when the PAH are adsorbed on activated carbon, under photochemical and nonphotochemical conditions.

References

1. a) K.W. Boyer and H.A. Laitenen, "Automobile exhaust particulates: Properties of environmental significance," Environ. Sci. Technol. 9, 457 (1975).

b) J.B. Edwards, Combustion: Formation and Emission of Trace Species, Ann Arbor, Ann Arbor Science, 1974, p. 64.

2. a) B.D. Tebbens, M. Mukai, and J.F. Thomas, "Fate of arenes incorporated with airborne soot: Effect of irradiation," Am. Ind. Hyg. Assoc. J. 32, 365 (1971).

b) B.D. Tebbens, J.F. Thomas, and M. Mukai, "Fate of arenes incorporated with airborne soot," Am. Ind. Hyg. Assoc. J. 27, 415 (1966).

3. National Academy of Science, Biological Effects of Atmospheric Pollutants: Particulate Polycyclic Organic Matter, Washington, U.S. Govt. Printing Office, 1970.

4. a) J.G. Hoggett, R.B. Moodie, J.R. Penton, and K. Schofield, Nitration and Aromatic Reactivity, Cambridge, Cambridge University Press, 1971.

b) A. Streitweiser, J.I. Branman, and J.B. Bush, "Application of the molecular orbital ω-technique to aromatic substitution," Tetrahedron 19, Suppl. 2, 379 (1963).

c) M.J.S. Dewar, T. Mole, and E.W.T. Warford, "Electrophilic substitution. VI. The nitration of aromatic hydrocarbons; partial rate factors and their interpretation," J. Chem. Soc. 3581 (1956).

5. a) R.C. Pierce and M. Katz, "Dependency of polynuclear aromatic hydrocarbon content on size distribution of atmospheric aerosols," Environ. Sci. Technol. 9, 347 (1975).

b) C. Golden and E. Sawicki, "Ultrasonic extraction of total particulate aromatic hydrocarbons from airborne particles at room temperature," J. Intern. Anal. Chem. 4, 9 (1975).

References (contd.)

c) R.C. Lao, R.S. Thomas, H. Oja, and L. Dubois, "Application of a GC-MS data processor combination to the analysis of the polycyclic aromatic hydrocarbon content of airborne pollutants," Anal. Chem. 45, 906 (1973).

d) R.J. Gordon, "Distribution of airborne polycyclic aromatic hydrocarbons throughout Los Angeles," Environ. Sci. Tech. 10, 370 (1976).

6. a) M.P. Groenewege, "Some regularities in the infrared spectra of aromatic compounds in the C-H wagging region," Spectrochim. Acta 11, 579 (1964).

b) C.G. Cannon and G.B.B.M. Sutherland, "The infra-red absorption spectra of some aromatic compounds," Spectrochim. Acta 4, 373 (1951).

7. C.J. Pouchert, ed., Aldrich Library of Infrared Spectra, Milwaukee, Aldrich Chemical Company, 1975.

8. J.T. Looker, "Mononitration of perylene, preparation and structure proof of the 1 and 3 isomers," J. Org. Chem. 37, 3379 (1972).

9. M.J.S. Dewar and T. Mole, "Electrophilic substitution. II. The nitration of napthalene and perylene," J. Chem. Soc. 1441 (1956).

10. A. Streitweiser, Molecular Orbital Theory for Organic Chemists, New York, Wiley, 1961.

11. J. March, Advanced Organic Chemistry, New York, McGraw-Hill, 1968.

12. E. Havinga and J. Cornelisse, "Aromatic photosubstitution reactions," Pure and Appl. Chem. 47, 1 (1976).

SECTION III

FIELD STUDIES

Characterization of Winter Air Pollution Episodes

C. D. Hollowell, R. L. Dod, R. D. Giauque, G. W. Traynor, and T. Novakov

One of the aims of our field studies is to establish what differences, if any, can be found in the chemical composition of urban aerosol particles in winter and in summer, i.e., when the photochemical activity is low and when it is intense. It is important to understand the relative contributions of both nonphotochemical reactions and photochemical (ozone-olefin) reactions in the formation of aerosol particulate air pollution. This is especially important because existing pollution controls are specifically aimed at the control of photochemical oxidant, which is believed to be an essential precursor for the formation of particulates from gaseous pollutants such as SO_2, NO, and certain hydrocarbons.

We have recently initiated an extensive field study to characterize winter and summer air pollution episodes. The work reported here represents the first phase of this field program. During winter months the San Francisco Bay Area has frequent, intense particulate air pollution episodes in spite of low or negligible ozone concentrations. The initial work has focused on a characterization of aerosol particles during typical winter air pollution episodes. The program will be extended into the summer months when the photochemical oxidant is at maximum concentrations. A comparison of the chemical composition of the aerosol particles sampled under these two distinctly different conditions should identify the species associated specifically with oxidant-related aerosol-particulate-forming reactions and should lead to a better understanding of the significance of nonphotochemical, especially heterogeneous, reactions in the formation of secondary particulates. During the course of these field studies, the LBL Mobile Atmospheric Research Laboratory (MARL)[1] will be used at several

San Francisco Bay Area locations during both photochemical and nonphotochemical seasons. The field laboratory, MARL, is a self-contained unit designed to provide a complete chemical and physical characterization of the gaseous and particulate portions of the ambient aerosol. It is capable of supporting field studies at almost any location and is readily movable to new sampling sites without requiring extensive time and effort. It contains the latest state-of-the-art air pollution monitoring and sampling equipment, meteorology instrumentation, automatic calibration equipment, and data acquisition and control systems necessary for routine measurements and special studies in the field.

We have characterized two episodes during the winter of 1976-1977. The sampling locations in Berkeley, California, and dates of sampling are shown in Figure 33, and the results of the episodes are shown in Figures 34 through 37. In early November, 1976, an episode occurred characterized by warm temperatures, low relative humidity, and generally stagnant air, as seen in Figure 34a. The light-scattering coefficient b_{scat} reached extremely high values during midday, as did the particle volume and concentration of condensation nuclei (Fig. 34e). The most striking feature in the gas data (Fig. 34b) is the high NO_2 and very low NO concentration. NO_2 exhibits maximum concentrations at midday, concurrent with the maximum concentrations of primary gaseous pollutants such as CO and SO_2. Ozone concentrations remained at the background level throughout the day. The diurnal concentration variations of total suspended particulates, particulate carbon, nitrogen, sulfur, lead, bromine, and chlorine are shown in Figures 34c and 34d. The particulate nitrogen concentrations were obtained by both combustion and proton activation analysis.

Sulfur, lead, bromine, and chlorine concentrations were obtained by X-ray fluorescence. It is of interest to note that the nitrogen concentrations are about a factor of 5 higher than the sulfur concentrations. The detailed particulate

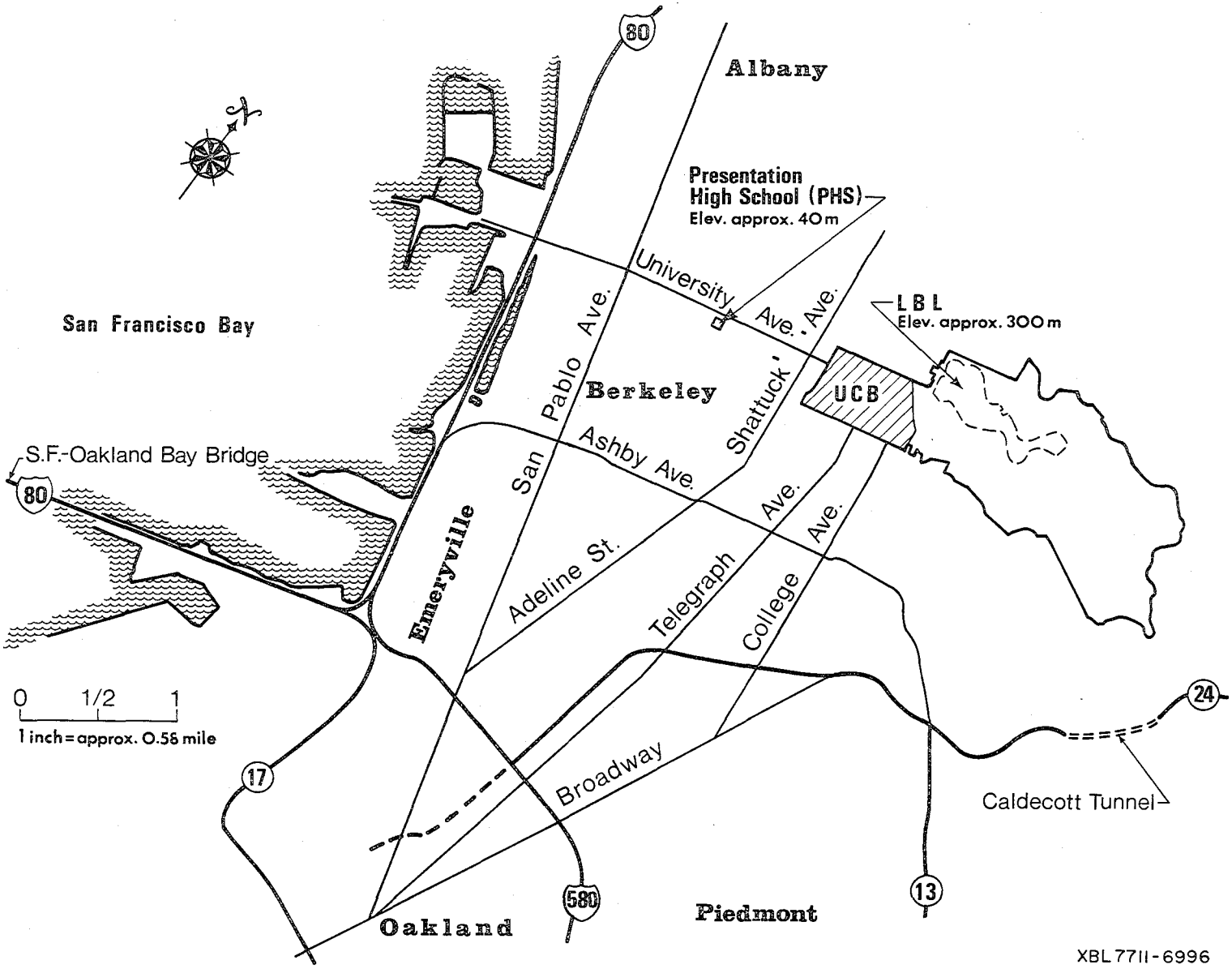

Figure 33. Location of Berkeley air pollution field monitoring sites.
LBL = Lawrence Berkeley Laboratory, November 4-7, 1976
PHS = Presentation High School, February 9-12, 1977

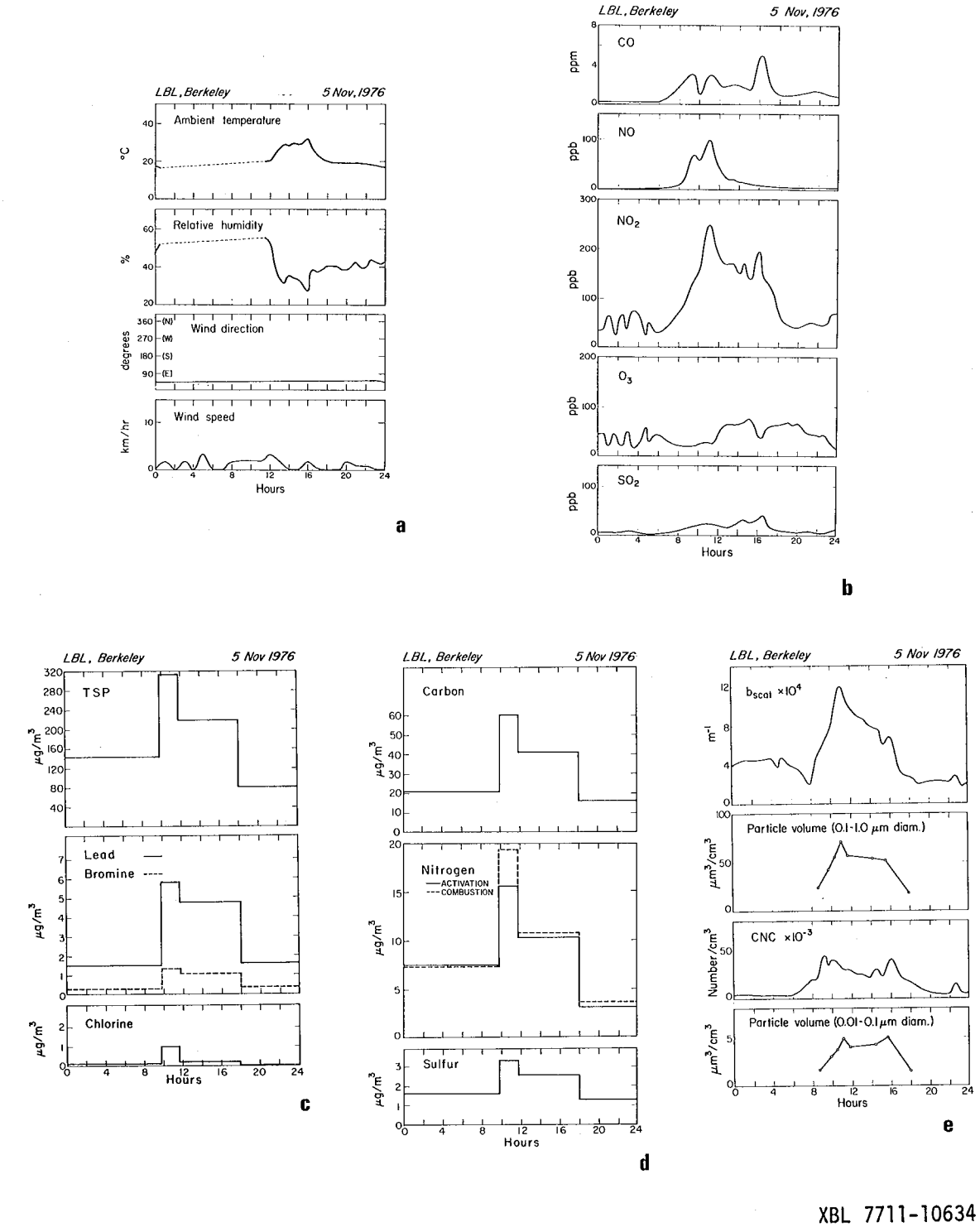

Figure 34. November episode.

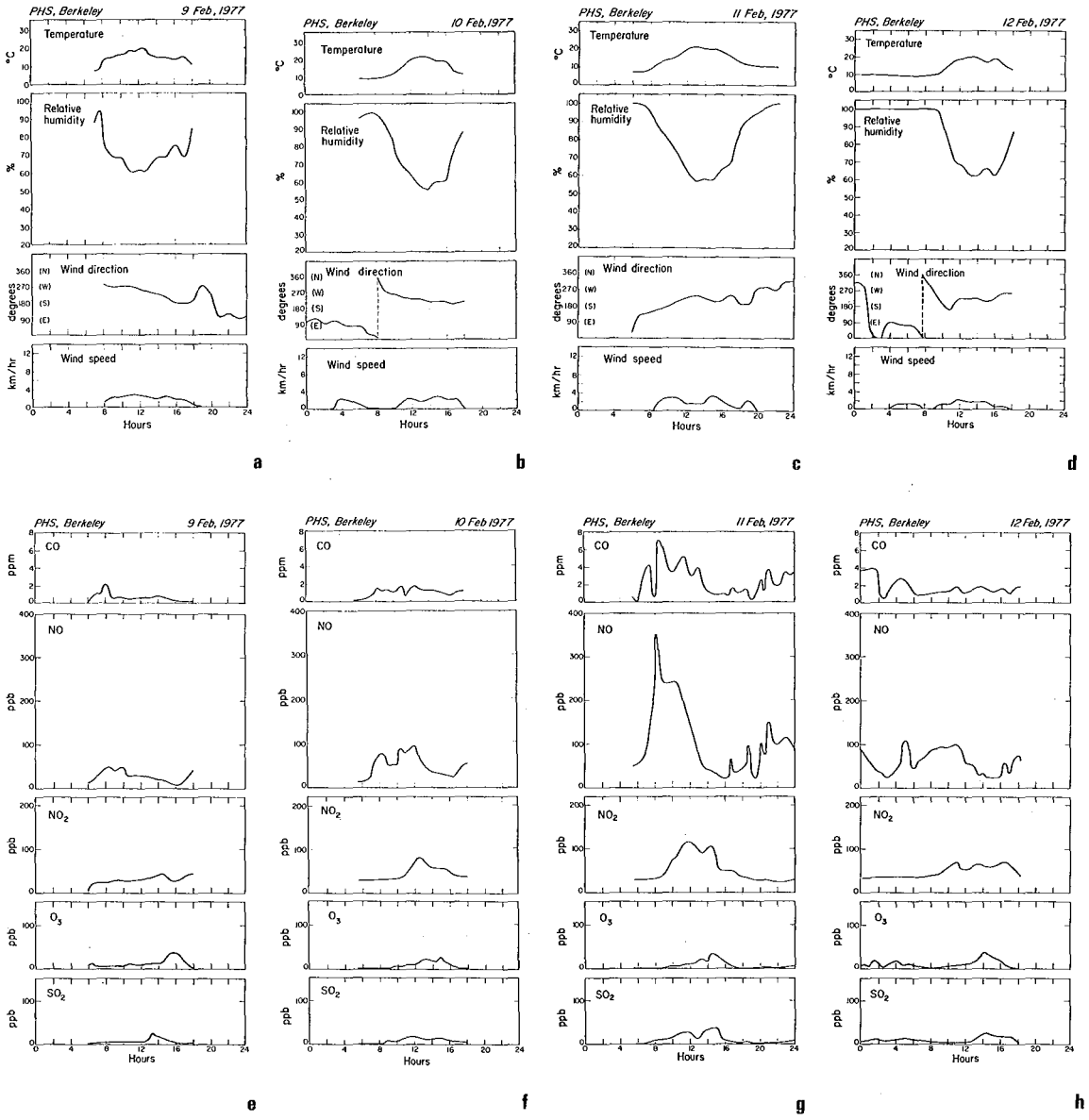

Figure 35. February episode.

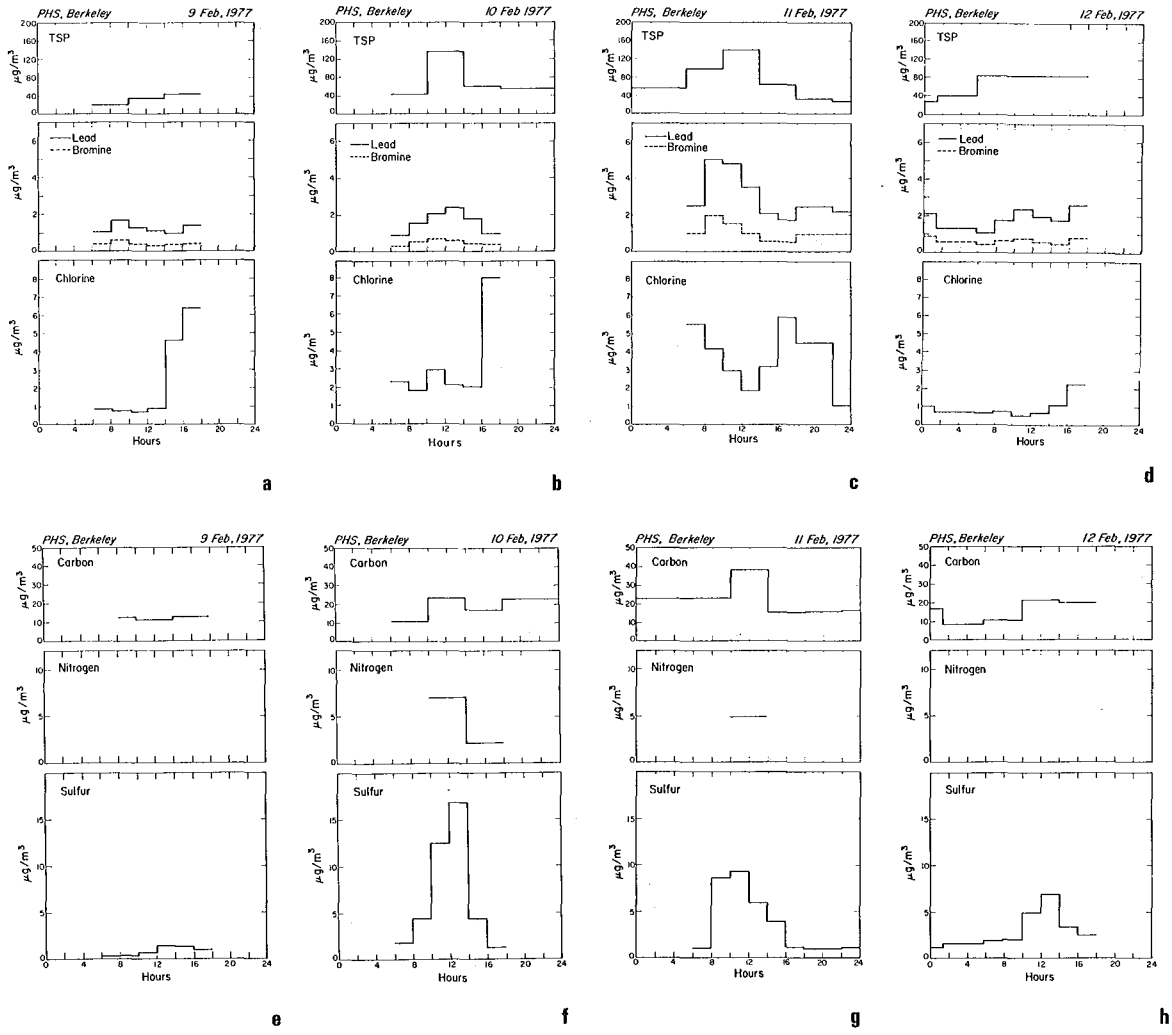

Figure 36. February episode.

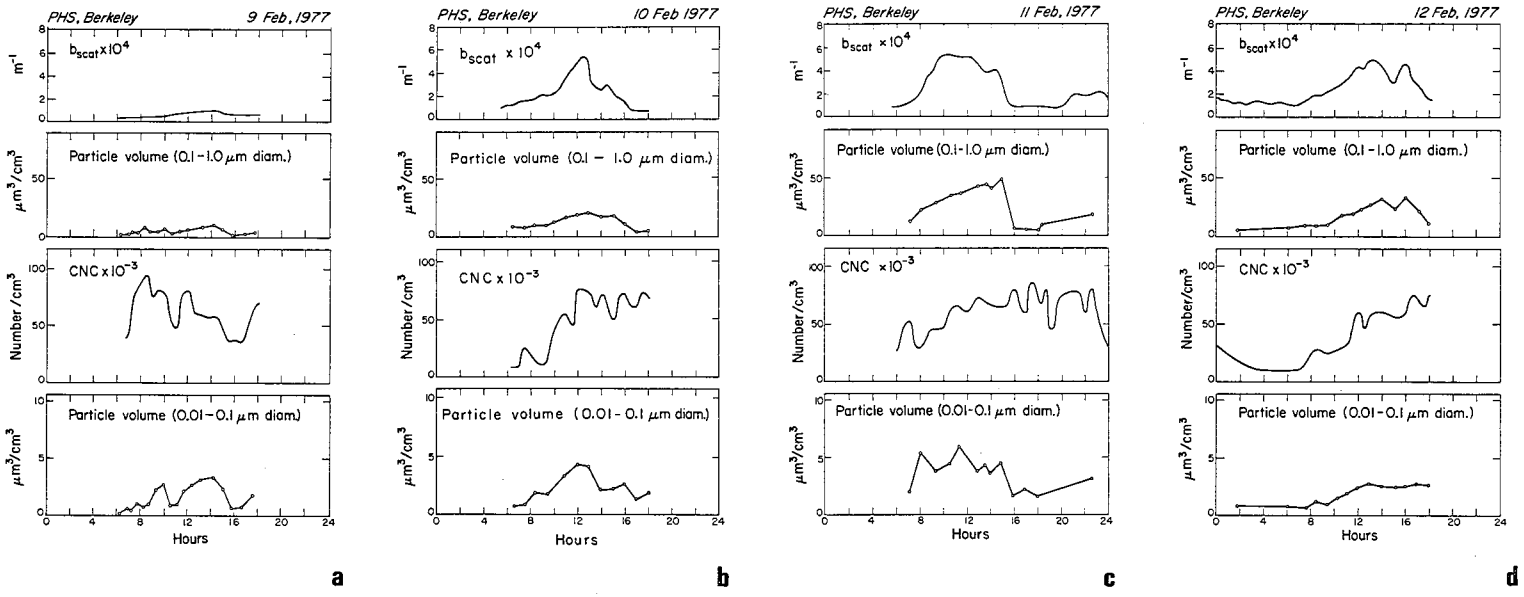

XBL 7711-10637

Figure 37. February episode.

composition for the November episode is tabulated in Table V. Comparisons of the concentrations of C, S, and N compounds determined by various techniques at LBL and Battelle, Columbus Laboratories,[2] are given.

The lateness of the season — thus the relative shortness of daylight hours and the low angle of the solar radiation — prevented conditions which could be classified as a photochemical episode. Photochemistry was also inhibited by sporadic high cloudiness during the period. In spite of these conditions, a heavy air pollution episode was experienced in the San Francisco Bay Area. The Bay Area Air Pollution Control District (BAAPCD) described the episode as a "winter mix" of high levels of suspended particulates, NO_2, and CO.[3]

A less severe episode in February 1977 was monitored (see Figures 35-37). Temperatures were moderate to warm, relative humidity rather high, and stagnation conditions prevailed (Figs. 35a-35d). This episode did not last as long as the November one, but it was monitored from inception following a light rain until its breakup by marine intrusion (see chlorine data, Figs. 36a-36d). Direct comparisons between the data taken in this episode and those taken in November are subject to some uncertainty due to a change of sampling location to a lower elevation within Berkeley. Similarities in the ozone, carbon monoxide, and sulfur dioxide concentrations and diurnal variation are evident in Figures 35e-35h. Nitrogen oxides, however, show a reversal to a regime more dominated by NO in February. This may be due to a different set of local sources or to a shorter history of episode development. Similarly, there is a reversal in the concentrations of particulate sulfur and nitrogen, with the February episode showing substantially more particulate sulfur (Fig. 36). No change in the chemical character of the particulate sulfur and nitrogen was observed by ESCA between the two episodes, with the sulfur being entirely in the form of sulfate, and the nitrogen being composed of approximately 25% nitrate, 25% ammonium, and 50% organic-type nitrogen.

Table V. Particulate composition ($\mu g/m^3$), November 5/6, 1976

Collection date			11-4/5-76	11-5-76	11-5-76	11-5/6-76	11-5/6-76	11-6-76
Collection time			18:39(11-4)-9:45(11-5)	9:54-11:40	11:48-18:00	18:05(11-5)-11:20(11-6)	18:05(11-5)-22:00(11-6)	11:25-22:00
Mass	TSP = 0.31 $g/m^3 \cdot b_{scat}$		143	313	229		81	
Carbon	Total C, combustion (LBL)		21.56	60.54	40.94		15.96	
	Total C, combustion (Battelle)		23.75	62.64	38.01		15.82	
Sulfur	Total S, XRF (LBL)		1.63±.16	3.37±.34	2.60±.26	1.30±.13		1.63±.16
	$SO_4^=$(as S), wet chemistry (Battelle)		3.31	4.32	5.20		1.28	
Nitrogen	Total N, proton activ. anal. (LBL)		7.53	15.60	10.29		3.06	
	Total N, combustion (Battelle)		7.40	19.15	11.14		3.69	
	NH_4^+(as N)	Proton activ. anal. and ESCA (LBL)	1.9-2.3	∿ 4	∿ 3		∿ 1.0	
	Organic N(as N)		3.8	∿ 8	∿ 4		∿ 1.2	
	NO_3^-(as N)		1.5-1.9	∿ 4	∿ 3		∿ 1.0	
	NO_3^-(as N), wet chemistry (Battelle)		5.07	14.16	5.87		2.58	
Hydrogen	Total H (Battelle)		13.19	64.88	23.12		5.25	
Calcium	Total Ca	XRF (LBL)	1.67±.07	4.07±.16	3.98±.16	1.16±.05		1.50±.06
Iron	Total Fe		2.40±.10	5.36±.21	6.12±.24	2.00±.08		2.36±.09
Zinc	Total Zn		0.13±.01	0.98±.04	0.63±.03	0.10±.01		0.10±.01
Bromine	Total Br		0.32±.01	1.36±.05	1.10±.04	0.35±.01		0.37±.01
Lead	Total Pb		1.53±.06	5.77±.23	4.78±.19	1.66±.07		1.76±.07

Table VI shows that the particulate chemical composition of these two winter episodes is quite similar to the composition observed in a photochemical environment such as the South Coast Air Basin (Los Angeles). The observed C/Pb

Table VI. Particulate composition (weight percent).

Species	Berkeley 11/5/76 1000-1400	Berkeley 2/10/77 1000-1400	Berkeley 2/11/77 1000-1400	South Coast Air Basin (typical)[a]
C	19	19	28	19
S	1	11	6	3
N	5	5	4	5
H	10			4
Pb	2	2	3	2
C/Pb	9.5	9.5	9.3	9.5

[a]Refs. 4, 5

ratio in all cases is approximately 10. Field experiments indicate that the halogen-to-lead ratio decreases with increasing aerosol particulate age, probably as the result of photodecomposition of lead bromochloride.[6] The Br/Pb ratios in Table VII compare the winter Berkeley episodes with ratios observed in fresh and aged aerosol particulate environments. The meteorological conditions and the locations of major freeways indicate the age of the Berkeley automotive-source-derived aerosol particulates to be about 2 hours old, similar to aged aerosol particulates in the South Coast Air Basin yielding a lower Br/Pb ratio. This may be an indication of less photodecomposition of PbBrCl and further evidence of low photochemical activity in the Berkeley studies.

During these two winter episodes of low photochemical activity, significant concentrations of carbon, sulfur, and nitrogen were present in the aerosol particles. The results show high concentrations of gaseous and particulate nitrogenous species, and low concentrations of SO_2, yet high levels of particulate sulfur.

The sulfate-to-SO_2 ratio is similar to that observed in the South Coast Air Basin during photochemical smog episodes; this indicates either significant primary sulfate, significant nonphotochemical SO_2-to-sulfate conversion, or both. The presence of a low level of oxidant and the area-wide use of predominantly low-sulfur fuels did not alleviate the problem of high gaseous and particulate nitrogen and particulate sulfur species, nor was the development of visibility restriction (comparable to a moderate-to-severe South Coast Air Basin photochemical smog episode) prevented.

Table VII. Br/Pb mass ratios.

Location	Br/Pb
Berkeley, 11/5/76	.22
Berkeley, 2/9/77	.25
Berkeley, 2/10/77	.29
Berkeley, 2/11/77	.33
Berkeley, 2/12/77	.33
PbBrCl	.40
Caldecott Tunnel (very fresh aerosol)	.55
Los Angeles freeway (fresh aerosol)	.40[a]
South Coast Air Basin (aged aerosol)	.16-.20[b]

[a] Ref. 7

[b] Refs. 6,7

The initial results of these studies indicate that the aerosol particulate composition of a nonphotochemical air pollution episode is similar in composition to "photochemical" episodes and gives strong support to the thesis that nonphotochemical reactions play a significant role in particulate aerosol formation in both summer and winter urban air pollution episodes in California. More extensive studies of winter and summer air pollution episodes are currently

in progress. These studies should help in assessing the significance of heterogeneous and homogeneous reactions in the formation of carbon, sulfur, and nitrogen aerosol particles and, furthermore, to assess the relative importance of humidity and various potentially important catalysts (e.g., carbon) for SO_2 conversion.

Several sampling sites will be used to account for both source-enriched and aged aerosol particles. The sites dominated by sources such as a power plant (Antioch), refineries (Richmond), and automotive and small commercial/residential point sources (Berkeley) will be studied as well as typical receptor sites such as the South Bay (Fremont-San Jose) and the Livermore Valley.

References

1. C.D. Hollowell and T. Novakov, "Mobile Atmospheric Research Laboratory," in Atmospheric Aerosol Research, Annual Report 1975-76, Report LBL-5214, Lawrence Berkeley Laboratory, University of California, Berkeley, CA 94720.
2. Analyses performed by Chester W. Spicer, Battelle, Columbus Laboratories, Columbus, Ohio 43201.
3. "Air Currents," Bay Area Air Pollution Control District, 20 (January, 1977).
4. C.W. Spicer, The Fate of Nitrogen Oxides in the Atmosphere, EPA Report #600/3-76-030.
5. G.M. Hidy, et al., Characterization of Aerosols in California (ACHEX): Final Report, Science Center, Rockwell International, Report SC524.25FR (1974).
6. S.G. Chang, R. Dod, R. Giauque, and T. Novakov, Photodecomposition of Lead Bromochloride, Report LBL-6360, Lawrence Berkeley Laboratory, University of California, Berkeley, CA 94720.
7. R.D. Giauque, private communication, 1977.

ESCA and X-ray Fluorescence Analyses of DaVinci II and III Particulate Samples

R. L. Dod, R. D. Giauque, C. D. Hollowell, and T. Novakov

Two manned balloons (Da Vinci II and III) were launched into the St. Louis urban plume during the summer of 1976. Since each balloon ideally operated as a Lagrangian platform, following and remaining within a single air parcel from the time of launch until descent maneuvering, the samples collected should, in principle, represent only that air parcel. Only by collecting in this fashion can enough particulate material be collected for analysis by many techniques while still maintaining assurance that each sample represents a common history. Successive samples thus reflect only chemical and physical changes within the particulate aerosol, modified by emissions into the parcel and deposition from it. The LBL Atmospheric Aerosol Research group participated in these studies by collecting onboard samples on membrane filters and analyzing the collected particulate aerosol by X-ray fluorescence (XRF) and X-ray photoelectron spectroscopy (ESCA) analysis.

The samples collected on cellulose ester filters during both flights were analyzed by X-ray fluorescence spectroscopy. (Those from DaVinci II were analyzed by neutron activation analysis also.) A listing of the most significant elements detected for DaVinci II is shown in Table VIII. Other elements were detected on some filters, but in general the loadings were below detection limit. Particulate sulfur concentration increased by nearly a factor of 2 during the DaVinci II flight, but no other trends were noted among the other elements. DaVinci III filters showed similar relationships among the various elements detected, but at lower concentrations.

Table VIII. Particulate elemental concentrations by X-ray fluorescence (partial listing).

Sample	Time	Concentrations, $\mu g/m^3$						
		S	Ca	V	Mn	Fe	Zn	Pb
Da Vinci II (6-8/9-76)								
1	0914-0930	7.1±.6	.82±.65	<.57	.11±.10	.29±.09	<.13	<.68
2	1022-1035	8.0±.6	<2.4	.35±.24	<.39	.28±.12	<.16	<.84
3	1106-1128	8.5±.7	.70±.49	<.43	.13±.07	.28±.07	<.10	.29±.17
4	1213-1232	9.4±.8	<1.6	<.48	.14±.09	.39±.08	<.11	<.58
[a]5	1307-1322	9.5±.8	.93±.70	<.63	.16±.11	.25±.10	.14±.05	<.75
6	1405-1425	11.0±.9	1.7±.57	<.48	.18±.09	.43±.08	.16±.04	<.58
7	1512-1529	7.5±.6	.91±.64	<.54	<.29	.19±.09	<.12	<.66
8	1605-1625	9.4±.8	<1.6	.17±.15	<.25	.38±.08	.06±.04	.50±.18
9	1701-1716	11.9±1.0	1.6±.73	<.64	<.35	.57±.11	.30±.05	.44±.25
10	1810-1830	12.4±1.0	.95±.55	.20±.16	.12±.09	.35±.08	.13±.04	.38±.19
11	1908-1937	11.7±.9	.52±.37	.20±.11	<.17	.36±.06	.04±.02	.14±.13
12	2011-2026	13.3±1.1	.88±.71	<.62	<.34	.32±.10	.07±.05	<.74
13	2206-2235	11.5±.9	<1.1	<.32	<.17	.60±.06	.10±.03	.16±.13
[b]14	0031-0105	13.6±1.1	.82±.31	<.27	.08±.05	.47±.05	.06±.02	.19±.11
[c]17	0556-0621	14.0±1.1						

[a]Sample dropped.

[b]Flow rate questionable.

[c]Samples 15 and 16 damaged.

The silver filters used for ESCA analysis were relatively lightly loaded, primarily due to a low pumping speed required to keep the power demand low. A sufficient sample was collected on each silver membrane filter to allow detection of sulfur, which was in all cases in the 6+ (sulfate) oxidation state. DaVinci II filters also showed varying amounts of nitrogen, primarily ammonium nitrogen, but with some nitrogen characteristic of organic amines. Lead concentrations on all filters were low.

For DaVinci II the filters collected near the end of the flight showed a somewhat higher apparent sulfate concentration than those taken near the beginning (Fig. 38). Ammonium nitrogen (binding energy, 402 eV) was present and measurable by the afternoon of June 8 and increased throughout the remainder of the flight. The molar ratio of ammonium to sulfate ions increased during this period by approximately a factor of 2, with the final observed ratio corresponding to a "compound" more ammonium rich than NH_4HSO_4 (Fig. 38). This may be the first field observation of the neutralization of acidic sulfate species by ammonia gas entering the air parcel within a plume.

Because the air parcel which DaVinci III traveled in was much cleaner, the filters contained no detectable nitrogen or lead and only small amounts of sulfur, again only as sulfate.

All filters from both flights were lightly loaded and required long periods in the high vacuum (10^{-8} torr) of the electron spectrometer in order to obtain measurable spectra. Consequently, volatile components of the collected particulate material (such as most nitrates) could easily have been lost by sublimation and their presence cannot be excluded.

From the results of the ESCA and X-ray fluorescence analyses of the DaVinci particulate samples, an estimate can be made of the practical detection limits for sulfur, nitrogen, and lead on silver filters. Using the S(2p) photoelectron peak, sulfur species can probably be detected in filter

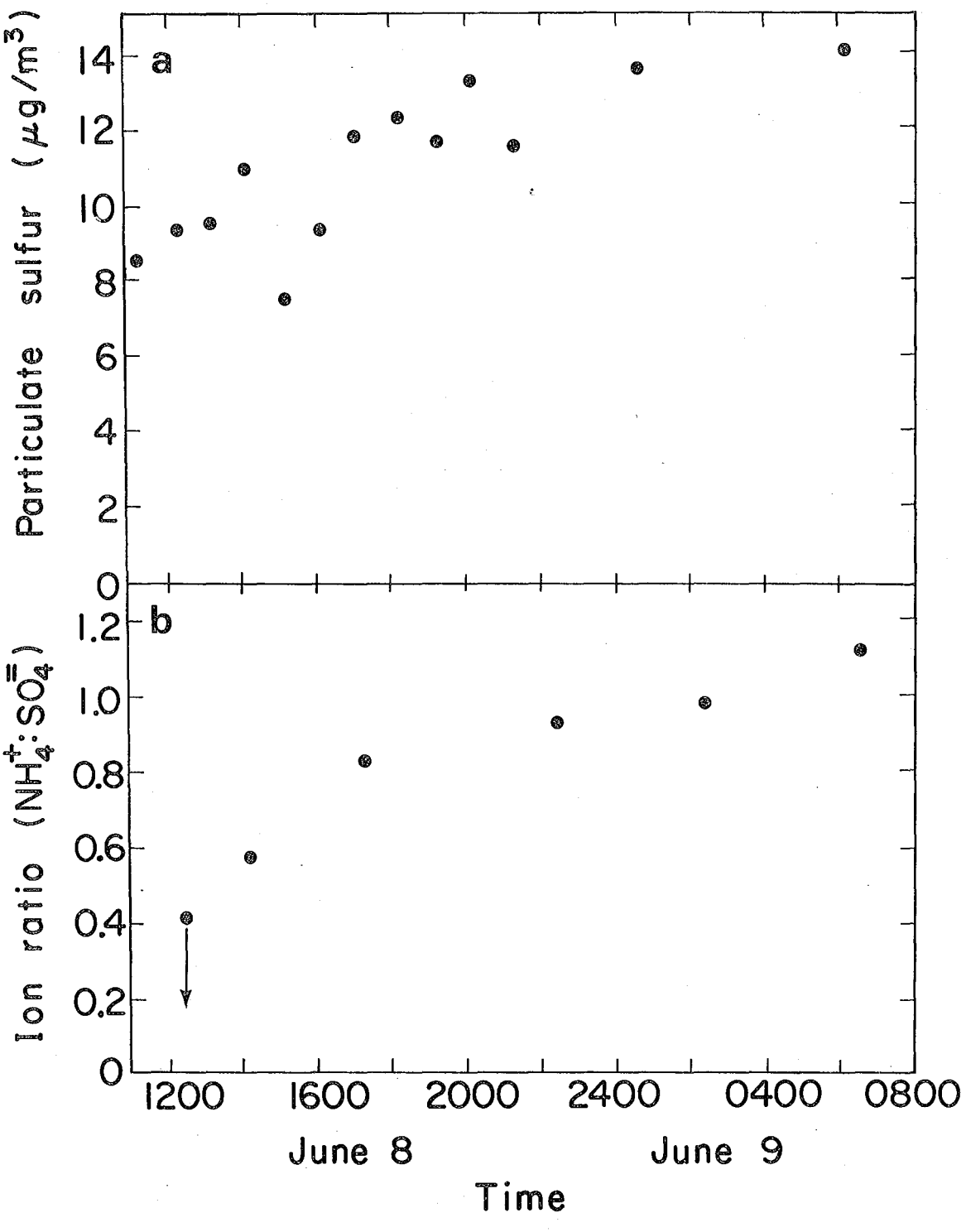

XBL772-362

Figure 38. Da Vinci II results as a function of flight time: a) Total particulate sulfur concentration by X-ray fluorescence. b) Ammonium-to sulfate ratio by ESCA.

concentrations as low as 0.1 $\mu g/cm^2$, with reasonably reliable measurement of peak intensity possible at 0.5 $\mu g/cm^2$. The nitrogen core electron peak lies on the energy loss spectrum of the silver 3d peaks and therefore requires a greater quantity of material to be detected. The detection limit is approximately 1 $\mu g/cm^2$ per chemical oxidation state. A similar detection limit is found for lead.

This report was done with support from the United States Energy Research and Development Administration. Any conclusions or opinions expressed in this report represent solely those of the author(s) and not necessarily those of The Regents of the University of California, the Lawrence Berkeley Laboratory or the United States Energy Research and Development Administration.